Karin Andrea Plimon, BSc

Comparison of ITU-R Models with Selected Measurements and Improvements

MASTER'S THESIS

for the acquisition of the academic degree

Diplom-Ingenieur

Master's Program Space Sciences and Earth from Space

submitted to

Graz University of Technology

Advisor

Ao.Univ.-Prof. Dipl.-Ing. Dr. Erich Leitgeb

Institute of Microwave and Photonic Engineering
Graz University of Technology

Dipl.-Ing. Dr. Michael Schönhuber
Joanneum Research

Graz, May 2014

Abstract

To design satellite links and assess the impact of atmospheric effects on satellite communication, different models that predict these effects have been developed. The International Telecommunication Union (ITU) is a department of the United Nations (UN) and is amongst others also concerned with the development and adoption of these models. The common goal is to optimize existing models in order to obtain predictions that are close to reality.
ITU propagation models that predict tropospheric effects for fixed satellite systems are evaluated. These models are relevant for satellite signals in the range between 10 GHz - 50 GHz. The reference dataset for evaluation consists of measurement data from beacon receivers, radiometers, a disdrometer and meteorological data.
After the evaluation of brightness temperatures, frequency scaling, specific rain attenuation, attenuation due to clouds and total attenuation as well as scintillation, fade statistics such as fade duration, interfade duration and fade slope results are analyzed. Based on these findings potential improvements are discussed and modified models as proposed in open literature introduced.

Kurzfassung

Für den Entwurf von Satellitenkommunikationsstrecken werden Modelle benötigt, die den Einfluss von atmosphärischen Effekten auf die Satellitenkommunikation für verschiedene Szenarien vorhersagen. Die International Telecommunication Union (ITU), eine Abteilung der Vereinten Nationen (UN), ist mitunter auch an der Entwicklung von Modellen zur Vorhersage von Signalausbreitung unter atmosphärischen Einflüssen beteiligt. Ziel ist eine möglichst wirklichkeitsgetreue Gestaltung der Modelle, damit die vorhergesagten Ergebnisse realen Bedingungen entsprechen.
ITU Signalausbreitungsmodelle, geeignet für die Prädiktion von troposphärischen Effekten bei Signalen von fixen Satellitenstrecken im Frequenzbereich zwischen 10 GHz - 50 GHz, werden herangezogen. Die ITU Modelle werden mit Messergebnissen von Bakensignalempfängern, Radiometern, einem Distrometer und meteorologischen Daten evaluiert. Nach der Evaluierung von Radiometermessungen, spezifischer Dämpfung durch Niederschlag, Dämpfung durch Bewölkung, sowie die absolute Dämpfung und Szintillation aber auch das Signalverhalten bei Dämpfungsereignissen und Frequenzskalierung werden die Ergebnisse anlysiert. Basierend auf diesen Ergebnissen werden potentielle Verbesserungsmöglichkeiten diskutiert und bereits entwickelte modifizierte Modelle aus der Literatur vorgestellt.

AFFIDAVIT
EIDESSTATTLICHE ERKLÄRUNG

I declare that I have authored this thesis independently, that I have not used other than the declared sources/resources, and that I have explicitly marked all material which has been quoted either literally or by content from the sources used. The text document uploaded to TUGRAZonline is identical to the present master's thesis.

Ich erkläre an Eides statt, dass ich die vorliegende Arbeit selbstständig verfasst, andere als die angegebenen Quellen/Hilfsmittel nicht benutzt, und die den benutzten Quellen wörtlich und inhaltlich entnommene Stellen als solche kenntlich gemacht habe. Das in TUGRAZonline hochgeladene Textdokument ist mit der vorliegenden Masterarbeit identisch.

Date / Datum

Signature / Unterschrift

Contents

List of Figures

List of Tables

List of Abbreviations

ITU International Telecommunication Union

UN United Nations

SG3 Study Group 3

ITU-R ITU - Radiocommunication

ITU-T ITU - Telecommunication Standardization

ITU-D ITU - Development

FSS fixed satellite service

2DVD 2D-Video-Disdrometer

ZAMG Zentralanstalt für Meteorologie und Geodynamik

IOT in-orbit test

RPG Radiometer Physics GmbH

ATPROP Atmospheric Propagation Profiler

UTC Coordinated Universal Time

ESA European Space Agency

CPA co-polar

CDF cumulative distribution function

HDF5 Hierarchical Data Format 5

TUG Graz University of Technology

OPEX Olympus Propagation Experimenters Group

r.m.s. root mean square

FFT Fast Fourier Transformation

ECMWF European Centre for Medium-Range Weather Forecasts

1 Introduction

In satellite communication atmospheric effects can have a strong impact on the transmission of information. This is why the avoidance of transmission impairments on satellite links is crucial. During the design of a satellite link it is important to assess possible atmospheric influences by modelling. Therefore, models which are close to reality are required to simulate real conditions on a satellite link as close as possible. The modelling however is quite difficult, because the conditions strongly depend on the area and thus the climate where the satellite receiver is stationed. Additionally, atmospheric effects also depend on frequency and elevation of the satellite link. By modelling various influences, expected signal strengths and variation results become known. Based on that knowledge measures can be taken to avoid outages and thus make a satellite communication more reliable.

An organization that is amongst others also concerned about improvement of satellite communication is the International Telecommunication Union (ITU) [33]. The ITU is an agency of the United Nations (UN) with the headquarters located in Geneva, Switzerland. The ITU is specialized in information and communication technologies and is structured in the following three sectors: the ITU - Radiocommunication (ITU-R), the ITU - Telecommunication Standardization (ITU-T) and the ITU - Development (ITU-D). The main task of the Radiocommunication sector is frequency allocation, efficient use of the frequency spectrum and the coordination of satellite orbits. Another important aspect of their work is the development of radio regulations and recommendations. ITU-R recommendations are usually developed by one of the six study groups in this sector that consist of experts from world wide ITU member states. Before a new recommendation developed by the ITU study group or a modified version of an already existing recommendation is released, the recommendation has to be approved by the ITU member states. The ITU is anxious to provide approved high quality models based on the latest findings and to keep these models up-to-date. Although these recommendations are not mandatory for satellite link design, they are eminent due to the high level of expertise. Study Group 3 (SG3) is one of the six study groups at the ITU-R sector mentioned above. This study group is concerned with radio wave propagation. One of their focuses is on the earth-space propagation.

Based on propagation models in form of ITU-R recommendations provided by the SG3 this thesis performs the evaluation of selected ITU-R propagation models for fixed satellite service (FSS) regarding their matching to real conditions. The core theme are especially propagation models that predict the influence of tropospheric effects.

The structure of this thesis is as follows: The problem and the procedure executed are presented in chapter 2. Chapter 3 talks about the relevant atmospheric effects. In chapter 4 the selected datasets that form the reference database are described. The algorithms of the chosen ITU models are introduced in chapter 5. Chapter 6 defines the evaluation tasks. In chapter 7 the implementation of the ITU models and data analysis routines is described. Chapter 8 presents the test procedure for the implemented software. Chapter 9 is concerned with the results of the evaluation. In chapter 10 modified propagation models are discussed. Based on the evaluation result potential improvements for ITU models are provided in chapter 11. Finally, chapter 12 draws conclusions and gives an outlook.

2 Problem and procedure

The objective of this thesis is the evaluation of models simulating atmospheric effects on radio wave propagation in a fixed satellite system. The measurement datasets are derived from instruments being part of the basic equipment of a beacon receiver terminal. These datasets define the reference database for the evaluation process. Based on the selected database, adequate propagation models have to be identified where the focus is on propagation models developed by the ITU.

The following actions were performed in the course of this thesis:

- Identification of measurement datasets for the reference database
- Description of the individual datasets forming the database
- Research on suitable ITU-R models matching the reference database
- Research on dependencies between ITU models
- Definition of the evaluation tasks
- Implementation of the ITU-R models and their dependencies
- Implementation of routines to prepare measurement data for further processing steps
- Implementation of data pre-processing routine as well as visual inspection of measurement data to remove perturbing effects in the data sets manually
- Implementation of data processing routines to compute the statistics
- Evaluation of the models
- Suggestions for potential model improvement

The initial step of the procedure was the identification of potential measurement datasets to create the reference database. In the course of this action, datasets derived from beacon receivers, radiometers, a disdrometer and a meteorological station, respectively a rain gauge, were considered. The selected datasets for the final reference database were described in further detail regarding their parameters and period of acquisition in section 4. Once the reference database was selected, suitable propagation models had to be selected from the models offered by the ITU. The model selection criteria, that have been identified based on the available dataset, defined a frequency range between 10 GHz to 40 GHz for beacon signals, focussed on fixed satellite systems and considered tropospheric effects only. Additionally, dependencies between the ITU models needed to be determined. These dependencies provide the possibility to generate input parameters

based on other models provided by the ITU. Finally, 10 tasks for the propagation model evaluation emerged from the research.
Subsequently the implementation process of the ITU models started. Software routines needed to be implemented in order to convert data sets into a common data format. This was necessary for the processing of the reference database, to simplify the data access and speed up further processing steps to create comparative values for the model evaluation. In the next step data pre-processing was performed. In this pre-processing step outliers were detected, removed and template extraction was performed as well. The data then was processed, the statistics computed and finally the evaluation step could be performed. In addition, modified prediction models as proposed in open literature are introduced and based on the evaluation results potential improvements for ITU models are discussed.
This chapter was intended to introduce the problem and give an overview of the executed procedure. The remaining chapters of this thesis will now examine these steps of the procedure in more detail.

3 Atmospheric effects

Micrometer- and millimeter-waves describe the wavelength in the frequency range between $1\,GHz$ with a wavelength of approximately $\lambda = 30\,cm$ and $300\,GHz$ with a wavelength of approximately $\lambda = 1\,mm$ [11]. The relation between frequency and wavelength can be derived according the following equation (1).

$$\lambda = \frac{c}{f} \qquad [m] \tag{1}$$

This formula is valid for free space where the parameter c denotes the phase velocity of light in vacuum with $3 \cdot 10^8 m/s$ and the frequency f is indicated in $[Hz]$ [27].

For satellite communication, consideration of the impact of the atmosphere on the signal propagation is crucial. Satellite communication commonly happens in the frequency range between 1 GHz and 50 GHz where frequencies up to Ka-band are considered operational and Q/V-band is currently used for experimental purposes. Therefore, this section focuses on atmospheric effects that influence the signal propagation in this frequency range. For frequencies above 1 GHz the ionosphere appears transparent, otherwise satellite communication would not be possible. This fact is explained in [3] by the critical frequency, respectively the plasma frequency which can be computed by the following equation (2).

$$f_c = 8.9788 \cdot 10^{-6} \cdot \sqrt{N} \qquad [MHz] \tag{2}$$

Here, N denotes the number of $electrons/m^3$ in the plasma.

Radio waves at frequencies below the critical frequency are reflected back to the Earth's surface but if the critical frequency is reached only partial reflection occurs. Thus, radio waves at frequencies higher than the critical frequency are able to travel through the ionosphere. With increasing frequency the absorption and reflection characteristics of the ionosphere decrease. The critical frequency threshold varies but it appears around 12 MHz. Hence, for frequencies above 1 GHz the influence of the ionosphere on propagation can be neglected and therefore the ionosphere is called transparent for micrometer- and millimeter-waves.
The most severe impact is caused by tropospheric effects, as the influence of the ionosphere is not relevant for signal propagation within the indicated frequency range used for satellite communication. For this reason, tropospheric effects are discussed in further detail in the following subsections.

3.1 Rain attenuation

In satellite communication the spectrum from 1 GHz to 300 GHz is divided in different frequency bands according to the letter band designation as explained by Luis Ippolito

in [27]. Many satellite communication systems operate in the frequency range above 3 GHz which are C-band, Ku-, Ka-band and for experimental operation the Q/V-band. Unfortunately, major impairments of propagation happen in this frequency range. Signal degradation by rain represents the phenomenon that causes the most serious propagation impairments in satellite communication. This category includes basically two effects which are induced by rain drops.
Attenuation by rain drops happens due to absorption and scattering of energy. This fact leads to a reduced amplitude of the transmitted signal.
Depolarization represents the second effect. The depolarization occurs due to the shape of the rain droplet which is usually not spherical but is rather flattened and thus similar to an ellipsoid. However, the shape of a raindrop is dependent on the mass and the fall velocity of the rain droplet. The polarization of a transmitted signal changes if a radio wave impinges on a non-spherical but rather flat raindrop because in the raindrop the energy gets transferred into another polarization state [27].
Effects on the signal induced by rain largely depend on the frequency of the transmitted signal but also on factors like rain rate, the drop size distribution and its shape. Nevertheless, the higher the frequency the more attenuation is caused by rain drops. Furthermore the presence of ice crystals respectively ice clouds can influence the strength of this effect to a large extend [27].

3.2 Cloud attenuation

The effect of attenuation due to clouds is not as strong as the rain attenuation, though, this effect is more present than the occurrence of rain events. While fog with water droplets of a diameter less than 0.1 mm effects radio waves at frequencies above 100 GHz, clouds usually consist of 0.1 mm up to 10 mm droplets. For this reason, attenuation induced by fog can be neglected for satellite links. Furthermore it is observed that attenuation due to clouds increases with increasing frequency and additionally also a decreasing elevation angle leads to an intensification of this phenomenon [27]. The effect of cloud attenuation might not be very strong for satellite communication frequencies but definitely has to be taken into account at Q/V band frequencies as it is reported by L. Luini in [29]. The specific attenuation due to clouds is related to the amount of liquid water contained in the cloud. The liquid water content depends on the type of cloud but generally varies between 0.1 g/m^3 and 2 g/m^3. However, also within the cloud the liquid water content is highly variable. The liquid water content of a cloud is assumed to have the maximum at the cloud base height and diminish towards the top of the cloud [6].

3.3 Gaseous attenuation

Regarding gaseous absorption, which is also outlined by [3], oxygen and water vapour are two gases that cause most absorption of the energy from the electromagnetic wave.

Moreover these gases have absorption lines in frequencies where resonant absorption occurs. The specific attenuation of oxygen (dry air) and water vapour (H_2O) over a frequency range of 1 to 350 GHz are illustrated in Figure 1. Considering the frequency band up to 350 GHz, water vapor has absorption lines at three frequencies which are 22.3 GHz, 183.3 GHz and 323.8 GHz. Some absorption lines for oxygen are at approxi-

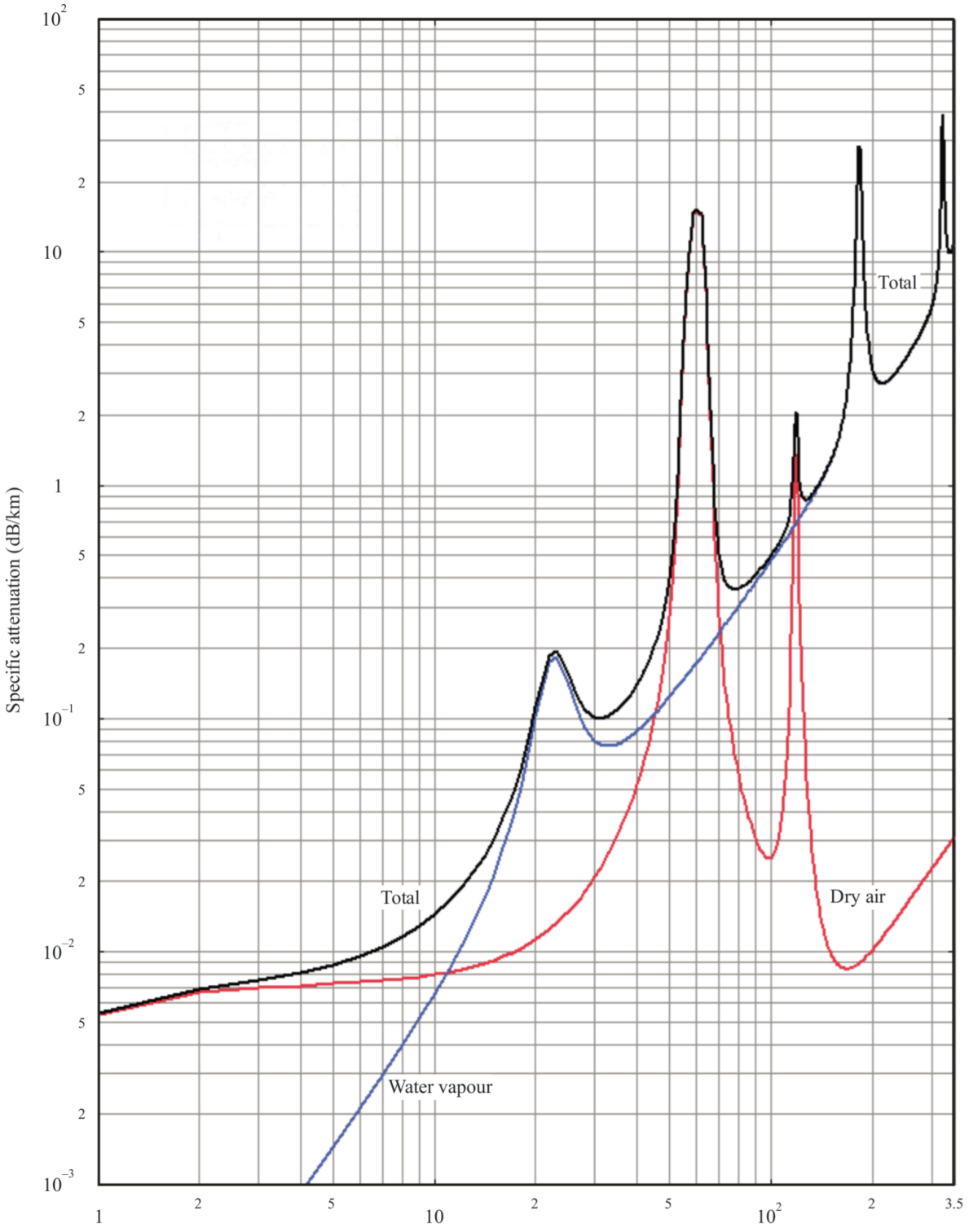

Figure 1: Specific attenuation due to dry air and water vapour [50]

mately 60 GHz and additionally there is one located at 118.74 GHz. The phenomenon of gaseous absorption is dependent on two parameters which are air pressure and temperature. Thereby, the dependency is inversely proportional, which means the attenuation increases with decreasing temperature. As illustrated in Figure 1, the total gaseous absorption value is composed of the specific attenuation of dry air on the one hand and the

specific attenuation of water vapor on the other. To determine the gaseous absorption along the satellite link path, integration of the specific attenuation is necessary. However, for the integration, the variation of temperature and air pressure along the path needs to be taken into account. Because of the fact that the impact of fog specific attenuation is minor at frequencies below 100 GHz, the influence due to fog is not relevant and can be neglected in this context as the used frequencies of the reference database are below 50 GHz.

3.4 Tropospheric scintillation

As it is described in the OPEX handbook [5], the phenomenon of fast variations in the refractive index that causes random fluctuations in the signal amplitude is called scintillation. The reason for scintillation, respectively these fluctuations, are turbulences in the atmosphere whereby the presence of clouds in the satellite link path are relevant as well. The impact of this effect becomes stronger with higher frequencies and lower elevation angles. Allnutt [3] reports that the effect of scintillation is not remarkably relevant at frequencies below the 1 GHz threshold. For frequencies larger than 10 GHz however, this effect gains influence and needs to be considered for propagation [5].

Scintillation generally occurs during clear sky as well as rain periods. Though during rain events the description of the process that is responsible for scintillation gets more complex since also parameters as the drop size distribution, rain rate, scattering, wind gusts, different air masses etc. additionally influence amplitude fluctuations. For this reason most scientific analyses focus on scintillation that occurs during clear sky respectively dry air [5]. This phenomenon is relevant for satellite communication because it leads to a significant degradation of the signal quality especially in higher frequency bands.
Figures 2 and 3 exemplarily illustrate the characteristics of scintillation and its effect on a transmitted signal at 11.2 GHz as shown by Cheffena in [9]. In Figure 3 the dashed line indicates the theoretical spectrum, the continuous line the measured one.

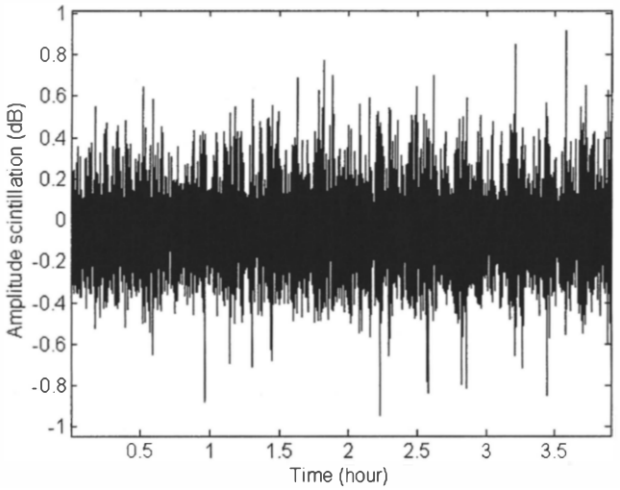

Figure 2: Clear-sky scintillation time series [9]

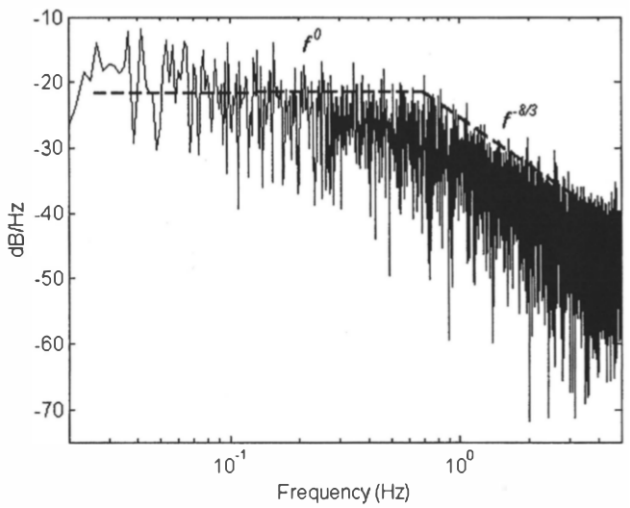

Figure 3: The scintillation spectrum [9]

3.5 Other atmospheric effects

Certainly impairments are caused by other atmospheric phenomenons as well, for example refraction and depolarization.
Allnutt explains in [3] that refraction occurs because the atmosphere is composed of multiple vertical layers with different refraction indices. This layered structure with various refractive characteristics is the reason why a radio wave does not travel straight through the atmosphere but a phenomenon called ray bending occurs. If the effect of refraction is not taken into account it can cause difficulties especially for antennas with a narrow beam width of some tenth of a degree.
Depolarization as discussed in [6] is another phenomenon that already has been shortly mentioned before. The effect of signal depolarization is induced by non-spherical rain droplets in the atmosphere. If a radio wave impinges on a flattened rain droplet, the signal gets to a certain extend depolarized. This change in depolarization leads to cross talk and can hamper communication enormously.
Of course these effects are no less important to satellite communication. Unfortunately, in this thesis they could not be covered by the reference data base and are therefore only shortly mentioned for the sake of completeness in this section.

4 Description of the database

The selected database consists of datasets that were collected at five different sites in the area of Graz during the last 30 years. Available measurements and graphical statistics, which are both representative and valid for point to point satellite links, were chosen for the database. These datasets involve satellite beacon measurements, radiometer data, disdrometer data, measured with a disdrometer of the type 2D-Video-Distrometer (2DVD), as well as meteorological data. Moreover, the available data to evaluate the ITU-R models is fundamental for the selection of the models to be compared. Therefore, especially datasets with measuring periods of one year or longer are preferred to derive statistics. Figures 4, 5 and 6 provide an overview of measurement sites and periods in the area of Graz. Table 1 represents the legend of Figure 4. Afterwards, each dataset is presented in detail.

Marker	**Site**	**Measurement data**
1	Weinitzen	Disdrometer (2DVD)
2	Inffeldgasse (TUG)	Radiometer (Report 1985)
3	Lustbühel	Olympus beacon receiver terminal
4	Hilmwarte	Alphasat beacon receiver terminal Radiometer Hilmwarte Meteorological station Hilmwarte
5	Graz University	Meteorological station (ZAMG)

Table 1: Legend of Figure 1

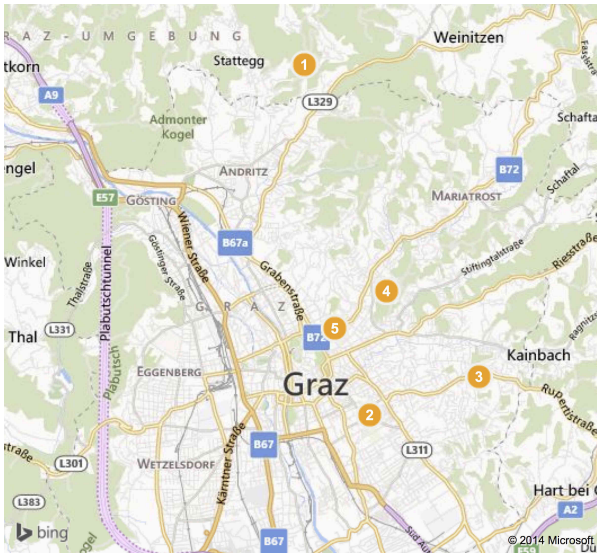

Figure 4: Database measurement locations in the area of Graz [13]

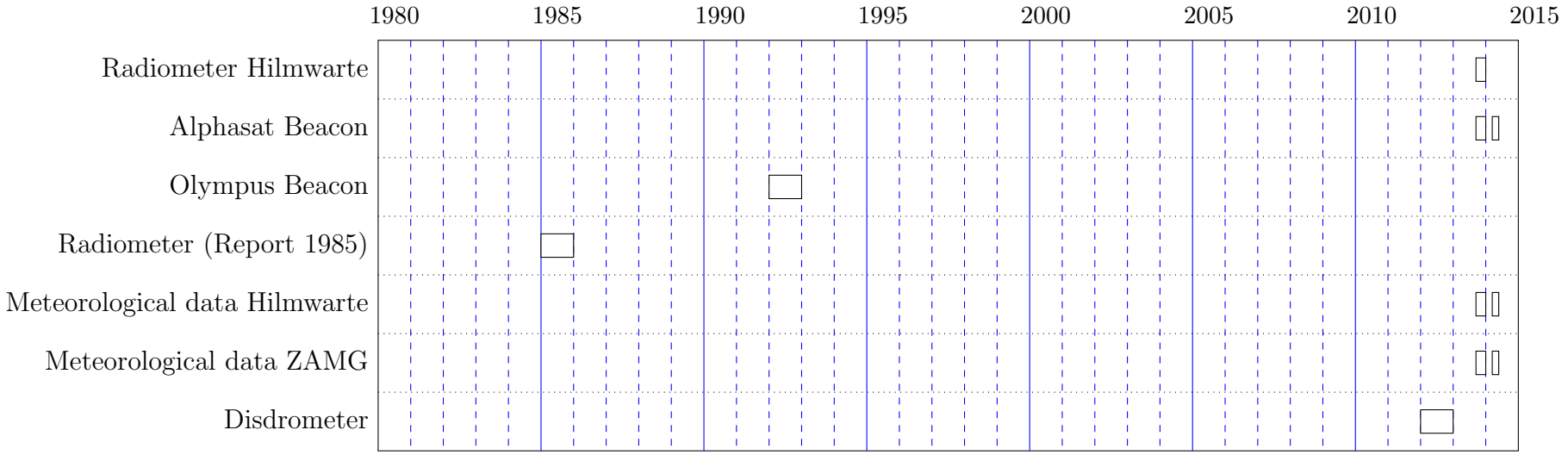

Figure 5: Time line of measurements in the reference database

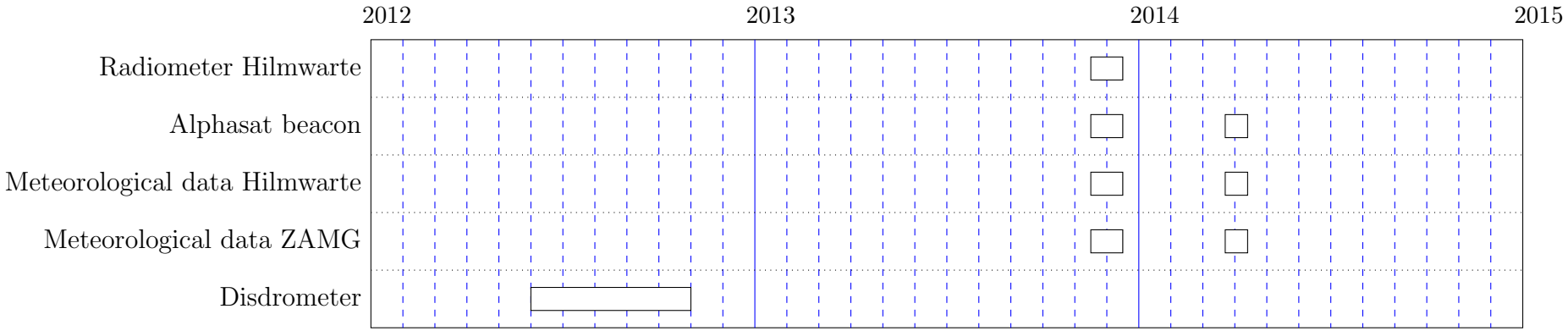

Figure 6: Detailed view of datasets measured between 2012 and 2014

According to the timeline illustrated in Figures 5 and 6, the datasets in the database are quite wide-spread in time. Nevertheless, this fact has no influence on the comparability neither with the ITU-R models nor the datasets amongst each other. The newest measurement data represents the Alphasat campaign which actually started in late October 2013 with the in-orbit test (IOT). The measurement period of this dataset is indicated with a duration of one month from mid-November to mid-December 2013 and approximately 14 days in March and April 2014. The Alphasat campaign presently has a nominal duration of three years. This dataset, however, was selected in order to avoid periods where equipment tests were executed. An important criterion was also to select data for the period of 1 month in order to calculate monthly statistics. Another important fact to be mentioned is that the datasets of radiometer and beacon data of the Alphasat campaign represent data which was measured at a very early stage of the campaign shortly after the IOT was executed. Due to this fact, the recorded data still contains outages and might show unusual behavior. Furthermore, the satellite shows significant orbital movement. In combination with other factors a template becomes visible in the recorded data. At that stage, no antenna tracking was installed at the beacon receiver, thus a first approach to extract the template from the dataset has been applied.

4.1 Radiometer Hilmwarte

At the Alphasat ground station at Graz Hilmwarte tower a combination of two radiometers of type Radiometer Physics GmbH (RPG) (Atmospheric Propagation Profiler (ATPROP) and 15/90 GHz) is installed.
The Hilmwarte tower was built in 1988 by the citizens commitee of Graz. Later, Joanneum Research became in charge of the Hilmwarte tower. In 1981 the tower was refurbished and became due to the excellent local characteristics for microwave experiments the new site of a weather radar station in Graz. Further detailed information about the building and characteristics of the weather radar are provided by Randeu in [36]. Recently the weather radar was removed however, the tower is still in use for signal propagation and communication research projects. In Figure 7 an image of the radiometer setup is shown.

Figure 7: Radiometer setup at Hilmwarte tower

The radiometers are measuring sky brightness temperatures [K] and thereby give information about the status of the atmosphere. In addition, this auxiliary data is consulted for the processing of Alphasat beacon data. The elevation of the radiometer is configurable. The accuracy of the measurements is strongly dependent on the quality of the calibration of each frequency channel. Table 2 gives an overview of the radiometer dataset characteristics.

Radiometer Hilmwarte (Alphasat ground station)	
Measurement period	21.11.2013 - 21.12.2013
Frequencies	15.3, 22.24, 23.04, 23.84, 25.44, 26.24, 27.84, 31.4, 51.26, 52.28, 53.86, 54.94, 56.66, 57.3, 58, 90 [GHz]
Elevation	35.07°, 90°[degree]
Measured value	brightness temperature
Status	raw data
Unit	K
Sampling-rate	non-uniform sampling rate (1s - 5s)
Time	UTC, local time (indicated by time flag in *.BRT) [seconds since 1/2001]
File format	.BRT (binary)
Viewer software	Matlab function developed by Vinia Mattiolli,PhD on behalf of Joanneum Research

Table 2: Dataset radiometer Hilmwarte

Since fall 2013 both radiometers are operational. Especially during the Alphasat in-orbit test IOT phase, the radiometers pointed in the direction of the satellite with an elevation of 35.1° and 182.9° in azimuth. However, during the measurement period, which is considered in the database, on 3 December 2013 the elevation was changed to 90°.

4.2 Alphasat receiver

The Alphasat satellite is a European telecommunication satellite that was launched in summer 2013 in French Guyana. The purpose of this geostationary satellite is to support the network of Inmarsat satellites that provide global mobile telecommunication services. The planned operational life time of the Alphasat satellite mission is 15 years [18]. The satellite carries multiple payloads and amongst others also the TDP#5 payload. The TDP#5 payload is planned to be operational for 3 years and hosts a propagation experiment (SCIEX) for Ka and Q band. The propagation payload transmits two beacon signals at 19.701 GHz (Ka-band) and 39.402 GHz (Q-band) for research on propagation impairments in these frequency bands [40] [12].
The Alphasat receiver was developed by Joanneum Research under ESA ESTEC/Contract No. 22354/09/NL/LvH with Mr. A. Martellucci as technical officer. Joanneum Research currently operates the receiver under ESA ESTEC/Contract No. 4000102639/10/NL/CLP with Mr. J. Rivera Castro as technical officer.

The characteristics of the Alphasat receiver dataset at Graz Hilmwarte tower are listed in Table 3.

Alphasat beacon	
Measurement period	21.11.2013 - 21.12.2013
	19.3.2014 - 10.4.2014
Frequencies	19.701 [GHz]
	39.402 [GHz]
Satellite in-orbit position	25 degree East
Elevation	35.1 degree
Status	raw data
Measured value	Beacon signal power level
Unit	Watt/1 Ohm
Polarity	co-polar (CPA)
Sampling-rate	10 Hz
Time format	UTC, format: 'Y-M-D h:m:ms'
File format	ASCII (text file)

Table 3: Dataset Alphasat beacon

An image of the Alphasat ground station outdoor unit at Hilmwarte tower is illustrated in Figure 8.

Figure 8: The Alphasat receiver setup at Hilmwarte tower.

The stability of the antenna at the Alphasat ground station receiver is defined by the design principle of a fly-away-antenna. Due to slight instabilities, strong wind could induce

oscillations in the signal that are similar to scintillation effects. The Alphasat receiver is stationed at the Graz Hilmwarte Tower. Figure 9 illustrates the Alphasat ground station at Hilmwarte (marked by the green dot in the upper part of the image) and the Alphasat satellite link path. The Alphasat satellite is at a geostationary in-orbit position of 25 degrees east.

Figure 9: View of the Alphasat satellite link path from Hilmwarte tower in Graz [28]

4.3 Olympus beacon data

The Olympus beacon measurement dataset is a historic dataset that has been derived during the Olympus measurement campaign in the early 1990s. Careful measurement and data pre-processing resulted in eventpackages that represent an ideal reference for the evaluation of ITU models.

The Olympus Propagation Experimenters Group (OPEX), as reported in [5], was founded quite some time before the actual launch of the Olympus satellite took place, with the intention of defining the objectives for the Olympus propagation experiments. In the course of this action, the group decided on three coherent beacon signals for propagation experiments which are near 12 GHz, 20 GHz and 30 GHz. The beacons at 12 GHz and 30 GHz were both vertically polarized. The 20 GHz beacon switched between horizontal and vertical polarized transmission. With this alternating polarization it was possible to measure the full transmission matrix for co-polar and cross-polar signals and their relative phases.
The basic Olympus receiver terminal was equipped with a beacon receiver, a radiometer and a rain gauge. Initially, antenna tracking was not needed due to the high orbit stability

of the satellite that kept its position within a window of 0.1 degree. Later on, however, due to fuel shortage, station keeping maneuvers no longer were performed. Thus, towards the end of the satellite's lifetime, during the last year of operation, tracking became required.

Olympus is a European Space Agency (ESA) research satellite. At the ground station in Graz, Olympus was visible at an elevation angle of 24.6 degree [41]. As explained in [5], the geostationary Olympus satellite was launched on 12 June 1989 in Kourou, French Guyana. The mission was planned for a period of five years. At that time Olympus was the largest civilian telecommunication satellite. The purpose of the mission was to develop and to test new technologies for satellite communication. Amongst three other payloads, the satellite carried also a 12/20/30 GHz beacon package intended for propagation experiments. Unfortunately, during summer 1991 the control of the satellite was lost but a successful recovery action got it operational again. Due to an incident that happened on the night of the 11th August 1993 the satellite could not fully reach its nominal lifetime of five years with a planned end in early 1994. Corrective measures lead to the fact that a shortage in fuel occurred. This fact led to the decision to transfer the satellite into another orbit and switch it off [19]. Table 4 presents the characteristics of the Olympus beacon receiver dataset.

	Olympus beacon
Measurement period	1992
Frequencies	12.502 GHz
	19.77 GHz
	29.656 GHz
Satellite in-orbit position	19 degrees West
Elevation	24.6 [degree]
Measured value	Beacon signal level
Unit	[dB]
Polarity	co-polar CPA
Sampling-rate	not constant
Time format	"YYY DOY HH MM SS"
Status	pre-processed
File format	.BEA (binary)
Viewer software	Software routine developed by Joanneum Research: "SDFSHOW.EXE"

Table 4: Dataset Olympus beacon

Due to technical problems on the satellite, as described above, transmission outage occurred. In the period of 29 May 1991 until 15 August 1991, no beacon signals were received. On 10 October 1992 the 30GHz beacon tube broke and stopped the signal transmission again. Once again on the 12 August 1993 technical problems at the satellite occurred.

Known issues regarding the recorded Olympus beacon are the inconsistency of the measured parameters. From the first day of the year (doy) 1992 until the 285 (doy) all three beacons were measured but rain rates are not recorded any more. Additionally, from 286 (doy) 1992 until the end of the campaign, there is no 30 GHz beacon data available.
Moreover, because of the low sampling rate of 1 Hz, it is not possible to compute scintillation from these measurements. The ground station receiver for the Olympus beacon was stationed at the Lustbühel Observatory which is located in the east of the city of Graz as shown in Figure 4.

4.4 Radiometer measurements (Report 1985)

In the 1980s the Institute of Communications and Wave Propagation (INW) installed in cooperation with Joanneum Research three radiometers in the region of Graz for site diversity experiments as reported by Randeu et al. in [37] and [38]. The radiometers pointed in the direction 223.16 degree azimuth and 26.43 degree elevation and were equipped with a tipping-bucket rain gauge. They were aligned in this direction because it was the planned geostationary position of the Olympus satellite at 19° degrees to the west. The sky noise temperatures T_{sky} were measured and afterwards converted into attenuation A with the following formula (3):

$$A = 10 \cdot log\left(\frac{T_{med} - T_c}{T_{med} - T_{sky}}\right) \tag{3}$$

$T_{med} = 270K$ ... estimated effective medium temperature
$T_c = 4K$ ... cosmic background noise temperature

After the transformation the cumulative distribution was derived [32].

One of these radiometers was located at INW, an institute of the Graz university of technology (TUG), as previously shown in Figure 4.
The attenuation statistics over 1 year derived by this radiometer at three different frequencies is provided in the report [26] as diagram. Table 5 provides more detailed information about this dataset.

Statistics	**Frequency [GHz]**	**Epoch**
Cumulative distribution of attenuation	19.9, 11.4, 29.9	1.1.1985 - 31.12.1985

Table 5: Radiometer report (1985) [26]

4.5 Meteorological data Hilmwarte tower

A meteorological weather station is part of the Alphasat ground station at Graz Hilmwarte tower. This station provides meteorological reference data for the Alphasat receiver antenna. The measured data is especially important for the analysis and identification of

rain and wind events in Alphasat beacon and radiometer measurements. In Table 6 more information about the measurement dataset is provided.

Meteorological data Hilmwarte tower	
Measurement period	since end of October 2013
Measured values and units	time stamp [p] air pressure [hPa] temperature [Celsius] humidity [%] rain rate [mm/h] wind speed [m/s] solar radiation [W/sqm]
Sampling rate	30 seconds, hourly files
File format	.h5 HDF5
Time format	CET, UTC (format indicated by flag)

Table 6: Dataset meteorological data

4.6 Meteorological data online

The homepage of ZAMG provides hourly updated meteorological data measured by the weather station at the University of Graz. It is the nearest weather station to the Alphasat ground station at Hilmwarte (approx. 1.4 km linear distance). ZAMG is an abbreviation for the Austrian governmental meteorological service. Information about the measured parameters are provided in Table 7.

Meteorological data ZAMG	
Measurement period	21.11.2013 - 21.12.2013 19.3.2014 - 10.4.2014
Weather station	Graz University
Parameters and units	temperature [Celsius] relative humidity [%] windspeed [m/s] rain rate [mm/h] sun [%] air pressure [hPa]
Sampling-rate	1hour, daily files
Time format	CET
File format	ASCII (text file)

Table 7: Dataset meteorological data ZAMG

4.7 Disdrometer data

The 2D-Video-Distrometer (2DVD) is a 2 dimensional video disdrometer (in German: Distrometer) that is manufactured by Joanneum Research. It detects and measures rain droplets and stores data for each individual particle. From that rain drop size distributions (DSDs) may be derived by counting the number of rain droplets with the same measured equivolumetric diameter in equally-spaced size bins. Furthermore it is able to derive the rain rate from these measurements. In 2012 a disdrometer was installed in the north of Graz at half the distance between the city center and mount Schöckl. A sample of the Low Profile 2DVD disdrometer as used in 2012 is shown in Figure 10.

Figure 10: Sample Low Profile 2DVD setup

Table 8 presents more details about the parameters measured by the disdrometer.

2DVD data	
Measurement period	26.5.2012 - 26.10.2012
Measured values and units	time stamp [15 seconds interval] rain rate [mm/h] rain drop size distribution (number of detected droplets per size bin)
Sampling-rate	every rain droplet is recorded by the disdrometer, data gets pre-processed to 15 second intervals
Time format	UTC
File format	ASCII (*.dbl file)
Viewer software	Viewer software developed by Joanneum Research

Table 8: Dataset disdrometer data

5 Description of ITU-R models and model selection

This chapter describes selection criteria for the ITU-R propagation models. Additionally, it illustrates the existing dependencies between the models, where in absence of measurement data, some input parameters can be derived by means of other models. A step-by-step description of each chosen model is provided as well. Please note that the derivations and underlying theories of these ITU-R models are not covered in this chapter because it would go beyond the scope of this thesis.

5.1 Model selection criteria

The selection of the ITU-R models for evaluation is based on the criteria defined by the available measurement database. Thus, models were chosen that simulate tropospheric phenomenons on a fixed satellite link. Additionally this selection is restricted to a frequency range between approximately 10 GHz and 40 GHz. Finally 10 ITU-R models were chosen that cover the modelling of specific attenuations, brightness temperature and second order statistics of a satellite link. In the following part of this chapter these models are described in further detail.

5.2 Description of selected ITU-R models

In the following sections the selected ITU-R models for evaluation are introduced. The idea and the step-by-step procedures are described in further detail. Some of the following models have dependencies on models presented in other ITU-R recommendations. In order to get an overview of dependencies between the models these relations are graphically visualized in Figure 11.

5.2.1 Noise from atmospheric gases

Recommendation ITU-R P.372-11 Radio noise [48] contains models for different sources of radio noise in the frequency range between 0.1 Hz to 100 GHz. In section 4 with the title "Noise from atmospheric gases and the Earth's atmosphere" a model for the prediction of the brightness temperature due to different sources is introduced. For the context of this thesis the sky noise caused by atmospheric gases, which are mainly oxygen and water vapour, is of special interest. Figure 4 and 5 in this recommendation [48] display simulated brightness temperature reference values versus frequency. These charts are calculated for an average atmosphere and cover a frequency range from 1 GHz to 340 GHz, respectively 1 GHz to 60 GHz. Moreover, both charts provide the brightness temperatures for different elevation angles at 0, 5, 10, 20, 30, 60 and 90 degrees. The average atmosphere is defined

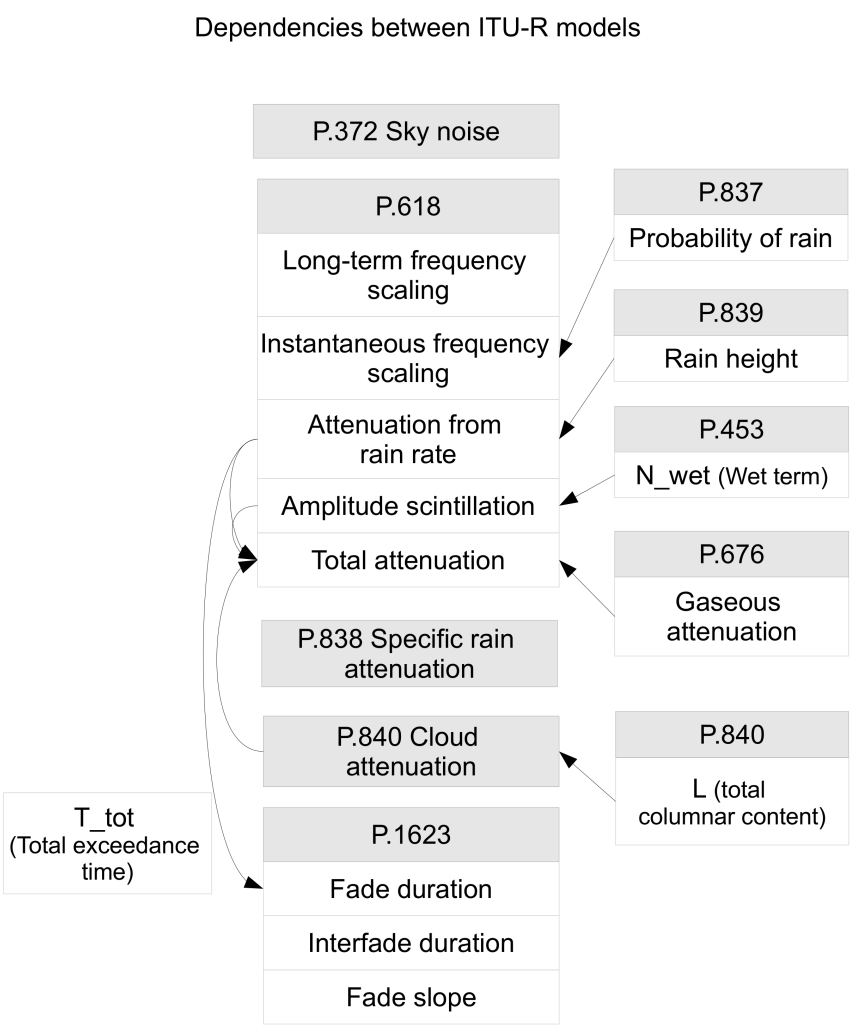

Figure 11: Dependencies between selected ITU-R models

with 7.5 $\frac{g}{m^3}$ water vapor density with a scale height of 2 km for water vapor, 15° Celsius surface temperature and an air pressure of 102 3 hPa [48].

5.2.2 Long-term frequency scaling of rain attenuation statistics

The frequency scaling of rain attenuation is a topic which is part of ITU recommendation P.618-10 with the title "Propagation data and prediction methods required for the design of Earth-space telecommunication systems" [49]. It is a comprehensive recommendation that treats especially topics like propagation loss but also noise temperature, depolarization effects, propagation delay, bandwidth limitations, angle of arrival as well as the statistics for non-GSO paths in detail. Therefore, this recommendation is one of the most important recommendations for the design of Earth-space systems. In chapter 2.2.1.2.2 this recommendation [49] presents a model for frequency scaling of rain attenuation statistics. The model is restricted to excess attenuation at frequencies between 7 GHz to 55 GHz. It enables to compute, for known attenuations A_1 at frequency f_1, the attenuations A_2 at frequency f_2 with the same probability of exceedance at both frequencies. Frequency f_1 usually represents the lower downlink frequency and frequency f_2 is the higher frequency which is the uplink. The attenuation ratio is calculated by the following eqs. (4)

to (6).

$$A_2 = A_1 \left(\frac{\varphi_2}{\varphi_1} \right)^{1-H(\varphi_1,\varphi_2,A_1)} \tag{4}$$

$$\varphi(f) = \frac{f^2}{1 + 10^{-4} \cdot f^2} \tag{5}$$

$$H(\varphi_1, \varphi_2, A_1) = 1.12 \cdot 10^{-3} \left(\frac{\varphi_2}{\varphi_1} \right)^{0.5} (\varphi_1 A_1)^{0.55} \tag{6}$$

If available, measured attenuation statistic instead of attenuation derived from rain rate is preferred for this long-term frequency scaling model [49].

5.2.3 Conditional distribution of the frequency scaling ratio of rain attenuation

This model is focused on instantaneous frequency scaling of rain attenuation and since the last revision in September 2013, it is also a content of the recommendation ITU-R P.618 [49] in chapter 2.2.1.2.1 . The difference compared to the long-term frequency scaling model before, is the fact that this model is based on the knowledge of the cumulative distribution of rain attenuation at the two frequencies $f1$ and $f2$ of interest. Here, it is again assumed that the frequency $f1$ is the lower one, which is the down link, and the frequency $f2$, where the attenuation a_2 $[dB]$ should be derived, is the uplink at a higher frequency. This method enables the prediction of the attenuation at $f2$ conditioned on the measured instantaneous attenuation level at $f1$ for a probability P [%] that the predicted attenuation value will be exceeded. The model is recommended for frequencies between 19 GHz to 55 GHz. Moreover, the model is also applicable for total attenuation, but its accuracy has not been fully evaluated by the ITU yet. In the following, the step-by-step procedure of this model is described.

In the first step, the probability of rain P_{rain} for the measurement site has to be determined. If necessary, this probability can be estimated by the ITU-R recommendation P.837 [45] that determines the probability at the indicated location from values of a numerical world map.

Step 2 describes the generation of pairs for both frequencies that indicate the probability P_i that a certain attenuation A_i is exceeded. However, only probabilities lower than the determined probability of rain and according attenuation values should be considered. $[P_i, A_{i,1}], [P_i, A_{i,2}]$ where $P_i \leq P_{rain}$.

In the next step the probabilities of exceedance need to be divided by the rain probability to get conditional rain attenuation probabilities: $p_i = \frac{P_i}{P_{rain}}$.

The following transformation of the pairs needs to be performed in step 4:
$[p_i, A_{i,1}]$ *to* $[Q^{-1}(p_i), lnA_{i,1}]$ and $[p_i, A_{i,2}]$ *to* $[Q^{-1}(p_i), lnA_{i,2}]$ where Q-function, as defined in ITU-R P.1057 [46], denotes the normal complementary cumulative probability integral.

In step 5 the values of mean μ and standard deviation σ for each of both pairs are determined by the least-square fit method:

$$lnA_{i,1} = \sigma_1 Q^{-1}(p_i) + \mu_1, \quad lnA_{i,2} = \sigma_2 Q^{-1}(p_i) + \mu_2$$

A more detailed description of the step-by-step procedure of this transformation is provided in the ITU recommendation P.1057 [46].

Step 6 computes the dependency factor ξ by the following equation (7).

$$\xi = 0.19 \left[\frac{f2}{f1} - 1 \right]^{0.57} \tag{7}$$

The conditional mean $\mu_{2/1}$ and standard deviation $\sigma_{2/1}$ are derived by the eqs. (8) to (9).

$$\mu_{2/1} = \frac{\sigma_2}{\sigma_1} \sqrt{1 - \xi^2}\, ln(a_1) + \left(\mu_2 - \frac{\sigma_2 \mu_1}{\sigma_1} \sqrt{1 - \xi^2} \right) \tag{8}$$

$$\sigma_{2/1} = \sigma_2 \xi \tag{9}$$

The complementary cumulative distribution that indicated the probability that the attenuation at f2 is exceeded on the condition that the attenuation at frequency f1 is $a1[dB]$ can be computed by the following equation (10).

$$P(A_2 > a_2 | A_1 = a_1) = Q\left(\frac{ln(a_2) - \mu_{2/1}}{\sigma_{2/1}} \right) \tag{10}$$

The attenuation a_2 at frequency $f2$ for a probability $P[\%]$ of interest can be derived by equation (11).

$$a_2 = exp\left(\sigma_{2/1} Q^{-1}(P) + \mu_{2/1} \right) \tag{11}$$

As a result, this model provides the complementary cumulative distribution function for the uplink which is conditioned on the information about the attenuation level provided by the downlink. Finally it has to be mentioned that the accuracy of this model is not fully determined yet due to its novelty [49].

5.2.4 Amplitude scintillation statistics

A model to predict monthly and long-term scintillation statistics is also part of the recommendation ITU-R P.618 [49]. There, in chapter 2.4.1 a technique to calculate scintillation statistics for elevation angles greater than 5 degrees is described. The model is applicable for frequencies up to at least 20 GHz. The scintillation strongly depends on the climate of the area where the ground station is located and additionally shows variations within the year. As many other ITU-R models, also this model shows some dependencies on parameters provided by other models.
The model consists of nine steps. In the first two steps the wet term N_{wet} of the radio refractivity, if not available, can be derived from a global numerical map provided by the recommendation ITU-R P.453 [44].

In step 3 the reference standard deviation σ_{ref} of the signal has to be computed.

$$\sigma_{ref} = 3.6 \cdot 10^{-3} + 10^{-4} \cdot N_{wet} \tag{12}$$

In the steps 4 and 5 the path length L as well as the effective antenna parameter D_{eff} need to be determined.

$$L = \frac{2h_L}{\sqrt{sin^2\Theta + 2.35 \cdot 10^{-4}} + sin\Theta} \tag{13}$$

$$D_{eff} = \sqrt{\eta} D \tag{14}$$

where $\Theta \geq 5°$ denotes the free-space elevation angle, $h_L = 1000m$ which is the height of the turbulen layer and η is the antenna efficiency which can be assumed with 0.5 if the actual value is unknown.
In step 6 the antenna averaging factor $g(x)$ is determined:

$$g(x) = \sqrt{3.86(x^2+1)^{\frac{11}{12}} \cdot sin\left(\frac{11}{6} tan^{-1}\frac{1}{x}\right) - 7.08 \cdot x^{\frac{5}{6}}} \tag{15}$$

where:

$$x = 1.22 D_{eff}^2 (\frac{f}{L}) \tag{16}$$

For values of $x \geq 7.0$ the square root is negative and thus the scintillation fade depth is zero for any time percentage and the computation can be aborted at this step.
In step 7 the standard deviation σ of the signal depending on the period and propagation path of interest has to be calculated.

$$\sigma = \sigma_{ref} f^{\frac{7}{12}} \frac{g(x)}{(sin\Theta)^{1.2}} \tag{17}$$

Step 8 determines the percentage factor a(p), where the time percentage p is $0.01\% < p \leq 50\%$.

$$a(p) = -0.061(log_{10}p)^3 + 0.072(log_{10}p)^2 - 1.71 log_{10}p + 3.0 \tag{18}$$

And step 9 finally calculates the attenuation A due to scintillation $[dB]$ for the indicated time percentage $p[\%]$.

$$A(p) = a(p) \cdot \sigma \tag{19}$$

5.2.5 Total attenuation

The model for the prediction of total attenuation statistics is also available in the ITU-R P.618 [49] in section 2.5. This model is especially recommended for frequencies above 18 GHz or very low operation angles because they are affected most by the sum of atmospheric attenuation by multiple sources. Due to the fact that atmospheric attenuation includes attenuation by gases, rain attenuation, attenuation by clouds and scintillation, this model is dependent on a number of other ITU-R prediction models which are: rain attenuation described in [49] section 2.2.1.1, cloud attenuation model in recommendation [51], gaseous attenuation presented in [50] and attenuation due to tropospheric scintillation explained

in [49] chapter 2.4.1.
All mentioned intermediate results are calculated for the probability that the attenuation was exceeded in the range between 0.01% to 50%. In case no meteorological data for gaseous attenuation is available at the defined percentage, the mean value should be calculated and used for the model instead.
The total attenuation can then be calculated with the following formula (20):

$$A_T(p) = A_G(p) + \sqrt{(A_R(p) + A_C(p))^2 + A_S^2(p)} \tag{20}$$

where:

$$A_C(p) = A_C(1\%) \quad for\ p < 1.0\% \tag{21}$$

$$A_G(p) = A_G(1\%) \quad for\ p < 1.0\% \tag{22}$$

here, A_T denotes total attenuation [dB], A_G is gaseous attenuation [dB], A_R denotes rain attenuation [dB], A_C cloud attenuation and A_S is attenuation [dB] due to scintillation for a percentage p of interest.
For percentages below 1%, two correction terms Ac and Ag as shown above have to be used. They consider the part of attenuation caused by gases and clouds that is already included in the rain attenuation term. The recommendation additionally states that when compared to real measurements significant variances in the root mean square (r.m.s.) error have been observed [49].

5.2.6 Specific attenuation due to rain

The topic of specific attenuation due to rain is covered by ITU-R recommendation P.838-3 [43]. With this prediction method it is possible to calculate the specific attenuation from measured rain rates. The model is recommended for frequencies in the range of 1 GHz to 1000 GHz. As the formula (23) indicates, the specific rain attenuation γ_R [dB/km] follows a power-law relationship.

$$\gamma_R = kR^\alpha \tag{23}$$

where R denotes the rain rate in [mm/h].

The parameters k and α are frequency dependent and can be derived as follows. a,b,c and m are constants and can be derived from the Tables 1-4 provided by the ITU-R recommendation [43].

$$log_{10}k = \sum_{j=1}^{4} a_j exp\left[-\left(\frac{log_{10}f - b_j}{c_j}\right)^2\right] + m_k log_{10}f + c_k \tag{24}$$

$$\alpha = \sum_{j=1}^{5} a_j exp\left[-\left(\frac{log_{10}f - b_j}{c_j}\right)^2\right] + m_\alpha log_{10}f + c_\alpha \tag{25}$$

where:

f: frequency [GHz]
k: either k_H or k_v
α: either α_H or α_v

Once k and *alpha* have been derived for horizontal and vertical polarization, the coefficients for the equation (23) can be derived from equation (26) and equation(27).

$$k = \frac{[k_H + k_v + (k_H - k_v)cos^2\Theta cos2\tau]}{2} \tag{26}$$

$$\alpha = \frac{[k_H\alpha_H + k_v\alpha_v + (k_H\alpha_H - k_v\alpha_v)cos^2\Theta cos2\tau]}{2k} \tag{27}$$

here, Θ denotes the elevation angle and τ the polarization tilt angle that is measured relative to the horizontal plane. For circular polarization τ has to be indicated with 45°.

5.2.7 Attenuation due to clouds

The prediction method for attenuation due to clouds is part of the ITU-R recommendation P.840-6 [51]. The formula (28) to determine the cloud attenuation is described in section 3 of this recommendation. The model is restricted to elevation angles Θ between 5°and 90°. Also this model is dependent on the specific attenuation coefficient that can be calculated as described below. A required input parameter is the columnar content of cloud liquid water L_{red}. The model recommends deriving this value either from radiometric measurements or from radiosondes. If no measurement data is available, the 'total columnar content of cloud liquid water' parameter can be interpolated for the location of interest from a numerical wold map that is also provided by this recommendation [51].

$$A = \frac{L_{red}\, K_l}{sin\Theta} \tag{28}$$

Here, K_l denotes the specific attenuation coefficient. This coefficient can be computed for $0°C$ water temperature by the following set of equations.

$$K_l = \frac{0.819f}{\epsilon''(1+\eta^2)} \tag{29}$$

The parameter f is the frequency in [GHz] and is valid for this model in a range up to 1000 GHz. The parameter η can be derived as follows:

$$\eta = \frac{2+\epsilon'}{\epsilon''} \tag{30}$$

The parameters $\epsilon(f)$ represents the dielectric perimittivity of water. Its derivations are:

$$\epsilon''(f) = \frac{f(\epsilon_0 - \epsilon_1)}{f_p\left[1 + \left(\frac{f}{f_p}\right)^2\right]} + \frac{f(\epsilon_1 - \epsilon_2)}{f_s\left[1 + \left(\frac{f}{f_s}\right)^2\right]} \tag{31}$$

$$\epsilon'(f) = \frac{(\epsilon_0 - \epsilon_1)}{\left[1 + \left(\frac{f}{f_p}\right)^2\right]} + \frac{(\epsilon_1 - \epsilon_2)}{\left[1 + \left(\frac{f}{f_s}\right)^2\right]} + \epsilon_2 \tag{32}$$

where the parameters ϵ_0, ϵ_1, ϵ_2 and θ are defined as:

$\epsilon_0 = 77.66 + 103.3(\theta - 1)$
$\epsilon_1 = 0.0671\epsilon_0$, $\epsilon_2 = 3.52$, $\theta = 300/T$

where T is the temperature that is indicated in Kelvin [K]. As it is recommended in [51], a temperature of $0°C$ which corresponds to 273.15 Kelvin should be used for cloud attenuation.
The parameters f_p and f_s are the principal and secondary relaxation frequency. These frequencies can be computed by equations 33 and 34 as follows:

$$f_p = 20.20 - 146(\theta - 1) + 316(\theta - 1)^2 \tag{33}$$

$$f_s = 39.8\, f_p \tag{34}$$

5.2.8 Fade duration statistics

Fade duration can be estimated by the model presented in the ITU-R recommendation P.1623 [42]. This recommendation focuses on the analysis and statistics of outage events in order to improve quality of service. Moreover, fade duration is also important for the choice of the forward error correction codes and coding schemes in satellite communication. The fade duration prediction model which is described in chapter 2.2 of this recommendation determines the fade duration statistics for fades caused by attenuation effects as well as scintillation that happen on the Earth-space path. The occurrence of fade duration can be described by two cumulative distribution functions that is why the prediction model is structured in two parts. The first distribution function is $P(d > D|a > A)$ the probability of fades with a duration longer than $D[s]$ for a predefined attenuation threshold $A[dB]$. The second one is the cumulative probability of exceedance $F(d > D|a > A)$ that indicates the total fraction of determined fade durations d longer than D, again for a defined attenuation threshold A.
The model is recommended for frequencies between 10 GHz to 50 GHz and elevation angles in the range of 5° to 60° degrees. Moreover, fade durations shorter than 1 second are not taken into account by the model because they are not expected to contribute significantly to outage events. The prediction model for fade duration distribution consists, as described in [42], of the following nine steps. Furthermore, there it is stated that the fraction of fading time by long duration fades that exceed a certain attenuation threshold, follows a log-normal distribution.
In step 1 its mean duration D_0 of the log-normal distributed fraction of long fades needs to be determined with:

$$D_0 = 80\varphi^{-0.4} f^{1.4} A^{-0.39} \tag{35}$$

where the parameter φ denotes the elevation angle, f the frequency [GHz] and A the attenuation threshold [dB].
Step 2 determines the standard deviation of the log-normal distribution for the fraction of fading time that is caused by long duration fades.

$$\sigma = 1.85 f^{-0.05} A^{-0.027} \tag{36}$$

In step 3 the exponent γ for the power-law distribution is computed for the fraction of fading time that is caused by fades of short duration.

$$\gamma = 0.055 f^{0.65} A^{-0.003} \tag{37}$$

In step 4 the boundary D_t between long and short fades is determined.

$$D_t = D_0 e^{p_1 \sigma^2 + p_2 \sigma - 0.39} \tag{38}$$

where p_1 and p_2 are determined as follows:

$$p_1 = 0.885\gamma - 0.814 \tag{39}$$

$$p_2 = -1.05\gamma^2 + 2.23\gamma - 1.61 \tag{40}$$

The mean duration of the log-normal distribution of the probability of occurrence of long fade duration $D2$ is calculated in step 5.

$$D_2 = D_0 \cdot e^{-\sigma^2} \tag{41}$$

In step 6 the share in total fade duration caused by fades of duration less than the threshold Dt is computed.

$$k = 1 + \left[\frac{\sqrt{D_0 D_1}(1-\gamma) Q\left(\frac{ln(D_t) - ln(D_0)}{\sigma}\right)}{D_t \gamma Q\left(\frac{ln(D_t) - ln(D_2)}{\sigma}\right)} \right]^{-1} \tag{42}$$

where Q is the standard cumulative distribution function for a normal distributed variable and is defined as follows.

$$Q(x) = \frac{1}{\sqrt{2\pi}} \int_z^\infty e^{-\frac{x^2}{2}} dx \tag{43}$$

In the next steps 7 and 8 the occurrence probability P and the exceedance probability F are determined. Both distribution functions have different calculation schemes for fades of short duration and fades of long duration.

Computation of the occurrence probability P:

$$For 1 \le D \le D1 \quad P(d > D | a > A) = D^{-\gamma} \tag{44}$$

$$For D > D_t \quad P(d > D | a > A) = D_t^{-\gamma} \cdot \frac{Q\left(\frac{ln(D) - ln(D2)}{\sigma}\right)}{Q\left(\frac{ln(D_t) - ln(D_2)}{\sigma}\right)} \tag{45}$$

Computation of the exceedance probability F:

$$For 1 \leq D \leq D1 \quad F(d > D|a > A) = 1 \left[1 - k \left(\frac{D}{D_t} \right)^{(1-\gamma)} \right] \tag{46}$$

$$For D > D_t \quad F(d > D|a > A) = (1 - k) \cdot \frac{Q\left(\frac{ln(D)-ln(D_0)}{\sigma}\right)}{Q\left(\frac{ln(D_t)-ln(D_0}{\sigma}\right)} \tag{47}$$

The recommendation also indicates that during the tests of this model, quite large natural variations of the standard deviation parameter were identified [42].

5.2.9 Interfade duration statistics

Apart from fade duration also interfade duration plays an important role for the quality of service and is thus also mentioned in the ITU-R recommendation P.1623 [42] in section 2.3. The interfade duration provides information about the time between consecutive fades. The recommendation does not provide a step-by-step model for interfade duration but states that interfade duration statistics follow a log-normal distribution. Short interfade duration statistics however, which are due to tropospheric scintillation are assumed to follow a power-law distribution [42].

5.2.10 Fade slope statistics

This prediction method is concerned with fade slope statistics and is part of the recommendation ITU-R P.1623 [42] as well. The analysis of fade slopes in the signal is crucial for systems that provide fade mitigation techniques that take measures to lower the impacts of fades on the communication link. To analyze the slope of a fade, the signal has to be filtered beforehand in order to eliminate the rapid variations. For this purpose the model recommends a low pass filter with a 3 dB cut-off frequency of 0.02 Hz. Another important factor to consider is that the fade slope parameter is highly sensitive to climate and changes in meteorological parameters.
The presented model is applicable for frequencies from 10 GHz to 30 GHz and elevation angles between 10° to 50° degrees. Furthermore, it specifies limits for the attenuation level A between 0 dB and 20 dB, the 3 dB cut-off frequency of the low pass filter to be in the range of 0.001 Hz to 1 Hz. This model deals with sampling intervals Δt between 2 and 200 seconds to compute fade slope statistics.

The fade slope at time t $\zeta(t)$ is calculated from the low pass filtered data as indicated in equation (48) below:

$$\zeta(t) = \frac{A\left(t + \frac{1}{2}\Delta t\right) - A\left(t - \frac{1}{2}\Delta t\right)}{\Delta t} \tag{48}$$

There are 3 steps needed to calculate the fade slope distribution. In step 1 the dependency on the chosen time interval at the cut-off frequency of the low pass filter f_B is determined by the function F where the parameter b = 2.3.

$$F(f_B, \Delta t) = \sqrt{\frac{2\pi^2}{\left(\frac{1}{f_B^b} + (2\Delta t)^b\right)^{\frac{1}{b}}}} \tag{49}$$

Step 2 calculates the standard deviation of the conditional fade slope σ_ζ, where the parameter s = 0.01.

$$\sigma_\zeta = sF(f_B, \Delta t)A \tag{50}$$

With these parameters the conditional probability can be determined in step 3. The conditional probability that the fade slope is equal to the fade slope for a given attenuation threshold can be computed with formula (51):

$$p(\zeta|A) = \frac{2}{\pi\sigma_\zeta \left(1 + \left(\frac{\zeta}{\sigma_\zeta}\right)^2\right)^2} \tag{51}$$

By the following equation (52) the probability for the exceedance of an absolute fade slope value can be computed:

$$P(|\zeta||A) = 1 - \frac{2\left(\frac{|\zeta|}{\sigma_\zeta}\right)}{\pi\left(1 + \left(\frac{|\zeta|}{\sigma_\zeta}\right)^2\right)} - \frac{2\,arctan\left(\frac{|\zeta|}{\sigma_\zeta}\right)}{\pi} \tag{52}$$

6 Task description

This thesis focusses on propagation effects on fixed satellite links. To design satellite links the ITU provides models to simulate single effects that occur during the transmission of electromagnetic waves from the satellite to the ground station and vice versa. Based on the requirements defined by the reference database, available ITU models that provide methods to simulate these propagation parameters, respectively their statistics, were selected as described in detail in the previous chapter 5. As a result of this investigation, 10 model evaluation tasks have been defined. In this chapter these identified tasks are introduced in more detail.

These 10 tasks are structured as follows:
Task 1 describes the evaluation of the modelled brightness temperature characteristic presented in the ITU-R P.372 [48] with measured brightness temperatures at different frequency channels by a radiometer. In Task 2 and Task 3 two frequency scaling models as recommended in the ITU-R P.618 [49] are evaluated. Task 4 evaluates the ITU scintillation statistic model presented in [49] with Alphasat beacon measurements. Task 5 is concerned with total attenuation and Task 6 evaluates the results of the ITU specific rain attenuation model. In Task 7 the ITU model for attenuation due to clouds is compared with Alphasat beacon and radiometer data. Task 8 to Task 10 evaluate fade characteristic models provided by ITU-R P.1623 [42] such as fade duration, interfade duration and fade slope statistics.

Table 9 provides an overview of all tasks. The column 'Description' in this table gives keywords that link the description of the used dataset to the ITU prediction model used for the individual evaluation task.

Task	Name	Description	ITU model	Model description	Data basis
1	Sky noise	Sky noise	P.372-10 4 Noise from atmospheric gases and the Earth's surface	Chap.5.2.1	Radiometer Hilmwarte measurements
2	Long-term frequency scaling	Radiometer report ↔ long-term frequency scaling	P.618-11 2.2.1.2.2 Long-term frequency scaling of rain attenuation statistics	Chapter 5.2.2	Atmospheric attenuation charts (Radiometer report 1985)
3	Instantaneous conditional frequency scaling	Olympus beacon ↔ instantaneous frequency scaling	P.618-11 2.2.1.2.1 conditional distribution of the frequency scaling ratio of rain attenuation	Chapter 5.2.3	Olympus beacon
4	Amplitude scintillation statistics	Alphasat beacon ↔ scintillation statistics	P.618-10 2.4.1 Calculation of monthly and long-term statistics of amplitude scintillation at elevation angles greater than 4°	Chap.5.2.4	Alphasat beacon
5	Total attenuation statistics	Radiometer report ↔ total attenuation statistics	P.618-10 2.5 Estimation of total attenuation due to multiple sources of simultaneously occurring atmospheric attenuation	Chapter 5.2.5	Atmospheric attenuation charts (Radiometer report 1985)
6	Specific attenuation from rain rate	Drop size distribution ↔ specific attenuation due to rain	P.838-3 Specific attenuation model for rain for use in prediction methods	Chapter 5.2.6	2DVD

Task	Name	Description	ITU model	Model description	Data basis
7	Attenuation due to clouds	Brightness temperature + Alphasat beacon ↔ attenuation due to clouds	P.840 3 Cloud attenuation	Chapter 5.2.7	Radiometer measurements + Alphasat beacon
8	Fade duration statistics	Olympus beacon ↔ fade duration statistics	P. 1623 2.2 Fade duration prediction method	Chapter 5.2.8	Olympus beacon, Alphasat beacon
9	Interfade duration	Olympus beacon ↔ interfade duration statistics	P.1623 2.3 Interfade duration	Chapter 5.2.9	Olympus beacon, Alphasat beacon
10	Fade slope statistics	Olympus beacon ↔ fade slope statistics	P.1623 3.2 Fade slope prediction method	Chapter 5.2.10	Olympus beacon

Table 9: Overview of defined tasks for model evaluation

6.1 Task 1 - Sky noise

The radiometer is an instrument that is able to measure the received thermal energy in form of sky brightness temperature respectively sky noise temperature. In the COST action IC0802 handbook [1] the relevance of radiometers for signal propagation studies is explained in more detail. This measured parameter is related to atmospheric attenuation and thus the radiometer is an important instrument to accurately measure tropospheric attenuations, especially at low attenuation values. For signal propagation analysis especially its ability to determine clear sky attenuation is of high interest. Whereby the attenuation at clear sky is induced by atmospheric gases in the atmosphere which are hydrogen and oxygen.
Thus, especially for beacon receivers the radiometer is of great value to determine the total attenuation. A chart of the sky brightness temperatures provided by the recommendation ITU-R P.372 [48] is presented in Figure 12. It was calculated for a standard atmosphere at clear sky and for a wide frequency range. In order to evaluate these reference values provided by the ITU, radiometer measurements recorded in the course of the Alphasat satellite campaign will be compared with the values presented by the model.

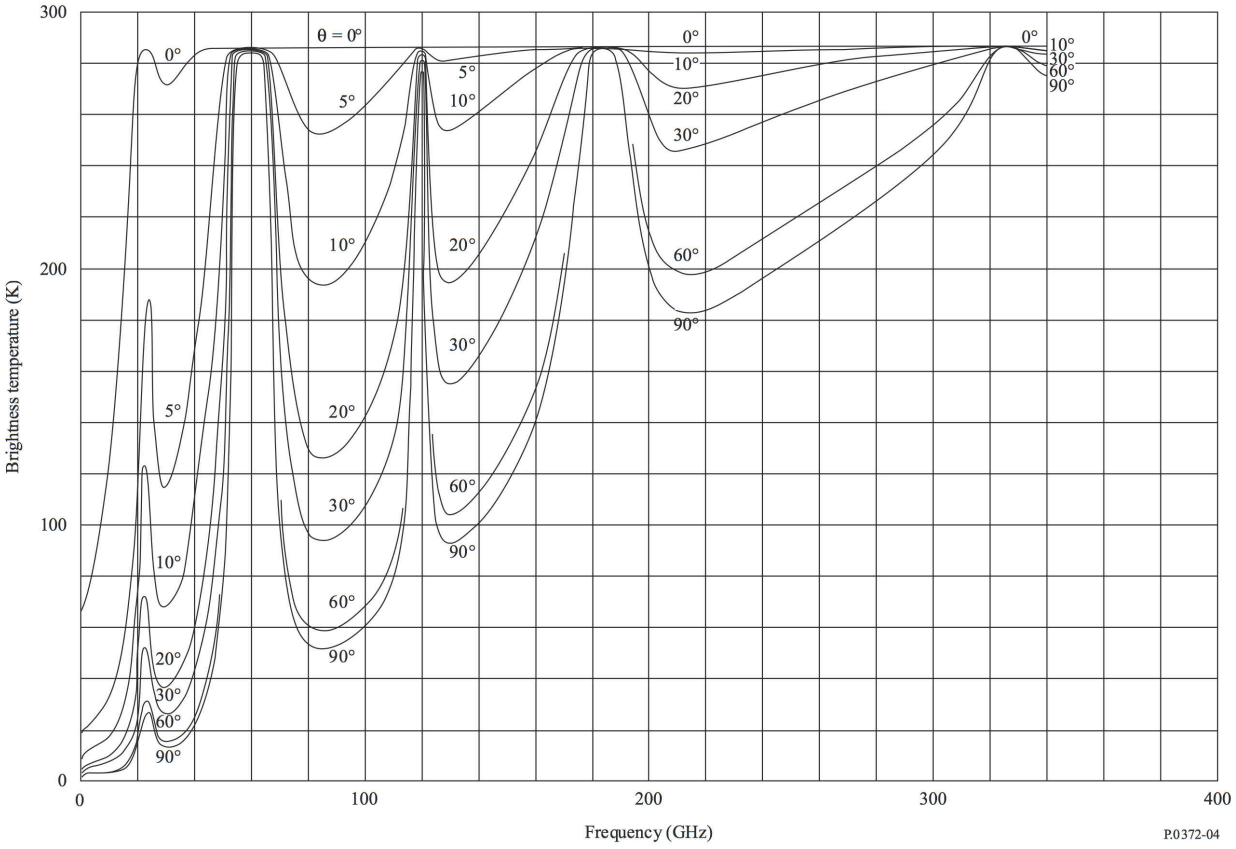

Figure 12: Characteristic of sky brightness temperatures with respect to frequency [48]

6.2 Task 2 - Long-term frequency scaling

Another interesting factor for the design of satellite links is the frequency scaling. At frequency scaling the attenuation at a higher frequency channel is related to the attenuation observed at a lower frequency channel. In order to do so, the ITU-R recommendation P.618 [49] presents two different methods. The long-term frequency scaling method is described by the recommendation in chapter 2.2.1.2.2 and is the topic of this task. The instantaneous frequency scaling method will be evaluated in Task 3 presented in the next section. The statistical frequency scaling method determines, for an attenuation at a certain level of probability, the attenuation at the second frequency that occurs with the same probability. To evaluate this method, attenuation statistics derived from radiometer measurements are used.

6.3 Task 3 - Conditional instantaneous frequency scaling

In this task the instantaneous conditional frequency scaling method as presented by the ITU-R recommendation P.618 [49] in chapter 2.2.1.2.1 is evaluated. This method is based on cumulative distributions of rain attenuation characteristics of both frequency channels. Nevertheless this method acts as an instantaneous frequency scaling compared to the method discussed in task 2. This model is evaluated by measured Olympus attenuation data at 12 GHz scaled to 20 GHz channel and 20 GHz scaled to 30 GHz channel. As input for the model the attenuation statistics for both channels and the rain probability for the station in Graz has to be determined.

6.4 Task 4 - Scintillation

The phenomenon of scintillation occurs in the troposphere and in the ionosphere. Ionospheric scintillation however is not relevant for the frequency range of interest in this context. The effect of tropospheric scintillation contributes to the total attenuation of a signal [49]. The reason why this effect occurs and what impact it causes on the signal is discussed in chapter 3. Figure 13 exemplarily illustrates how the scintillation effect superposes the signal and its low frequent component during transmission. In this task the ITU-R model for the prediction of attenuation statistic due to tropospheric scintillation presented in recommendation P.618 [49] is evaluated by scintillation statistics derived from beacon data measured in the course of the Alphasat campaign. To perform the evaluation the scintillation has to be extracted from the received Alphasat beacon data as shown in Figure 13 and afterwards the statistic has to be computed from the specific attenuation due to scintillation which is visible in Figure 13 c.

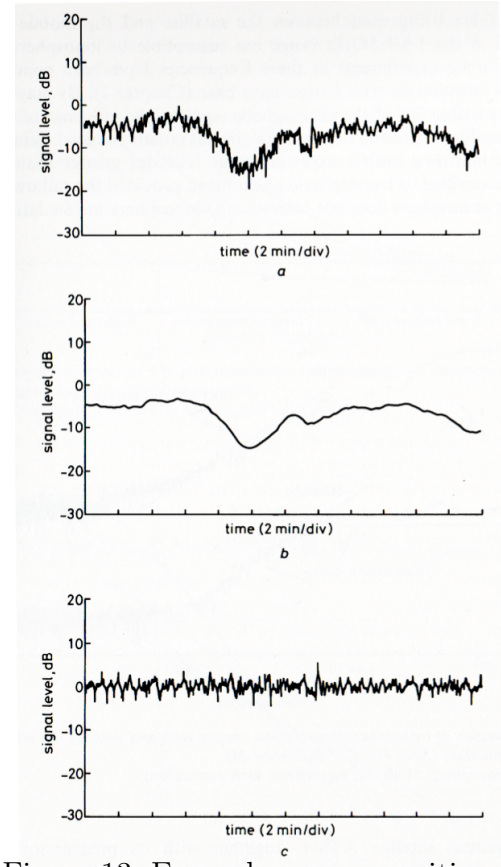

Figure 13: Exemplary superposition of scintillation on a signal [3]

6.5 Task 5 - Total attenuation

The statistics of total attenuation are of course fundamental information for the design of a satellite link. As indicated in ITU-R P.618 [49] the propagation parameter of total attenuation is composed of individual attenuations. The attenuations due to rain, clouds, atmospheric gases and scintillation contribute to the total amount of attenuation. To evaluate the results derived by the ITU model the data are compared with total attenuation statistics derived from radiometer measurements.

6.6 Task 6 - Specific rain attenuation

As already mentioned, the specific attenuation due to rain contributes most to the parameter of total attenuation. The specific attenuation due to rain can be calculated, based on known rain rates as it is described in the model provided by the recommendation ITU-R P.838 [43]. To evaluate the model, rain rates and rain drop size distributions measured by a disdrometer are used. The necessary scattering amplitudes are calculated by a software developed by Joanneum Research and ESA. Once the distribution and the scattering amplitudes for the frequency and elevation of interest are determined, the specific rain attenuation can be calculated.

6.7 Task 7 - Cloud attenuation

The focus of this task is the specific attenuation due to clouds. Of course this individual attenuation also contributes to the computation of total attenuation. In the ITU-R P.840 [51] a model is presented to simulate this attenuation. The evaluation of this model is performed based on beacon attenuations from the Alphasat campaign and brightness temperatures measured by the radiometer. Cloud attenuation can be derived from measurements by considering the attenuation at clear sky and the exclusion of rain events and of scintillation.

6.8 Task 8 - Fade duration

This task is concerned with the topic of fade duration. In Figure 14 the principle of fade duration together with interfade duration and fade slope, which are content of the following tasks, are illustrated. A fade is defined as the event that begins at the moment the signal crosses a certain attenuation threshold until the attenuation value is below the threshold again. Thus, the fade duration denotes the time between both level crossings. The analysis of fade duration is interesting regarding the prediction of expected outage events and their duration. The ITU recommendation P.1623 [42] provides a model to simulate the fade duration distribution for a given setting. The evaluation of this model is accomplished by the comparison with fade statistics of the Olympus beacon data set. In the course of the evaluation different attenuation thresholds and fade durations are be analyzed. For comparison with the ITU model, the probability of occurrence for different

fade durations and attenuation thresholds as well as the probability of exceedance are computed.

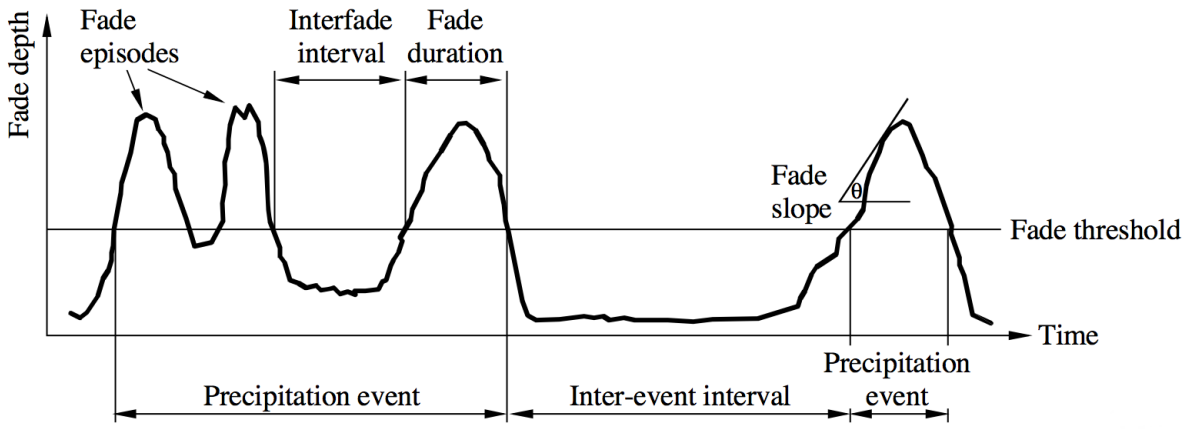

Figure 14: Characteristic of fade events [42]

6.9 Task 9 - Interfade duration

Besides fade duration also the time between fade events, which is called interfade duration, is of interest. The interfade duration thus indicates the time until the next fade event. This information is of great value for an operator because the interfade duration indicated the time until the next potential communication outage event occurs. This evaluation process is also executed with the statistics derived from the Olympus beacon data.
The ITU-R recommendation [42] unfortunately does not provide an interfade duration model. However, it is stated that the statistic of interfade duration events follows a log-normal distribution.

6.10 Task 10 - Fade slope

Not only the duration but also the slope of such a fade event is crucial. The so-called fade slope statistic is another important parameter for the prediction and analysis of potential outage events. As its two predecessors, also the fade slope prediction model is presented in the ITU-R P.1623 [42]. As for both methods before, also the fade slope model is evaluated by fade slope statistics derived from beacon data measured during the Olympus satellite campaign.

7 Implementation of models and data processing routines

In this chapter the implementation of the selected ITU models as well as the data analysis routines for the pre-processing and processing of the measurement datasets are described in further detail.

7.1 ITU models

The ITU algorithms have been implemented as MATLAB routines. The input and output variables together with their units have been well defined in the function header to ensure easy usability. A sample of a function header is shown in Figure 15. The code is commented to allow potential maintenance and to keep the code expandable, if needed.

```
%--------------------------------------------------------------------------
% File:     P838_SpecificAttenuationFromRain.m
% Purpose:  Method to model the specific attenuation from rain rate
% Language: Matlab 7.5.0(R2007b)
% Author:   Karin Plimon
% History:
% Version |    Date    |     Name     | Change history
%   v1.0  | 23/09/2013 |    Plimon    | First version
%   v2.0  | 03/11/2013 |    Plimon    | Second version
%--------------------------------------------------------------------------
%
% Method is valid for frequencies between 1GHz to 100GHz
%
% input parameter:
% - theta      path elevation angle [degree]
% - tau        polarization tilt angle (relative to the horizontal)[degree]
%              (tau = 0° for horizontal,tau = 45° for circular polarization)
% - f          frequency [GHz]
% - R          rain rate [mm/h]
%
% output parameter:
% - gamma_R    specific attenuation [dB/km]
%
%--------------------------------------------------------------------------
```

Figure 15: Sample Matlab function header for an implemented ITU model

To include the dependencies between some models, these models have been included in the function as enhancement and will be called if the parameter in question is not available by the user and therefore cannot be provided as input. By indicating this parameter as empty and providing required additional information for example, about the station which is needed by the embedded model, this missing parameter will be provided within the function automatically.
The functions also perform plausibility checks on input parameters to consider the model constraints and avoid misleading results.

7.2 Data analysis routines

The data analysis routines have also been implemented in MATLAB. The data analysis routines are structured in four groups.
The first group consists of preparation routines. The purpose of these functions is the modification of the file format and in addition they have the objective to fasten the data processing step. Preparation routines are intended to be applied only once and to store their output as modified database for further processing steps. The application of processing routines is strongly dependent on the status of the available measurement data format. The second category of software routines is concerned with the pre-processing of the data set. In the course of the pre-processing template extraction was executed. The third group is formed by processing functions. These Matlab routines focus on the processing of the measurement dataset. Time series are processed to determine propagation parameters and finally calculate statistics. The fourth group of functions describes the evaluation routines. These functions take the results of ITU models as well as propagation data statistics computed by processing routines as input. For the model evaluation, statistic parameters such as mean and standard deviation are computed.
The individual algorithms of implemented data pre- and processing routines are explained in the following sections. In Figure 16 an overview of the implemented software routines is given. Routines indicated with a dashed line are optional and are not needed for every dataset.

7.2.1 Pre-processing of Alphasat beacon data

For Alphasat data, the pre-processing step includes the transformation of measured signal power $[Watt/1Ohm]$ to $[dBm]$ by equation (53).

$$P_{dBm} = 10 \cdot \log_{10} \frac{P_W}{1W} + 30; \tag{53}$$

The beacon power levels in decibel then get inverted to obtain positive attenuation values. Then, in the next step template extraction was applied, outliers were detected and removed manually by visual inspection.
This paragraph shortly explains, as outlined by [2], the reason why a template is observed in the received beacon signal.
Amongst the theoretical motion of a satellite according to the Keplarian laws also perturbing forces act on the satellite since in practise non-ideal conditions exist.These perturbing forces cause a satellite movement that deviated from theory. The forces are caused by the presence of gravitational bodies such as sun and moon but also by solar pressure, the oblateness and the non-homogeneous gravitational field of the Earth and atmospheric drag. Due to this satellite motion, a sinusoidal template is induced in the transmitted signal. To avoid this effect, antenna tracking would be needed to adjust the antenna pointing to the current satellite position in order to receive the maximum signal strength.
Before the received signal can be processed, the sinusoidal template has to be extracted. This procedure has to be performed for Alphasat beacon data because during the considered period of measurements, the antenna tracking system was not yet installed. The

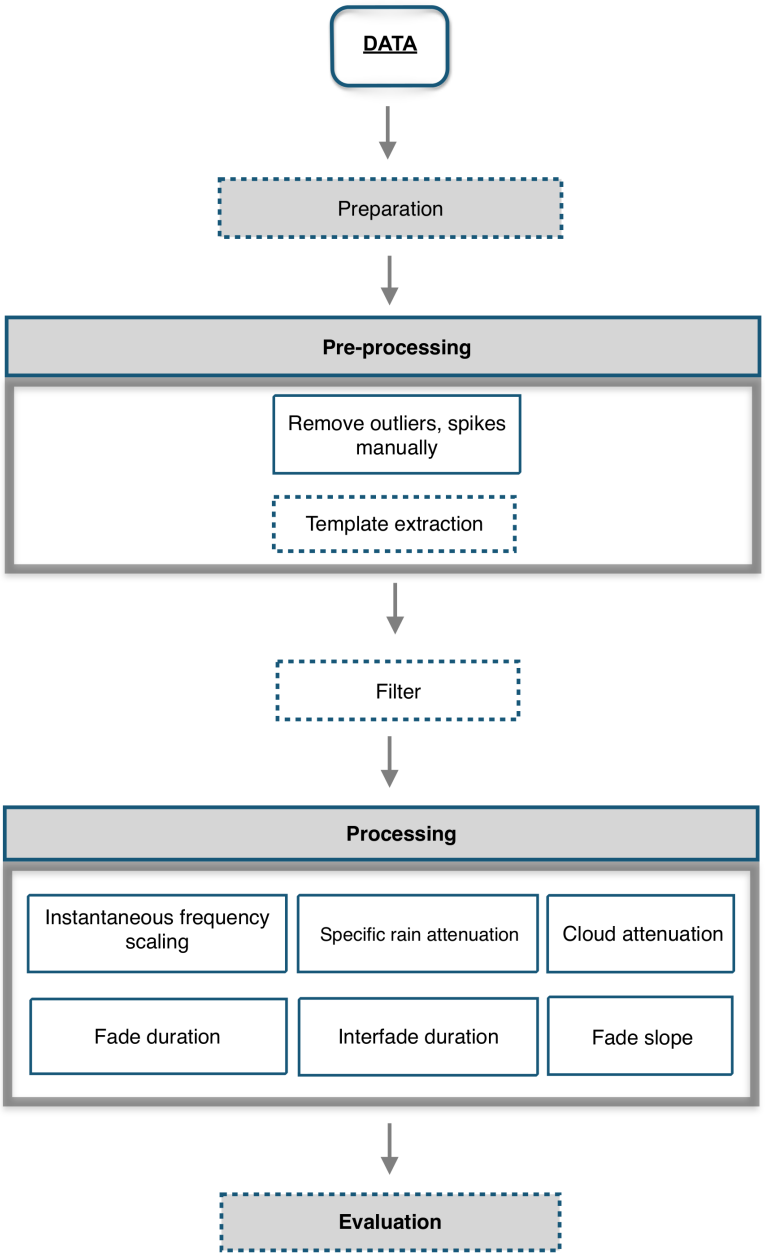

Figure 16: Overview of implemented data analysis software routines

Alphasat satellite follows a diurnal elliptical movement where the movements in elevation are bigger than those in azimuth. The pointing of the antenna was fixed and performed manually. Therefore it can be assumed that the pointing was not ideally in the center of this ellipse. This fact caused a non-symmetrical template which makes an automated template extraction even more complicated. Since no actions are planned by the satellite operator to stabilize the satellite movement, the daily variations are persistently increasing.
Antenna tracking is considered as nominal mode, therefore a first approach to extract this template by Fast Fourier Transformation (FFT) was implemented for this thesis. Against the recommendation in [1], signal artefacts were not excluded for this process beforehand, because artefacts, rain events and wind events could not be detected automatically with sufficient accuracy. As a result, the template was not extracted in an optimal way and small oscillations remained in the signal. Nevertheless, this procedure is fast and acceptable as first approach because program track is required for the measurements and will supersede the fixed antenna pointing mode in the near future.
The procedure of the template extraction is described in the remaining paragraph:
For the extraction of the Alphasat template, the FFT of the received beacon signal was computed. The Alphasat beacon signal was recorded with a sampling rate of 10 Hz. The extraction algorithm considered each 3 consecutive days to make the method more stable. Then, the derived result for the second day in the middle was stored. According to the number of FFT points, the FFT resolution was determined. The FFT extraction was finally performed for this time series where periodicities up to 6 hours where filtered out of the signal. This resulted in the fact that all low frequencies up to the frequency determined for the 6 hour periodicity and thus all low-frequency FFT coefficients were set to zero.
For Alphasat data the template actually could be removed by radiosonde data if available, because these measurements are much more accurate. For this procedure the measured brightness temperatures must be converted to attenuations at satellite elevation and frequencies. A routine to calculate this was implemented by Vinia Mattioli on behalf of Joanneum Research for measurements during the IOT of Alphasat. The zero dB level of the measured data by the beacon receiver then can be determined by subtracting the attenuations derived by the radiometer from the attenuation levels measured by the receiver [1]. For the considered period of Alphasat beacon data, however, antenna tracking was not activated and therefore antenna mis-pointing effects have to be removed from the signal as well. Apart from that, the radiometer setting was changed during this interval and this leads to the effect that measurements are not fully comparable. Considering this situation, the decision was made to extract the template by Fast Fourier transformation as it is suggested in [1].
Figure 17 shows a sample template extraction of approximately 5 days at the Alphasat Q-band beacon.

7.2.2 Pre-processing other data sets

Pre-processing of radiometer, disdrometer and meteorological data was not performed, since neither outliers in the recorded measurements were observed, nor was a resampling necessary.
Olympus beacon measurements were provided by so-called event packages as described in [37]. These event packages contain already pre-processed and template extracted bea-

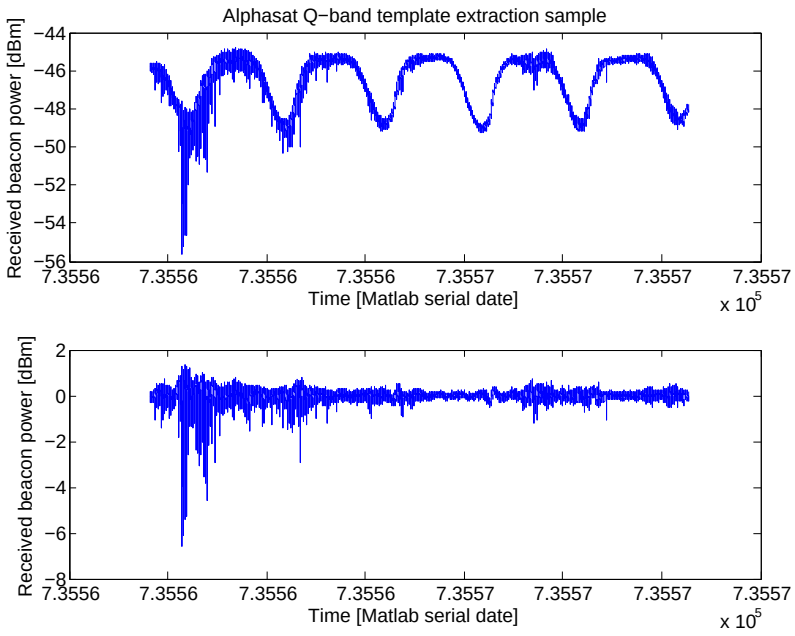

Figure 17: Sample template extraction shown at Alphasat Q-band

con attenuations. Since the data was available as binary files, the file format was converted to ASCII files by preparation methods. Visual inspection was performed to identify outliers or artefacts that occurred due to the file conversion. Moreover the 0dB-level needed to be determined by FFT to eliminate an offset.

7.2.3 Conditional distribution of instantaneous frequency scaling

To determine the cumulative distribution function (CDF) of instantaneous frequency scaling, Olympus beacon measurements at 12 GHz, 20 GHz and 30 GHz were used. This means, the frequency scaling was performed for two scenarios which is the scaling from a lower frequency of 12 GHz to 20 GHz and the second scenario from 20 GHz to 30 GHz. Due to the fact that this task is concerned with instantaneous frequency scaling, samples at a lower frequency f_1 and higher frequency f_2 measured at the same time stamp were determined. Then, samples at the lower frequency for a defined attenuation threshold were selected. For these samples, the instantaneous attenuation at the higher frequency channel were observed. As output the CDF of observed attenuations at f_2 for a specified attenuation level at f_1 was calculated.

7.2.4 Scintillation statistic

To determine scintillation statistic, the beacon attenuation data was low pass filtered to extract the low-frequency component. As recommended by [52] the low pass filter was designed with a cut-off frequency of 0.02 Hz to avoid distortion of the signal scintillation characteristic. The extracted low-frequency component was then subtracted from the beacon attenuation signal. The remaining part of the signal then represented scintillation.

The statistics were derived by the number of sampled that exceed a scintillation attenuation threshold divided by the total amount of samples.

7.2.5 Attenuation statistic

The attenuation statistics was computed by the histogram of the recorded Alphasat beacon attenuations. The bin size of 0.1 dB resolution was chosen. The statistic then can be derived by the number of values that exceed a certain attenuation threshold divided by the total number of samples.

7.2.6 Specific rain attenuation statistic from drop size distribution

The specific rain attenuation for horizontal and vertical polarization was computed on basis of the drop size distribution recorded by the disdrometer. The drop size distribution indicates the detected number of drops per an equivolumetric size bin. Constant bin sizes of 0.1 mm to 8 mm with a bin width of 0.1mm are considered. Additionally, the derived rain rate [mm/h] was provided as measurement parameter by the 2DVD distrometer. Based on the frequency of interest, temperature and path elevation, scattering amplitudes were computed by a software provided by Joanneum Research and ESA. As explained by Schönhuber in [41] the specific attenuation due to rain for horizontal respectively vertical polarization can be computed by equations 54 and 55.

$$A_H = 8.686 \cdot \frac{2 \cdot \pi}{k^2} \cdot 10^3 \cdot \int_{D=0}^{\infty} Re[S_{HF}(D)] \cdot N(D) dD \quad [dB/km] \tag{54}$$

$$A_V = 8.686 \cdot \frac{2 \cdot \pi}{k^2} \cdot 10^3 \cdot \int_{D=0}^{\infty} Re[S_{VF}(D)] \cdot N(D) dD \quad [dB/km] \tag{55}$$

Where k denotes the propagation constant with $k = \frac{2\pi}{\lambda}$. The parameter D describes the equivolumetric diamter of the sphere [mm] and N(D) is the drop size distribution $[1/m^3 mm]$. The Parameter S denotes the forward scattering amplitude with the subscript HF for linear horizontal polarization and VF stands for linear vertical polarization.

7.2.7 Cloud attenuation

Based on the fact that radiometer and beacon data for the same period and location are available in the reference database, a first approach was done to determine attenuation caused by clouds. For that purpose the measured brightness temperatures have to be converted to attenuations at the same elevation and frequency of Alphasat. This step has to be applied if the radiometer is not pointing in satellite link path direction and if brightness temperatures were measured at other frequencies, which is usually the case.
The conversion to satellite settings can be done by coefficients which are specifically derived for the location and climate of Graz. As the radiometer attenuations are computed, these zero dB values at clear sky get subtracted from the attenuations. By the exclusion of rain events, the resulting attenuations indicate the attenuation that is caused by clouds.
A first approach to determine a cloud attenuation statistic from Alphasat Q-band beacon

measurements was performed as described in the following. As radiometer data is available for the period of approximately one month but at two distinct configurations, the data set measured during the setup at 90° elevation was chosen. For this period of time, the measured brightness temperature by the radiometer have been converted to attenuations at Alphasat elevation and frequencies. Whereby, only attenuations derived for Q-band are of interest in this context. This conversion routine was developed by Vinia Mattioli on behalf of Joanneum Research in the course of a project and was made available by Joanneum Research for this thesis. The conversion algorithm developed by Vinia Mattioli in course of the Alphast IOT is documented in [31]. To determine the total attenuation at radiometer frequencies, the mean radiating temperature T_{mr} needs to be known. With equation (56) these temperatures can be determined.

$$T_{mr}(\Theta, f) = d_0 + d_1 \cdot T_s + d_2 \cdot P_s + d_3 \cdot R \cdot H \tag{56}$$

The parameters d_i are location specific coefficients that need to be determined for elevation and frequency of interest. For the location of Graz, these monthly coefficients were determined from radiosonde observation archive data as explained in [31]. Then equation 57 can be applied to compute the attenuation at radiometer frequency channels.

$$A(f, \Theta) = 10 \cdot log_{10}[(T_{mr}(f, \Theta) - T_c)/(T_{mr}(f, \Theta) - T_B(f, \Theta)] \quad [dB] \tag{57}$$

Finally, the attenuation at the Alphasat satellite link for an elevation of 35.1° and a frequency of 39.4 GHz for Q-band can be determined. Since there is always a trade-off between accuracy and computation time, radiometric frequency channels at 23.8 GHz, 27.84 GHz, 31.4 GHz, 51.26 GHz and 52.28 GHz were used to obtain the attenuation. For this purpose equation 58 was applied.

$$A_i(\theta, f) = a_0 + \sum_{j=1}^{m} a_j \cdot A_j(\Theta, f_i) \tag{58}$$

Where the parameter Θ is the elevation of 35.1° and the f_i represents the frequency of 39.4 GHz. The parameters a_j are location specific attenuation coefficients that are determined from radiosonde observations. Additional information regarding this topic is also provided by the COST IC0802 handbook [1].

After this conversion step, attenuation measured by the Alphasat receiver at Q-band and attenuations derived by radiometer measurements are available for the same period of observation as explained in [31]. In order to determine attenuation due to clouds, attenuation induced by other atmospheric phenomenons such as rain and attenuation by atmospheric gases needs to be excluded from the dataset. Rain events were detected and removed by visual inspection of meteorological data. Furthermore, also artefacts due to wind and antenna pointing were excluded. After the template extraction, the attenuation measured by the radiometer during two days of clear sky were was determined. Since available meteorological data only provided information about the visibility of the sun, days that indicate 100% visibility and no rain are assumed to be clear sky. Of course classification due to cloud coverage data would be more reliable and therefore preferred. In addition to the considered gaseous attenuation also the scintillation of the beacon signal was removed. Finally, the conditional distribution of cloud attenuation was computed.

7.2.8 Fade duration statistic

Fade duration statistics were obtained for different attenuation and duration thresholds from Olympus beacon attenuation data. If a signal crosses a specific attenuation threshold, a fade is detected. Once the signal attenuation is below the threshold again, the fade duration is computed and checked if the duration exceeds a specific duration. If both criteria are met, the counter is increased and the fade duration information stored. Thus, different lengths of duration thresholds are applied for one attenuation level. The probability of occurrence is determined by the number of observed fades that exceed a certain duration divided by the total number of fades that exceed the duration of 1 second. The probability of exceedance is computed by the the fraction of observed fading time divided by the total fading time observed at a certain attenuation level.

7.2.9 Interfade duration statistic

The statistic for interfade duration is related to the fade duration statistic. This means, not the fade is identified but the time between two fades. The principle of computation basically remains the same as for the fade duration statistics explained above.

7.2.10 Fade slope statistic

The fade slope statistics determines the probability that a slope at the rising respectively falling edge of a slope is exceeded at a certain attenuation. For a data sample of interest the slope is determined by its predecessor and antecessor which leads to a time interval of 2 seconds for a sampling rate of 1 Hz. The CDF is then again determined by the fraction of the number of samples that exceed a certain slope to the total amount.

8 Test procedure and execution

In this section measures are described to verify the software functions. Verification is necessary to ensure correct implementation and thus correct output values. This step is crucial and had to be executed before proceeding to the next step which is the evaluation of the ITU-R models on the basis of measurement data.

8.1 Verification of ITU-R model implementations

Although the ITU-R recommendations provide detailed descriptions of the models, there are still ambiguities and dependencies between different models. For this reason the verification of the implemented models becomes even more important.
As noticed in the task description introduced in chapter 6, not all prediction methods used in this context require an implementation. Explicitly for the ITU recommendation P.372 [48] there is no need for verification because the measured radiometer data was compared to the chart presented by the recommendation in figure 4 and figure 5.
According to the recommendation P.1623 [42] interfade duration follows a log-normal or rather power-law distribution for short interfade durations that result from tropospheric scintillation. However, no detailed model is at the moment available to predict the signal uptime due to interfade duration simulations [42]. Therefore, for this method also no verification is possible.
In the course of the revision of recommendation P.618 [49] the section about instantaneous frequency scaling has been added. Due to the rather new status of this model in the recommendation [1] no official validation data is available yet. Therefore, verification of the results derived by this model cannot be verified with reference data.
For some models however, the ITU does provide verification data on the homepage to confirm the correctness of the implementations. The selected prediction models of the recommendations P.840-4, P.676-9, P.838-3 and P.618-10 could be verified by means of this verification data sheet [23]. Concerning the model for total attenuation statistics, which is part of P.618 [49] chapter 2.5, there is a very high dependency on individual attenuations provided by other ITU-R models. As described in chapter 5, the total attenuation model scales and merges results derived by other ITU recommendations in one formula. Due to the fact that all partial results derived by other ITU-R models were verified by the validation excel sheet [23] and no explicit verification data for the total attenuation prediction model is available, the verification was performed by plausibility checks of the final result.
A similar scenario arises with the models provided by recommendation P.1623 [42] and P.618 [49] in chapter 2.2.1.2. . Unfortunately, also for these models neither sample charts of model output nor verification data is provided by the ITU for these models. Therefore,

[1] This model was officially included in the 11th version (P.618-11) published in September 2013.

also in this case, plausibility checks of the simulation results with results published in papers like [17] for fade duration, [4] for fade slope and [24] for long-term frequency scaling was done. Table 10 sums up the test plan for the implemented models.

Name	**ITU model description**	**Verification**
Sky noise	Chapter 5.2.1	No verification
Long-term frequency scaling	Chapter 5.2.2	Plausibility check [24]
Instantaneous conditional frequency scaling	Chapter 5.2.3	No verification
Scintillation	Chapter 5.2.4	Verified with [23]
Total attenuation	Chapter 5.2.5	P.618 (chapter 2.2.1.1) verified with [23] P.840 verified with [23] P.676 verified with [23]
Specific rain attenuation	Chapter 5.2.6	Verified with [23]
Specific cloud attenuation	Chapter 5.2.7	No verification
Fade duration	Chapter 5.2.8	Plausibility check [16], [17]
Interfade duration	Chapter 5.2.9	No verification possible
Fade slope	Chapter 5.2.10	Plausibility check [4]

Table 10: Test plan for implemented ITU models

Figure 19 and 18 show a sample plausibility check of the implemented ITU fade duration model with the ITU model results at 50 GHz and 40 degrees elevation as presented by Garcia del Pino et al. in [16].

8.2 Verification data analysis routines

The verification of data analysis routines was predominantly performed by plausibility checks and visual inspection because no verification data exists for them.
Preparation routines designed for the conversion of data types and layout were verified by visual inspection of their input and output files.
The routines that read and concatenate the content of files are also verified by visual inspection.

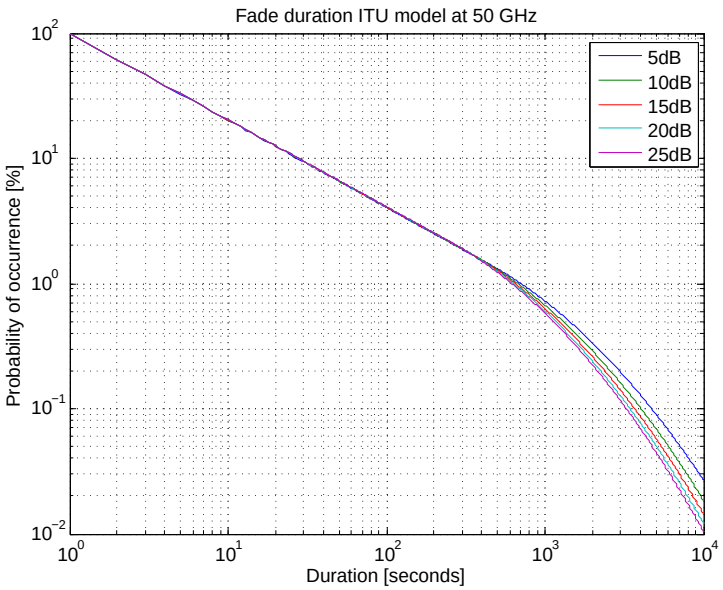

Figure 18: Fade duration statistic obtained by the implemented ITU model [42]

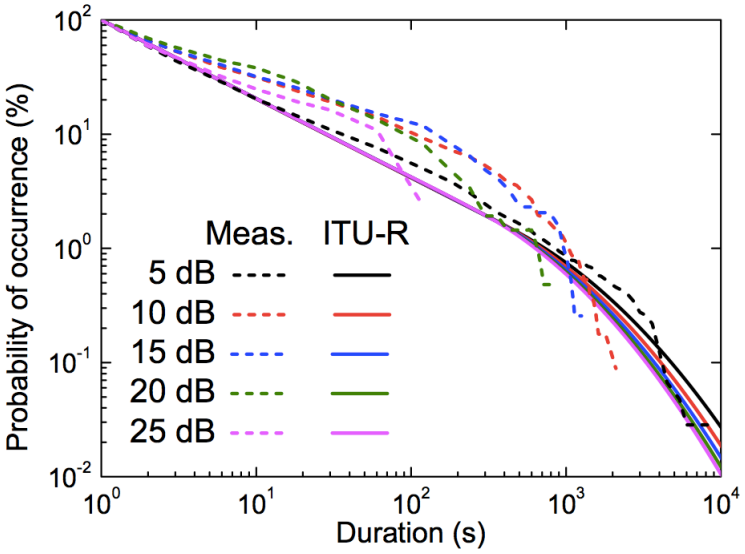

Figure 19: ITU modelled fade duration results as presented in [16]

Processing routines that derive statistics and calculate the parameters of interest were verified by plausibility checks with results derived by scientific papers.
The routine that computes the scintillation statistic was verified by the comparison of Alphasat beacon Ka-band statistics with statistics derived by [15]. The data illustrated in this paper [15] was measured in Madrid with a 19.7 GHz beacon. Therefore, a plausibility check of the statistics derived by the Alphasat beacon at Ka band with a similar frequency of 19.7 GHz is possible.
The verification of the function that derives rain attenuation from disdrometer measurements was performed by means of the results published in [10]. In this paper specific attenuation in Ka-band was computed from 2D-Video-Distrometer measurements in Taiwan. Of course the meteorological conditions such as temperature etc. are different in

Taiwan, nevertheless, the determined distribution function and similarity of results is expected to be qualified for a plausibility check.
The verification of the function that determines the cloud attenuation was performed based on the values presented in [39]. This paper presents results for cloud attenuation measured at 42° elevation at the 31.7 GHz frequency channel. The attenuation due to clouds is derived from Alphasat Q-band beacon measurements. For comparison also radiometer measurements transformed to the elevation and frequency of Alphasat Q-band are consulted as well. Due to measurement results at similar frequency and elevation presented by the paper, these results are used for plausibility check.
Fade duration as well as interfade duration statistics is performed by the same function in order to reduce processing time. The fade duration routine was verified by plausibility check with the results presented in the papers [4], [16] and [14]. Results of interfade duration statistics are rare in open literature. The interfade duration results have been verified by [17], [14] and [16].
Verification for the fade slope computation routine can be performed with Olympus beacon data at 12 GHz, 20 GHz and 30 GHz. Max van de Kamp treated this topic in detail in his doctoral thesis [52]. In the course of his thesis he provided fade slope statistics for Olympus beacon frequencies. Therefore these results can be used as plausibility check.
Table 11 relates the software analysis routines to their verification scheme. If available, it additionally provides information about the measurement data that was used for verification with data from published papers.

Type	**Verification**	**Verification data**
Cleaning routine	Visual inspection	none
Layout conversion routine	Visual inspection	none
Reading routine	Visual inspection	none
Scintillation statistics	Plausibility check [15]	Alphasat Ka-band
Specific rain attenuation	Plausibility check [10]	Disdrometer data
Cloud attenuation	Plausibility check [39]	Radiometer data and Q-band beacon of the Alphasat campaign
Fade duration statistics	Plausibility check [4], [16], [14],	Olympus beacon data
Interfade duration statistics	Plausibility check [17], [14], [16]	Olympus beacon data
Fade slope statistics	Plausibility check [52]	Olympus beacon data

Table 11: Test plan for the software analysis routines

The Figures 20 and 21 represent a sample for the evaluation of fade slope measurement

results by plausibility check with results presented by Kamp in [52].

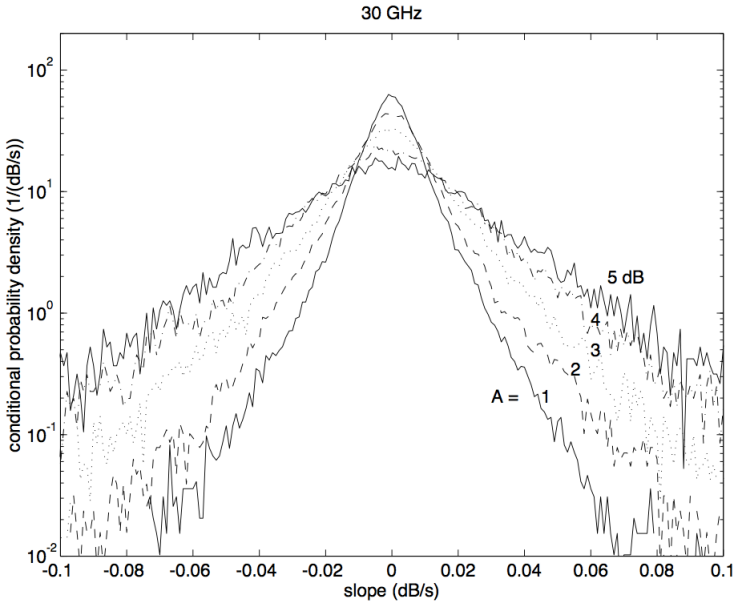

Figure 20: Fade slope statistics at 30 GHz as presented in [52]

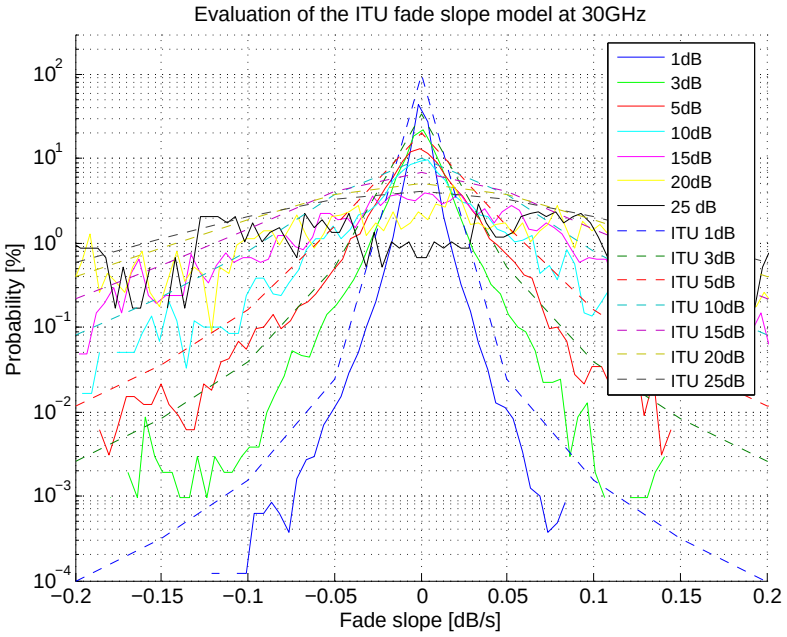

Figure 21: Fade slope statistics at 30 GHz as derived from the Olympus beacon dataset

9 Evaluation of ITU models

At the beginning this chapter shortly introduces the evaluation procedure for the ITU model results. Afterwards, the evaluation results of the 10 Tasks are presented.

9.1 Evaluation procedure

Guidelines for correct evaluation of ITU models by measured data are the content of recommendation P.311 [47]. This recommendation defines criteria for datasets that can be taken for model evaluation purposes. The most important and obvious criterion is that the measurement data has to be suitable for the model and subsequently qualified for comparison. The evaluation procedure is based on a testing variable. This testing variable is defined as the minimum mean between the two comparable datasets, respectively the minimum standard deviation of their difference. Additionally, testing procedures for fade duration and fade slope are explained in further detail.

9.1.1 Fade duration

Comparison of fade duration is also performed by means of a testing variable. The procedure to derive this variable is described in the recommendation ITU-R P.311 [47]. The fade duration has to be defined at fixed fade durations D as well as fixed attenuation thresholds. The testing variable is defined as the natural logarithm of the ratio between the predicted and the measured duration. Afterwards, the calculation of mean and standard deviation provide necessary statistics for comparison.

The process is described in more detail below:
In principal the statistics for fade duration can be described by the probability density function on the one hand and the cumulative exceedance probability on the other hand. Therefore two testing variables, one for each distribution function have to be determined. The testing variable for the probability density distribution can be computed with equation (59).

$$\epsilon_{P,i}(D,A) = ln\left(\frac{P_p(D|A)}{P_m(D|A)}\right) \tag{59}$$

By equation (60) the testing variable for the exceedance probability distribution can be derived.

$$\epsilon_{N,i}(D,A) = ln\left(\frac{1-F_p(D|A)}{1-F_m(D|A)}\right) \tag{60}$$

Here, the parameter i indicates different radio links.
The test variables have to be computed for each combination of the parameters' duration D and attenuation A.
In the next step the mean and standard deviation $\epsilon_{P,i}$, respectively $\epsilon_{N,i}$, have to be calculated for all attenuation thresholds A.

The best prediction method for the dataset will produce the smallest statistical parameters.

9.1.2 Fade slope

ITU-R recommendation P.311 [47] also defines a testing variable for the evaluation of fade slope models. The testing variable has to be derived by the natural logarithm of the ratio of measured to simulated data. For the fade slope validation there are fixed attenuations and percentages of time defined, for which the testing variable has to be calculated by the following equation (61).

$$\epsilon_i(\zeta, A) = 2 \cdot \frac{P_p(\zeta|A) - P_m(\zeta|A)}{P_p(\zeta|A) + P_m(\zeta|A)} \tag{61}$$

As described in the method before, the mean value and standard deviation must be calculated for all attenuation thresholds. The model that simulates the measurement results best is characterized by the smallest statistical parameters.

9.1.3 Evaluation procedure for other ITU models

For other ITU-R prediction models no algorithms for the evaluation of the models is proposed in the recommendation P.311 [47]. Therefore, a similar concept for the evaluation, as exemplarily described for fade duration and fade slope above, is adapted to the evaluations of the remaining tasks. The testing variable is, as recommended in [47] computed as the difference between the ITU model results and the results derived from measured data at defined probability levels. Then, mean and standard deviation are derived which give information about the quality of the model.

9.2 Task evaluation

This section presents the graphical and numerical evaluation results of the 10 tasks that have been defined in chapter 6. Additionally, first results of Alphasat measurements that cover a few days of observation are presented in this section as well. It is a first approach to analyze the new measurement data, therefore evaluation with ITU models cannot reliably be performed but they are illustrated to present a future outlook.

9.2.1 Task 1 - Sky noise

In this task the measured brightness temperatures at Hilmwarte tower are used for comparison with modelled results presented in the ITU-R P.372 recommendation [48]. The reference charts in the recommendation are computed for a standard reference atmosphere for clear sky. Retrospectively, based on the available measurement data it is not possible to determine clear sky periods for sure. A parameter of the meteorological data provided by ZAMG, however, indicates the sunshine [%] measured every hour. Thus, this parameter was taken as a reference to determine periods where sunshine was indicated with a very high percental level and thus clear sky was assumed during these periods. By correlation with this parameter and the cross-check with measured rain rates, a few potential clear sky

days were identified. Radiometer measurements from these selected days were therefore used to evaluate the ITU model.
Unfortunately, the pointing of the radiometer was changed during the measurement period of 31 days. The set of measurements started on 21 November 2013 with a radiometer configuration that was chosen to point directly to the Alphasat satellite at 35° elevation. Later, on 3 December 2013, the radiometer's pointing was changed to 90° elevation. The charts illustrated in P.372 present the sky brightness temperatures for different elevation angles and different frequencies. For evaluation, the mean value of clear sky day measurements for each each of both radiometer configuration was calculated and drawn into the chart for comparison.
Brightness temperatures measured by the RPG radiometers were read by a Matlab routine that is partly based on a Matlab procedure developed by Vinia Mattioli on behalf of Joanneum Research. The selected days with maximum recorded sunshine are 29 November 2013, 1 December 2013, and 2 December 2013 for a radiometer pointing at 35° elevation. For the radiometer setting of 90° elevation pointing, the measurements of 3 December 2013, 4 December 2013 and 16 December 2013 were identified for evaluation.
The mean values of measured brightness temperatures are presented in the appendix. Figure 58 shows measured mean brightness temperatures for 35° elevation configuration and Figure 59 shows the results for the 90° elevation for assumed clear sky.
In Figure 22 and Figure 23 the results are compared to the modelled data as provided by the ITU recommendation.
Table 12 and 13 show the mean value testing variables for all frequency channels at 35°, respectively 90° elevation setting of the radiometer at Hilmwarte.

Frequency [GHz]	15.3	22.24	23.04	23.84	25.44	26.24	27.84	31.4
$\boldsymbol{mean\ T_{Bright}}$ **[K]**	3.47	22.47	23.09	20.68	17.2	24.98	13.73	16.67

Frequency [GHz]	51.26	52.28	53.86	54.94	56.66	57.3	58	90
$\boldsymbol{mean\ T_{Bright}}$ **[K]**	144.78	192.34	264.22	271.91	272.7	272.72	272.77	45.26

Table 12: Mean brightness temperatures at 35° elevation

Frequency [GHz]	15.3	22.24	23.04	23.84	25.44	26.24	27.84	31.4
$\boldsymbol{mean\ T_{Bright}}$ **[K]**	4.55	17.28	16.41	15.19	12.85	14.34	11	12.14

Frequency [GHz]	51.26	52.28	53.86	54.94	56.66	57.3	58	90
$\boldsymbol{mean\ T_{Bright}}$ **[K]**	103.27	147.25	247.38	273.68	276.77	276.63	276.49	30.77

Table 13: Mean brightness temperatures at 90° elevation

The results show quite significant deviation from the model values at elevations of 35 and 90 degrees. Although the measured brightness temperatures at lower frequencies are

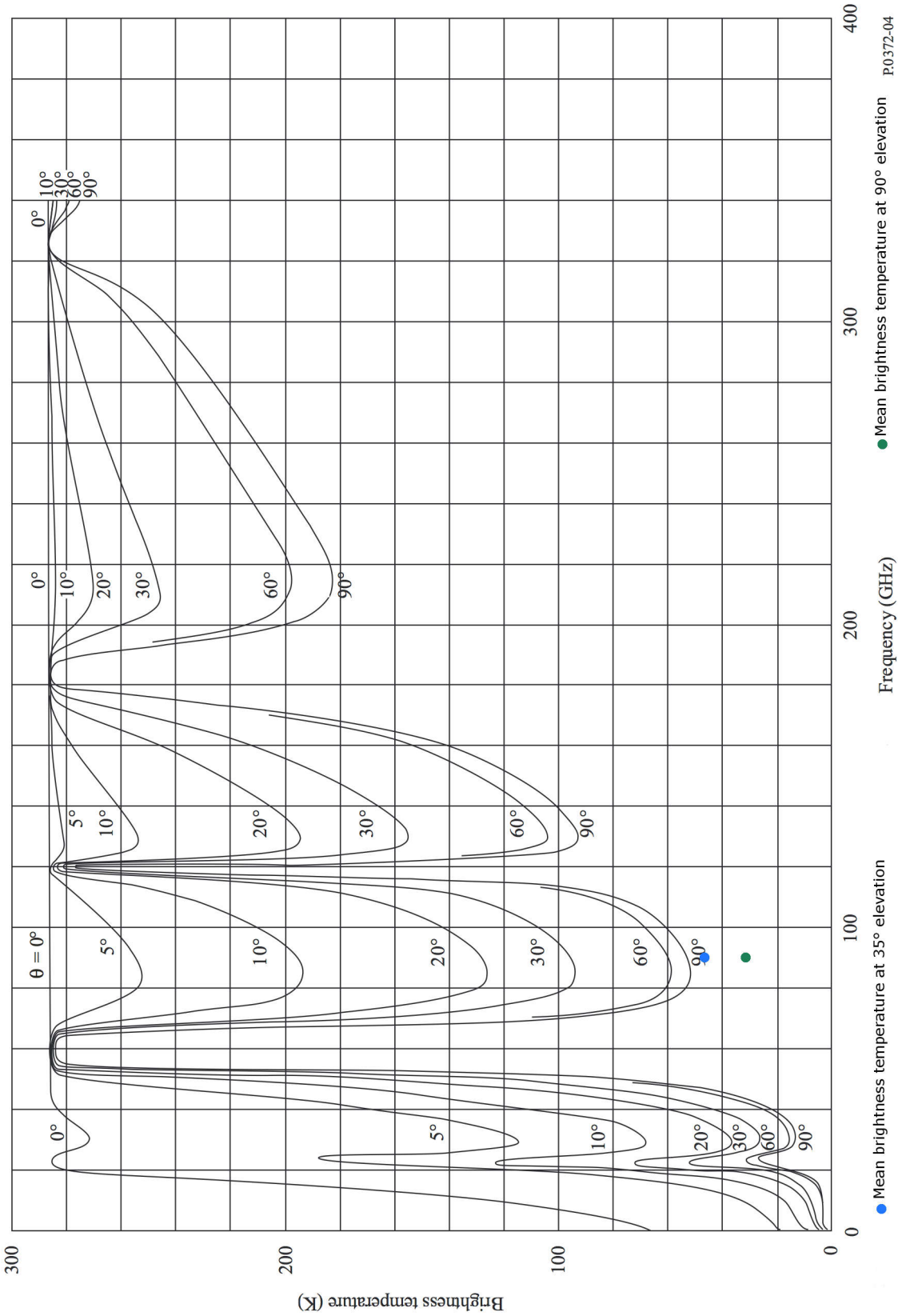

Figure 22: Brightness temperatures for the frequency range from 0 GHz to 400 GHz adopted from [48] and modified

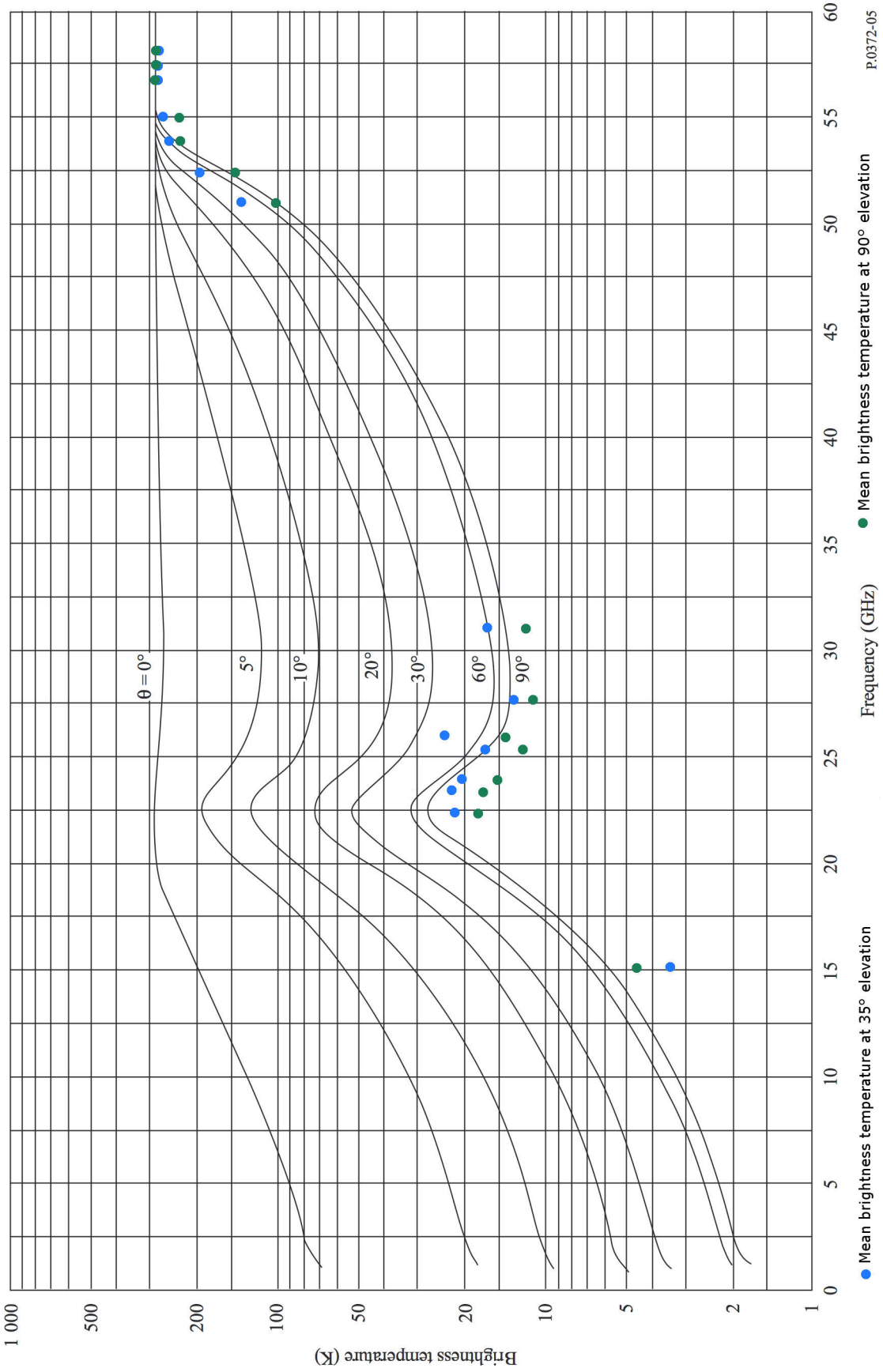

Figure 23: Brightness temperatures for the frequency range from 0 GHz to 60 GHz adopted from [48] and modified

below the expected values, the ratio between the values measured at 35 and 90 degrees elevation are plausible. Additionally, a parallel trend of the radiometer measurements to the modelled results derived by the ITU with a certain offset is noticeable. The measured value is larger at an elevation of 35 degrees than at 90 degrees. This fact can be explained because at lower elevations the path through the atmosphere is longer and causes more attenuation.
Especially two channels at 26.24 GHz and 15 GHz show unexpected behaviour. This phenomenon could be caused by inadequate calibration of these channels. Moreover, the structure of the atmosphere strongly depends on the location and season. Since the results presented by the ITU were simulated based on predefined standard atmosphere conditions, it is very unlikely to match these conditions exactly during real measurement.
In the reference handbook COST255 [30] the sky noise temperatures have been calculated as well. As it is further explained in the handbook, the calculation was performed with a so-called MPM93 model that estimated the results based on radiosonde measurements of the five regions indicated in Figure 24. The brightness temperatures were computed for a frequency range between 1 GHz and 300 GHz for a non-scattering atmosphere. The results for all five regions are presented in Figure 24. Due to the difference in temperature and integrated water content, the derived model results show a rather large difference among the results for those stations.

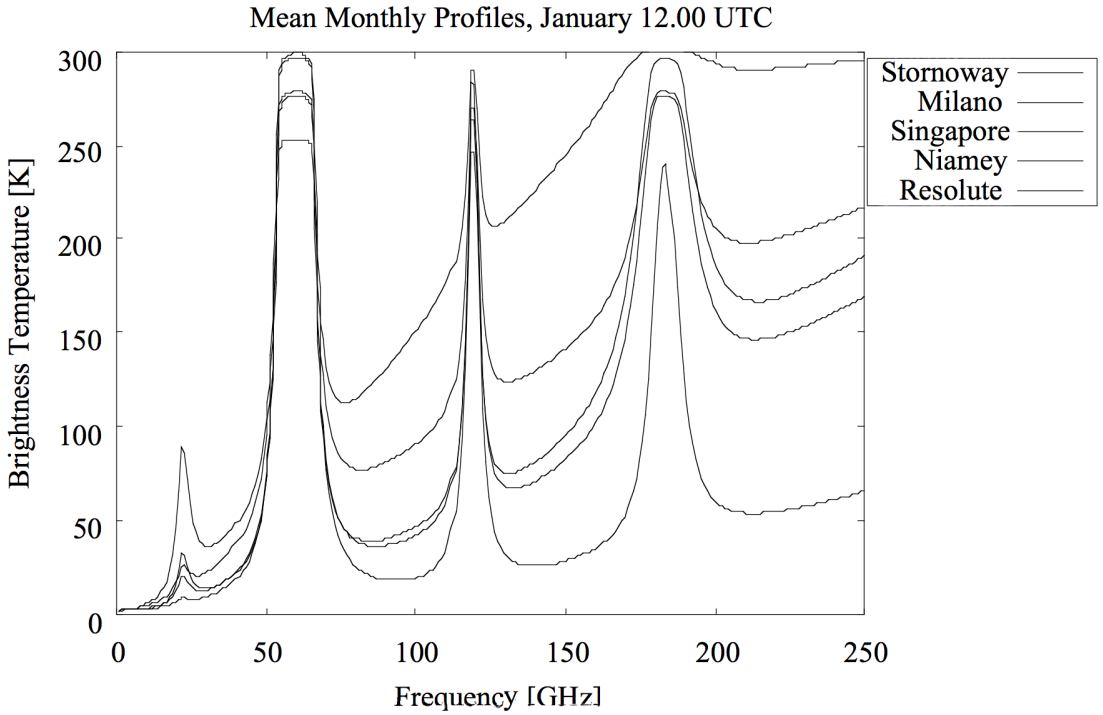

Figure 24: Brightness temperatures derived from the MPM93 model as presented in [30]

9.2.2 Task 2 - Long-term frequency scaling

The purpose of frequency scaling is to predict - based on attenuations observed at a lower frequency - the attenuation probability at a higher frequency. Statistics at 11.4 GHz respectively 19.9 GHz were used as reference values to evaluate the atmospheric attenuation model. The model provided in the ITU-R recommendation P.618 [49] predicts attenuation at the higher frequency for the same probability level as the attenuation value used as input at the lower frequency. Figure 25 and Figure 26 illustrate the results of the comparison.

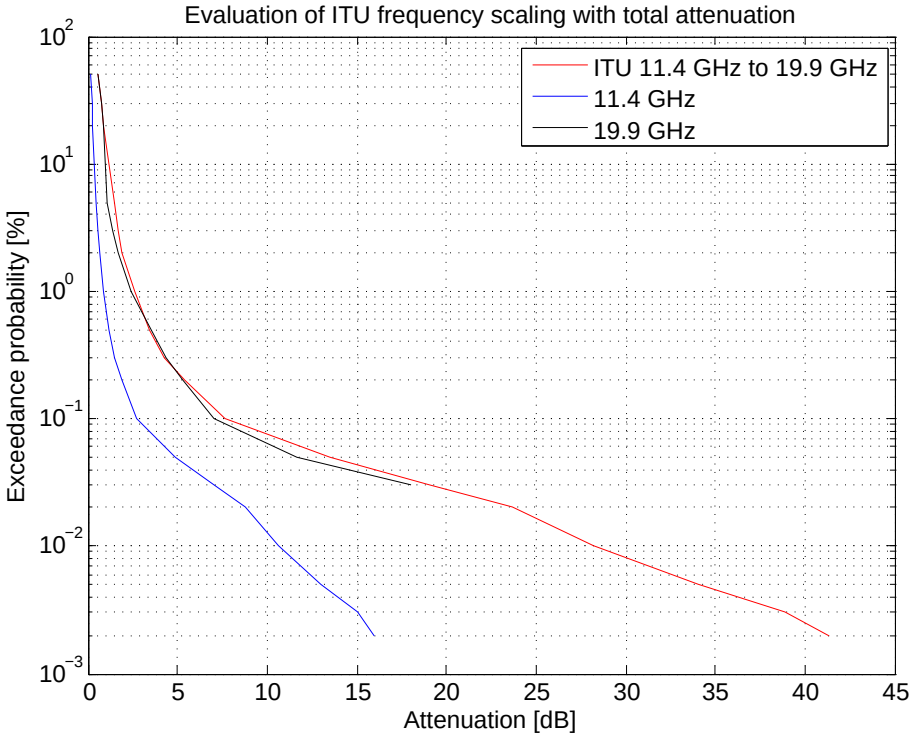

Figure 25: Evaluation of ITU frequency scaling 11.4 GHz to 19.9 GHz

Table 14 presents the results of the testing variable for the evaluation of the frequency scaling model.

Testing variable	**11.4 GHz to 19.9 GHz**	**19.9 GHz to 29.9 GHz**
mean	0.32 dB	0.8 dB
standard deviation	0.53 dB	0.42 dB

Table 14: Evaluation of the ITU frequency scaling model

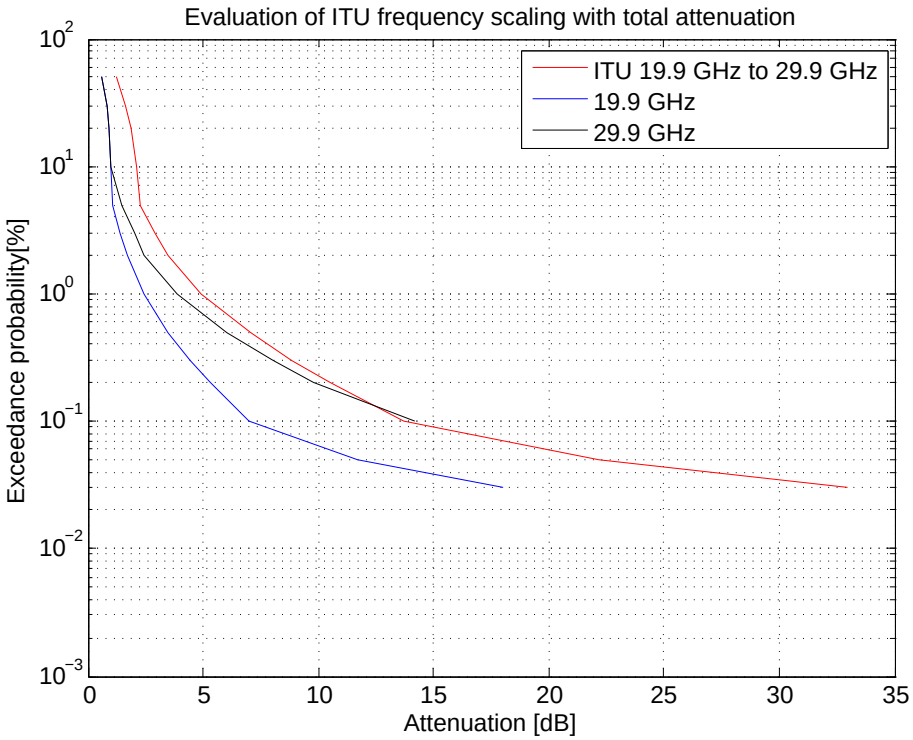

Figure 26: Evaluation of ITU frequency scaling 19.9 GHz to 29.9 GHz

The evaluation reveals that the ITU frequency scaling method achieves better results at lower frequencies such as 11.4 GHz to 19.9 GHz. In the second evaluation scenario, where the attenuation at 19.9 GHz is scaled up to 29.9 GHz, especially at low attenuations the model overrates the measured results.

9.2.3 Task 3 - Conditional instantaneous frequency scaling

The model presented in recommendation P.618 [49] was evaluated with Olympus beacon data at the frequencies 11.4 GHz, 19.9 GHz and 29.9 GHz. The results of the evaluation are presented in Figure 27 for the frequency scaling from 11.4 GHz to 19.9 GHz. Figure 28 presents the results of the frequency scaling from 19.9 GHz to 29.9 GHz. For different attenuations at the lower frequency (downlink), which are indicated in the legend, the CDF of attenuations measured at higher frequency (uplink) are shown.

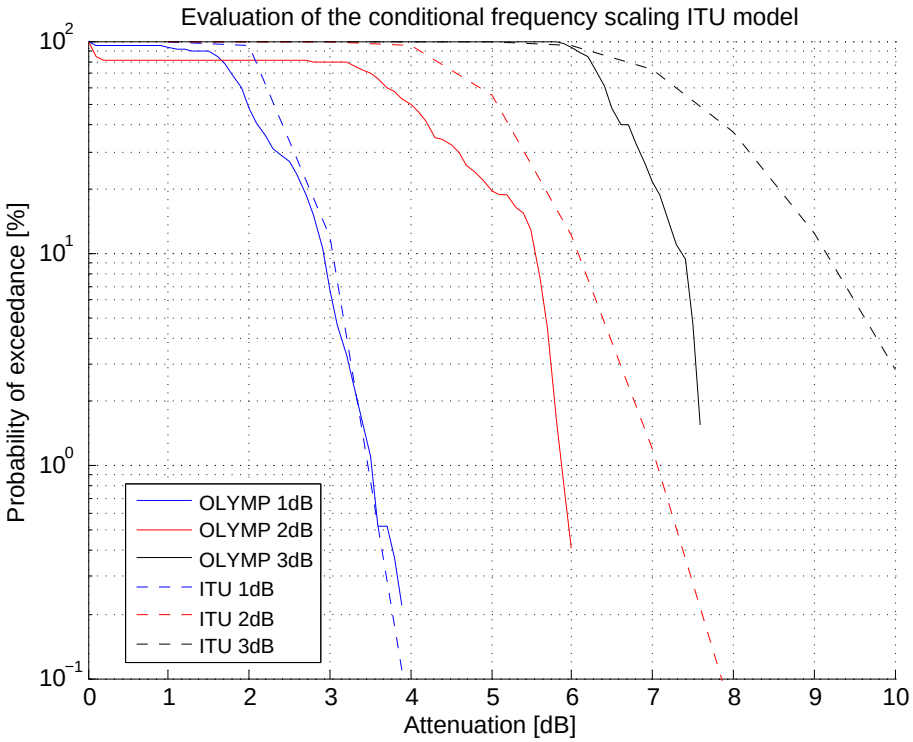

Figure 27: Evaluation of the CDF frequency scaling method for 11.4 GHz to 19.9 GHz

The evaluation results for the frequencies 11.4 GHz and 19.9 GHz are shown in Table 15.

attenuation [dB]	**1 dB**	**2 dB**	**3 dB**
mean	0.51 dB	1.27 dB	1.81 dB
standard deviation	0.31 dB	0.42 dB	0.49 dB

Table 15: Evaluation of the conditional instantaneous frequency scaling model for the frequencies 11.4 GHz and 19.9 GHz

Evaluation results of the conditional instantaneous frequency scaling for the frequencies 19.9 GHz and 29.9 GHz are provided in Table 16.

attenuation [dB]	**1 dB**	**2 dB**	**3 dB**	**4 dB**	**5 dB**	**6 dB**	**7 dB**
mean	-0.74	-0.41	0.35	1.93	2.68	3.53	3.85
standard deviation	0.16	0.42	0.73	1.11	1.22	0.98	0.72

Table 16: Evaluation of the conditional instantaneous frequency scaling model for the frequencies 19.9 GHz and 29.9 GHz

Figure 27 shows that at 11.4 GHz the modelled values match the measurement results best at 1 dB on the downlink f_1. For higher attenuations the model clearly overestimates the measurements. In Figure 28 instantaneous frequency scaling for higher frequencies 19.9

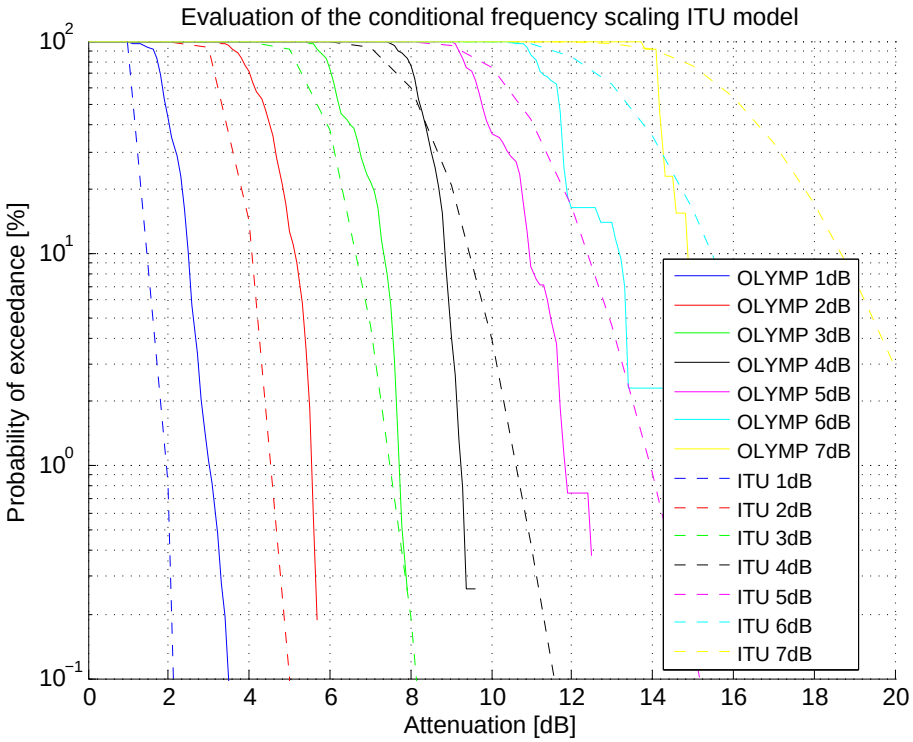

Figure 28: Evaluation of the CDF frequency scaling method for 19.9 GHz to 29.9 GHz

GHz to 29.9 GHz is illustrated. Here, the model underestimates the measured attenuation values at low attenuations. The model output fits the measured results best at 3 dB attenuation values at f_1. At larger attenuation values 4 dB to 7 dB the model starts to overestimate the measured attenuation values. It is noticeable that the overestimation becomes larger with increasing attenuation level at f_1.
As it is stated by the model description in [49], the accuracy of this model has not been determined by the ITU yet. The model is recommended for the frequency range between 19 GHz and 55 GHz. Hence, the first evaluation presented in Figure 27 for frequency scaling from 11.4 GHz to 19.9 GHz is actually not in the intended range of the model. The Olympus beacon measurements served as reference data for this evaluation. Samples recorded at the same time in both frequencies where identified. Then, samples at the lower frequency that meet the attenuation threshold were selected. For these selected samples, the recorded attenuation at the higher frequency was observed and a statistic computed. Another factor that adds uncertainty is the fact that the implementation of this model could not be verified since the model was first published in the latest version of this recommendation, which is version 11, and no reference data for the verification of the implementation model is provided by the ITU yet.

9.2.4 Task 4 - Scintillation

In this section the results of the ITU scintillation model evaluation are presented. The evaluation was performed for the Ka and Q-band Alphasat beacon signal recorded over the period of one month. At this point it needs to be mentioned that the scintillation model provided by the ITU is recommended for frequencies up to 29 GHz. But for reasons of comparison this limit was neglected and the scintillation at Q-band at a frequency of approximately 39 GHz was modelled as well. The results of the evaluation are shown in Figure 29 for Ka-band respectively in Figure 30 for Q band.

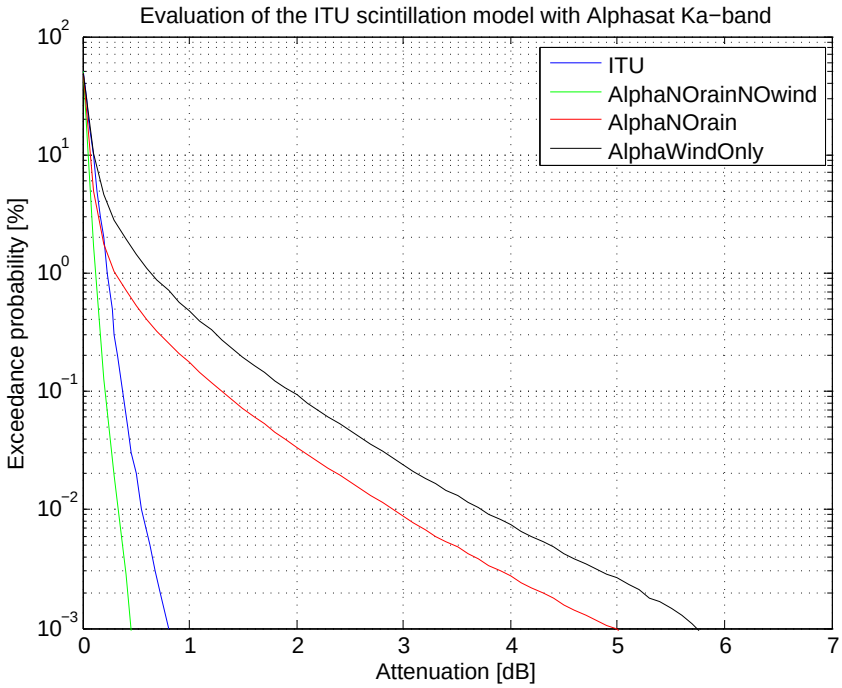

Figure 29: Evaluation of the ITU scintillation statistic model at Ka-band

Testing variable	**Ka band**	**Q band**
mean	0.14 dB	0.16 dB
standard deviation	0.1 dB	0.09 dB

Table 17: Evaluation of the ITU scintillation model at Ka- and Q-band for periods without rain and strong wind events

In Figure 29 and 30 the statistics of specific attenuation due to scintillation are shown for Ka- and Q-band. The results at both figures are quite similar. For evaluation, the rain events had to be excluded from Alphasat beacon measurements. The identification of the rain events was performed by visual inspection and manual removal. As visible in Figure 29 and figure 30, the exclusion of rain events resulted in unusual high attenuations in the scintillation statistics (red curve) compared to the simulated result by the model. The Alphasat beacon receiver in Graz is based on a fly-away type antenna, defining the system's stability against wind. Due to this fact, the antenna is very sensitive to wind

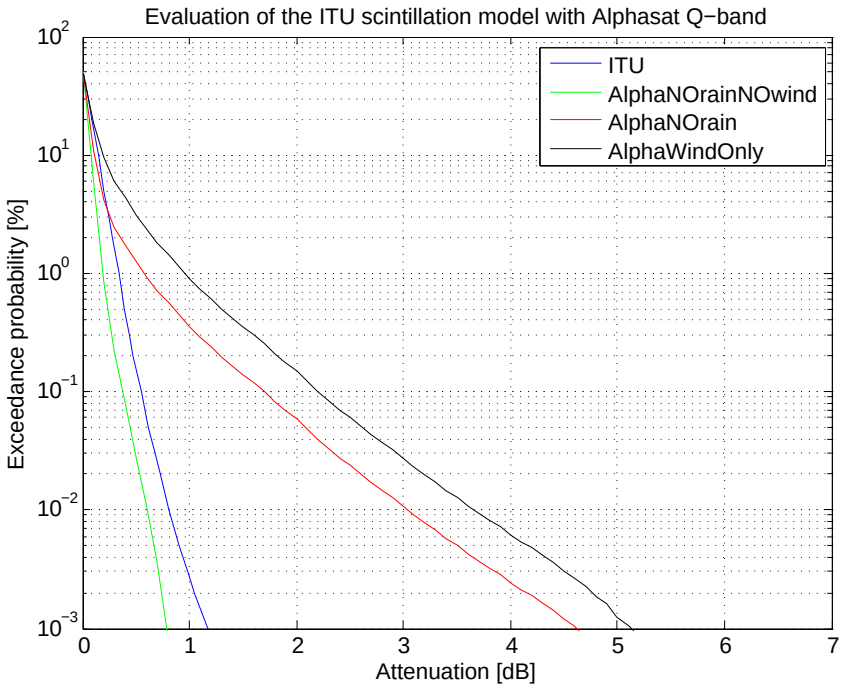

Figure 30: Evaluation of the ITU scintillation statistic model at Q-band

events. This is the reason why strong wind events that occurred over a longer period of time and exceeded a windspeed of approximately 4 $[m/s]$, had to be excluded for the evaluation. The results of the scintillation statistic for this data set (green curve) are actually more plausible compared to the model results. To demonstrate the impact of major wind events the scintillation during wind events has been determined as well and is shown in the figures as black colored curve. The resulting CDF of scintillation at Ka- and Q- band is lower than the curve predicted by the ITU model. This effect could be caused by the exclusion of strong wind events. Scintillation is caused by turbulences in the atmosphere. During wind events turbulences are assumed to be higher. Therefore the curve is expected to approximate the result derived from the ITU model if wind events would be considered as well.

9.2.5 Task 5 - Total attenuation

For the evaluation of the total attenuation model recommended in ITU-R P.618 [49], total atmospheric statistics charts derived from radiometric measurements are used. In order to evaluate the accuracy of the model, parameters valid for the location of Graz and matching values for the setup of the radiometer regarding frequency and elevation were used as input for the simulation model. The rain rate at 0.01% of the time was assumed with 50 mm/h on average. The water vapor density was assumed with 7 g per cubic meter as average value, which is also in the range of the water vapor density charts published by the ITU.

In Figure 31 the evaluation results of the total ITU total attenuation model are illustrated.

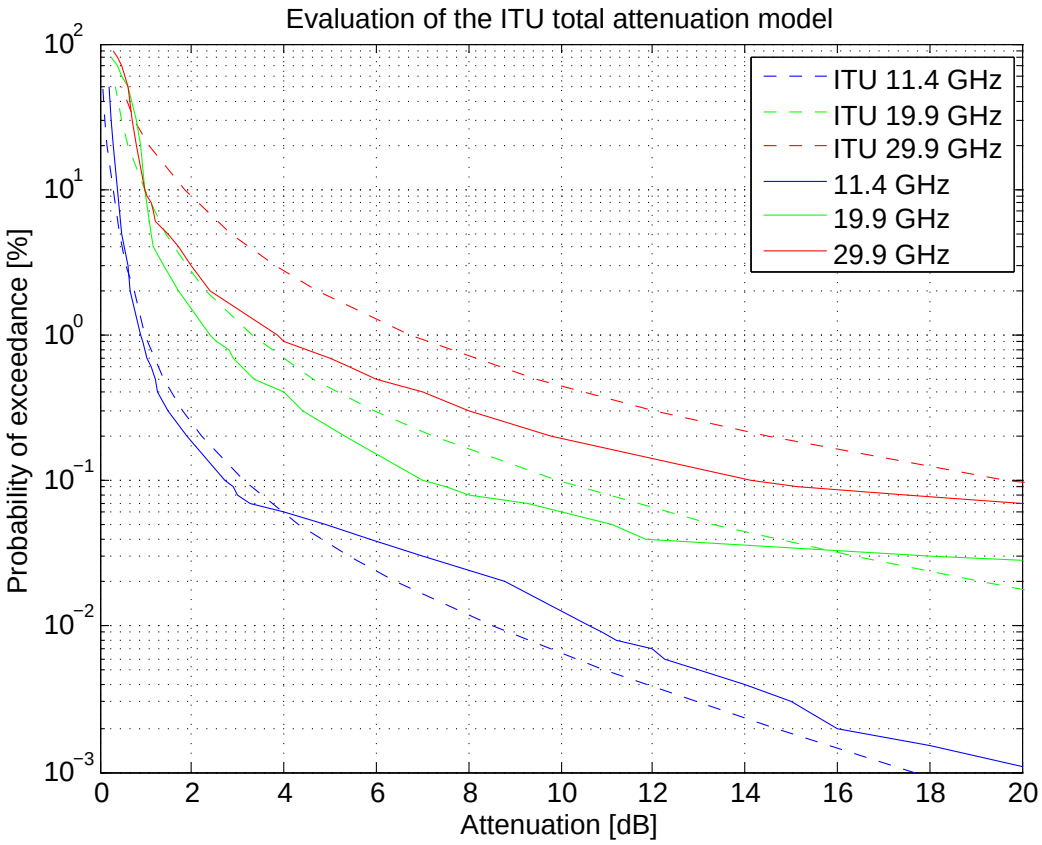

Figure 31: Total attenuation statistics evaluation of ITU model [49] compared with total attenuation derived from radiometer measurements

Table 18 presents the individual results of the testing variables for all three frequencies.

Testing variable	**11.4 GHz**	**19.9 GHz**	**29.9 GHz**
mean	-0.58 dB	0.64 dB	2.26 dB
standard deviation	0.97 dB	1.16 dB	1.88 dB

Table 18: Evaluation of the total attenuation statistics model

Except for the results at 11.4 GHz, the ITU model tends to overestimate the attenuation statistics derived from measurements. Based on the results derived by the testing variable, it could be assumed that the deviation between the measured and predicted attenuation statistics increase with increasing frequency.

In the following part of this section first attenuation statistics of the Alphasat mission are presented.
On 18 March 2014 the fixed satellite pointing of the Alphasat receiver antenna was readjusted due to the increasing satellite movement. By the readjustment a smaller daily

variation and a higher received signal power level was achieved. During the following 14 days the Ka- and Q-band beacon was recorded. The first Alphasat attenuation statistics for the period of 19.03.2014 until 01.04.2014 was computed and the results are presented in Figure 33 and Figure 34 below.

During the period of interest, unusual dry weather conditions were observed and only three minor rain events were measured.
In Figure 32 the measured rain events are shown, with an integration time of 1 hour. The three rain events were recorded during the measurement period from 19.03.2014 to 01.04.2014 by the ZAMG meteorological station at Graz University.

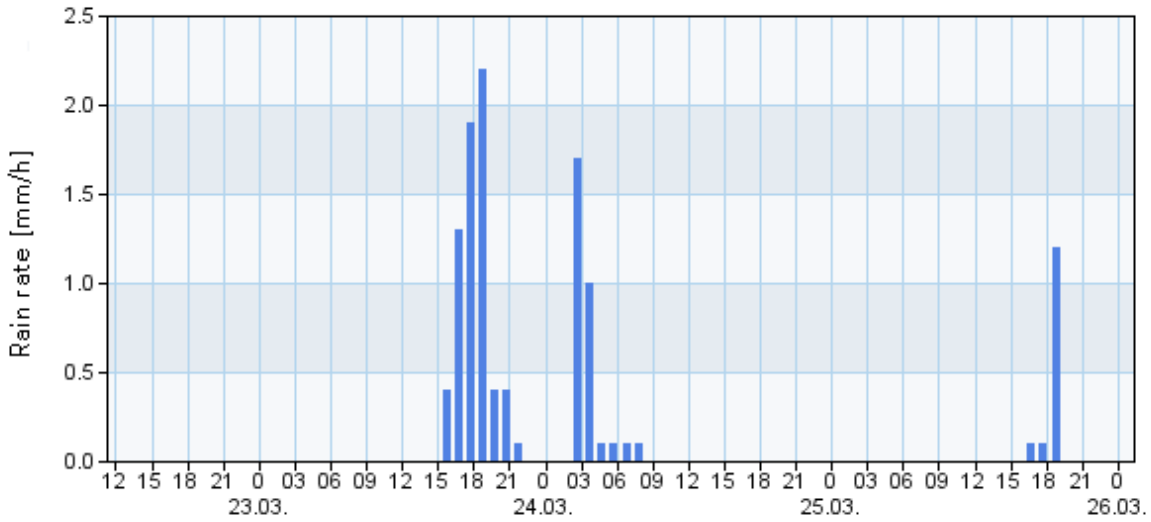

Figure 32: Recorded rain events taken and modified from the ZAMG website [21]

The ITU model recommended in P.618 [49] which was already evaluated above, predicts the rain attenuation for the indicated location, weather conditions and satellite link parameters for one year. Even though evaluation is not possible because of different conditions, the predicted ITU model results for the Alphasat Ka- and Q-band also have been added to the plots. It is expected that for a measurement period of one year the Alphasat attenuation statistic will approach the curve determined by the ITU model. However, due to the present conditions such as the very short measurement period and lack of rain events the significant gap between both curves was expected.

In Figure 33 and Figure 34 the first result of Alphasat attenuation statistics for Ka-band and Q-band are presented.

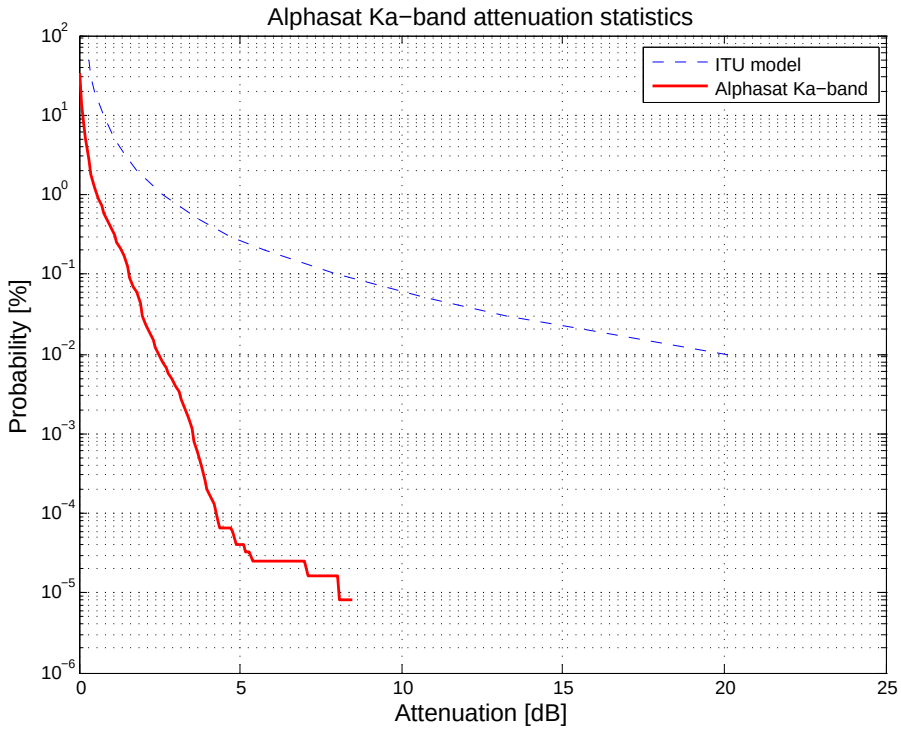

Figure 33: Alphasat Ka-band 14 days attenuation statistic

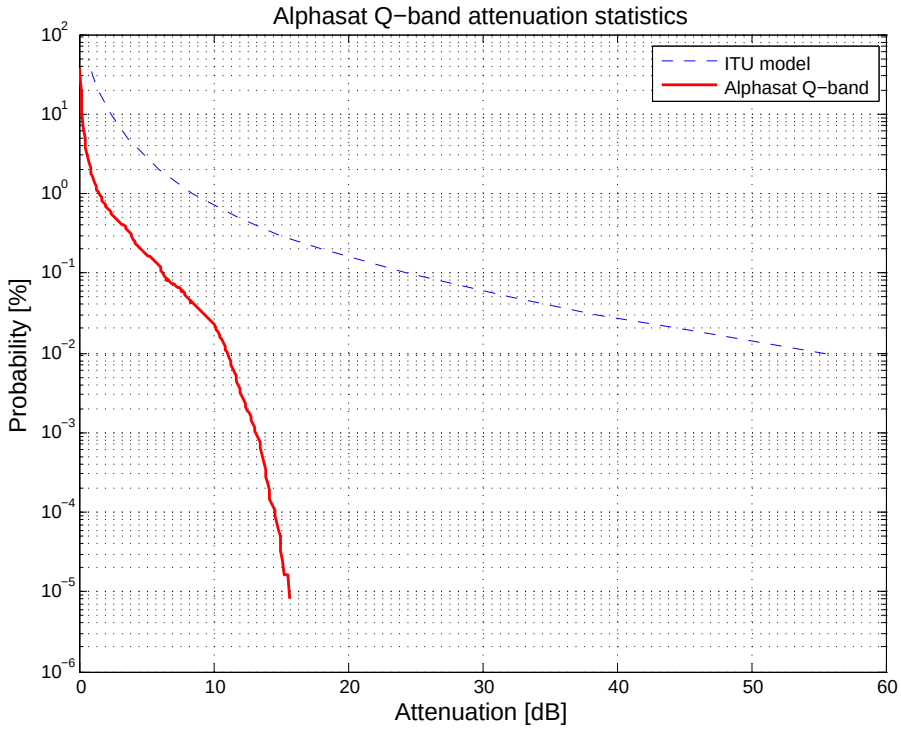

Figure 34: Alphasat Q-band 14 days attenuation statistic

9.2.6 Task 6 - Specific rain attenuation

The evaluation was performed with an equivolumetric rain drop size distributions measured by a 2DVD. Figure 35 presents the result for Ka-band. The figure shows the actual measured drop size distribution converted to specific attenuations due to rain (Ka2DVD) for both vertical and horizontal polarization. Furthermore, curves that represent the results derived by the ITU model and the theoretical result where the DSD was modelled with Marshall Palmer (MP) [41] are presented as well.

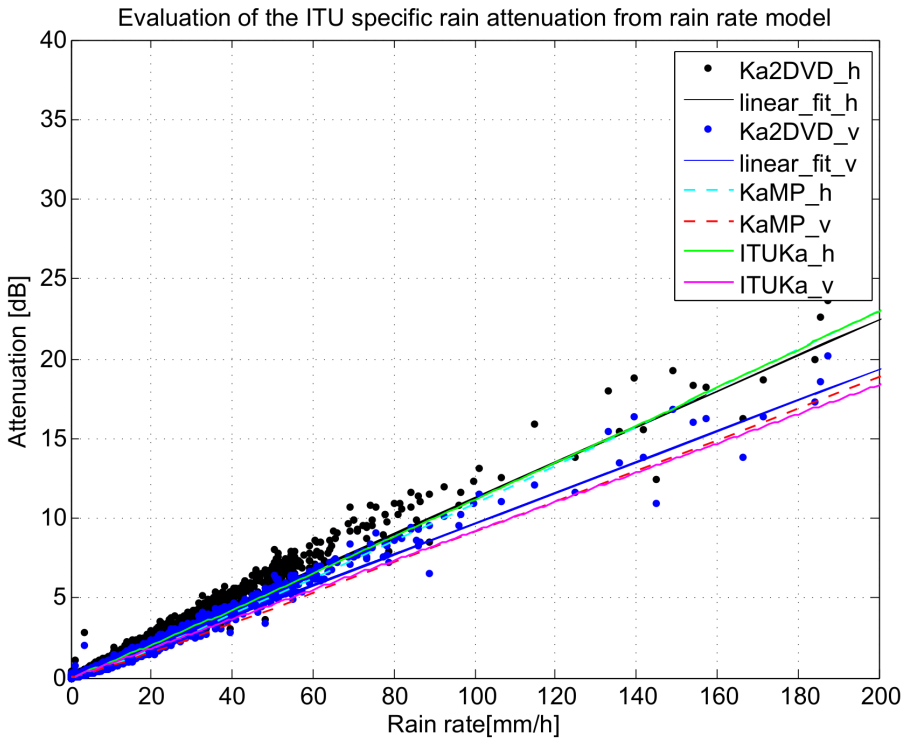

Figure 35: Evaluation of the ITU specific attenuation from rain rate model at Ka-band

The testing variables for the horizontal and vertical case are presented in Table 19 for Ka-band.

Testing variable	**horizontal**	**vertical**
mean	0.44 dB	-0.82 dB
standard deviation	0.63 dB	0.48 dB

Table 19: Evaluation of the specific rain attenuation model at Ka-band

Figure 36 illustrates the evaluation of the model results for Q-band at a frequency of 39.4 GHz. Amongst the specific rain attenuation for vertical and horizontal polarization also the theoretical rain attenuation based on Marshall-Palmer and the predicted results by the ITU model are presented.

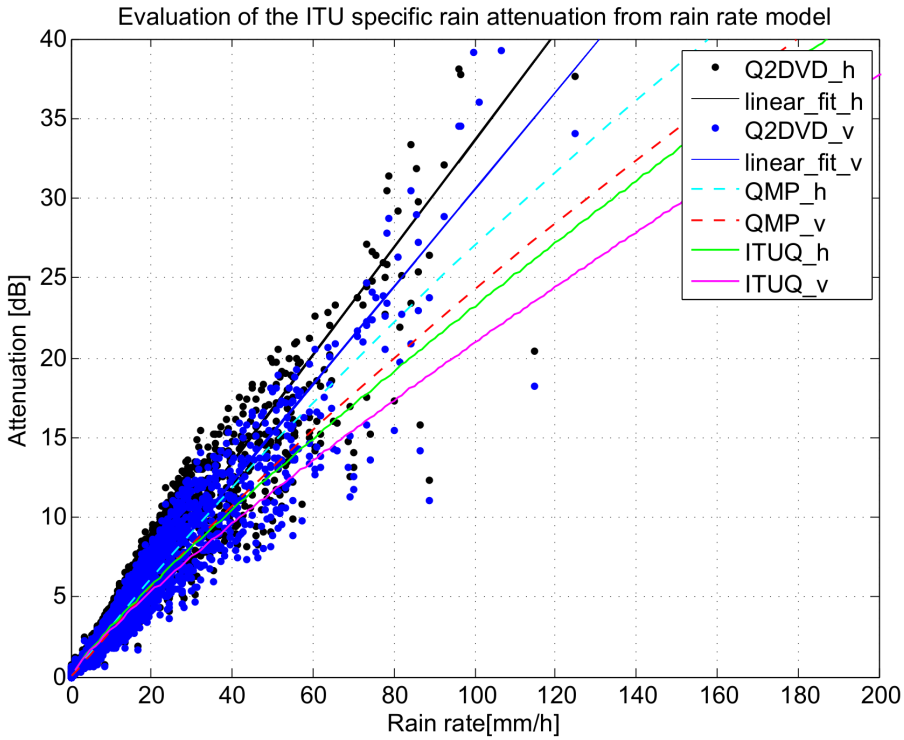

Figure 36: Evaluation of the ITU specific attenuation from rain rate model at Q-band

Table 20 presents the testing variable for horizontal and vertical polarization at Q-band.

Testing variable	**horizontal**	**vertical**
mean	-21.17dB	-19.89 dB
standard deviation	14.15 dB	13.44 dB

Table 20: Evaluation of the specific rain attenuation at Q-band

As a sample, Figure 37 shows the drop size distribution of a detected rain event on 15 October 2012. For direct comparison the theoretical approximation by Marshall-Palmer is indicated as yellow line as well. As the figure shows, the Marshall-Palmer does not accurately take into account rain drops with a large diameter. This fact could explain, why in Figure 35 and 36 these deviations between the measured and theoretically determined specific rain attenuation for different rain rates occur. The results derived by the theoretical rain drop size distribution and the ITU model are very similar. However, the ITU model requires the rain rate as input and therefore is not able to predict the event with high accuracy because no information about the actual drop size distribution is available. Rain drops with large equivolumetric diameter cause more attenuation and since they were not considered by the Marshall-Palmer distribution, the theoretical result underestimates the attenuation derived from the measurements. The evaluation also shows that large rain drops cause more attenuation in Q-band than in Ka-band.

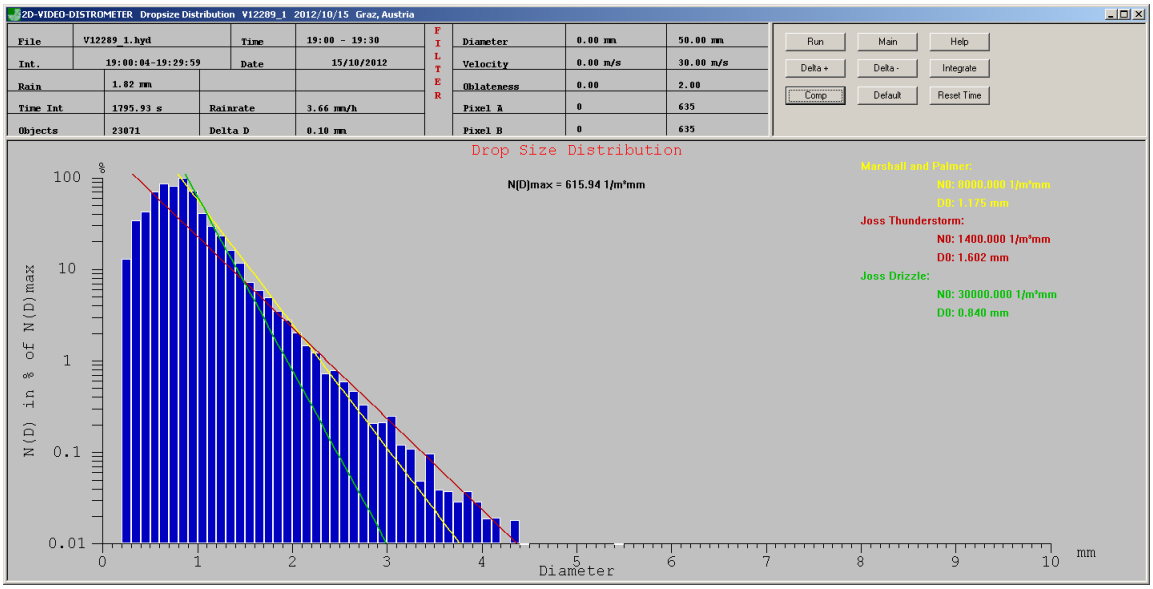

Figure 37: Sample drop size distribution generated with the disdrometer viewer software developed by Joanneum Research

9.2.7 Task 7 - Cloud attenuation

This task was performed to investigate the effect of cloud attenuation on the measured Q-band Alphasat beacon signal. To determine the cloud attenuation, the measurements by the radiometer were considered as well. The evaluation of the cloud attenuation ITU model provided in P.840 [51] rather corresponds to a plausibility check of actual measurements for three reasons. The available data set of Alphasat and radiometer measurement data covers less than a half month of observation. From the available dataset periods of rain, strong wind, and outages had to be excluded. Therefore, a period of clearly less than 14 days has been considered for this calculation. The ITU specific cloud attenuation model however was applied to compute cloud attenuation statistic for the month of December. For this reason, it was not expected that results derived from Alphasat measurements meet the curve provided by the ITU model. This comparison is understood as plausibility check because it is assumed that for a longer observation of one month, the curve will better approximate the result derived by the ITU model. Additionally, the statistics derived by the radiometer were added to cross-check the results derived by the beacon signal.
Another fact that additionally contributes to the deviation of this statistics is the template extraction of the signal. Since the Q-band beacon signal showed artefacts, the occurrence of rain events could not be detected automatically and therefore was not removed beforehand. The FFT template extraction was performed to remove low-frequent periodicities up to 6 hours. This threshold of 6 hours was chosen in order to avoid distortion of rain events.
The third reason, which is the lack of accurate information about clear sky periods adds additional significant uncertainty to the derived result. The radiometer setting of 90° elevation was used for testing. During the first two days, the sun was visible 100% of the day and thus these measured radiometric attenuations were considered to approximate the gaseous attenuation at clear sky. Thus, as a first approach, the clear sky variation was assumed to be constant.

The cloud attenuation statistics derived from Alphasat beacon data and those derived from radiometer measurements are illustrated in Figure 38. Additionally, the predicted attenuation due to clouds by the ITU model is illustrated there as well.

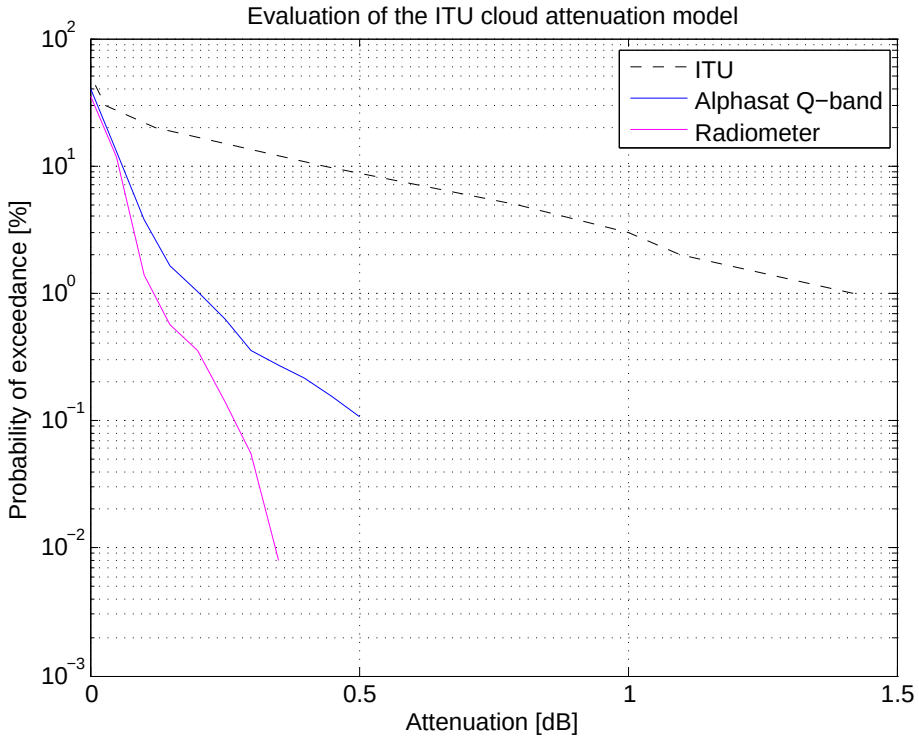

Figure 38: Cloud attenuation statistics from Q-band and radiometer measurements and the ITU model

According to the results in Figure 38, less cloud attenuation was observed by the radiometer. The radiometer results are considered to be more accurate because the Q-band beacon signal is distorted by small oscillations due to non optimal template extraction. This effect might not have much impact on large fade events but for cloud attenuation high sensitivity is needed. This could potentially be the reason why the cloud attenuation statistics at Q-band reports higher attenuation values.

9.2.8 Task 8 - Fade duration

The evaluation of the ITU fade duration model was executed with Olympus beacon measurements at 12 GHz, 20 GHz and 30 GHz. The fade duration probability of occurrence statistics are shown in the Figure 39, 40 and 41. For direct comparison, the predicted statistics derived by the ITU have been added to the figures. The evaluation at these three frequencies reveals that the ITU model matches the statistics best at 30 GHz. However, there is still room for improvement due to the large divergence.

The testing variables for the fade duration evaluation at 12 GHz, 20 GHz and 30 GHz are presented in Table 21, Table 22 and Table 23.

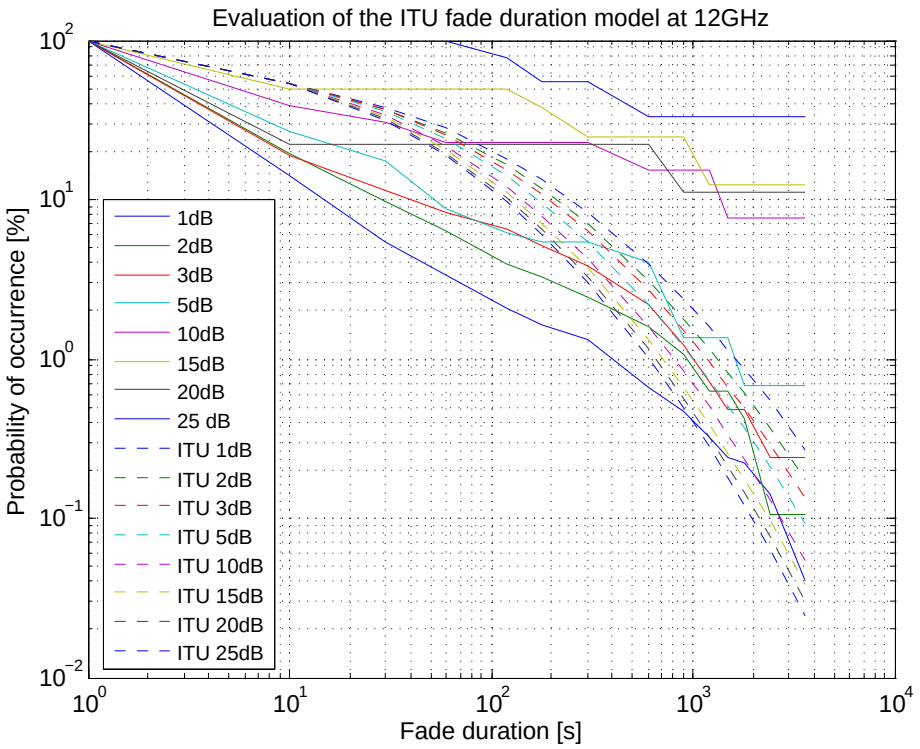

Figure 39: Evaluation of the ITU fade duration model at 12 GHz

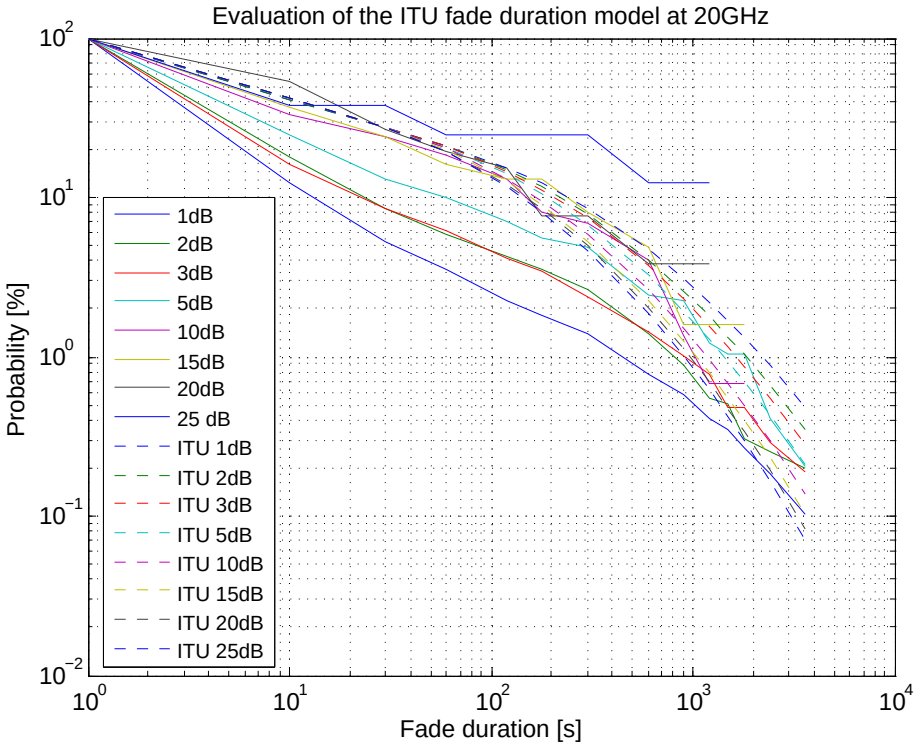

Figure 40: Evaluation of the ITU fade duration model at 20 GHz

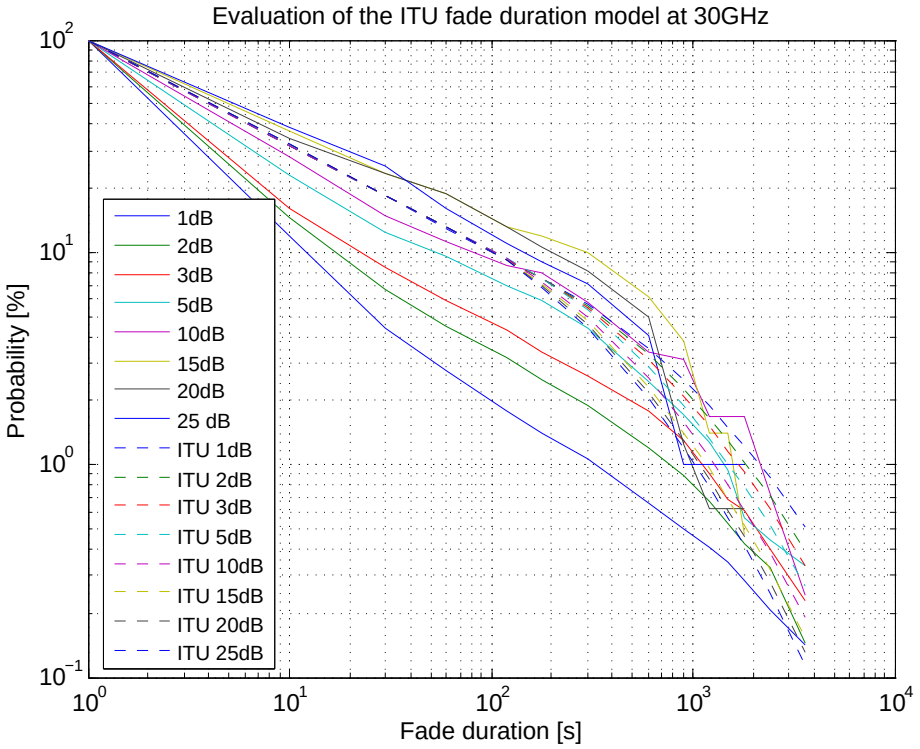

Figure 41: Evaluation of the ITU fade duration model at 30 GHz

Attenuation threshold [dB]	**1**	**2**	**3**	**5**	**10**	**15**	**20**	**25**
mean	1.64	0.87	0.47	-0.13	-1.91	-2.46	-2.12	-3.34
standard deviation	0.55	0.46	0.48	0.85	1.72	1.83	2.12	2.18

Table 21: Evaluation of the fade duration ITU model at 12 GHz

Attenuation threshold [dB]	**1**	**2**	**3**	**5**	**10**	**15**	**20**	**25**
mean	1.55	0.99	0.85	0.24	0.02	-0.38	-0.44	-1.14
standard deviation	0.48	0.34	0.36	0.37	0.22	0.51	0.60	1.09

Table 22: Evaluation of the fade duration ITU model at 20 GHz

Attenuation threshold [dB]	**1**	**2**	**3**	**5**	**10**	**15**	**20**	**25**
mean	1.39	0.89	0.56	0.17	-0.26	-0.44	-0.23	-0.32
standard deviation	0.44	0.28	0.22	0.17	0.38	0.35	0.31	0.30

Table 23: Evaluation of the fade duration ITU model at 30 GHz

First fade durations statistics of Alphasat Q-band for different attenuation and fade duration thresholds are presented in the following as well. Figure 42 presents the probability of occurrence statistic for Q-band. The probabilities of exceedance of fade duration for Q-band are presented in Figure 43.

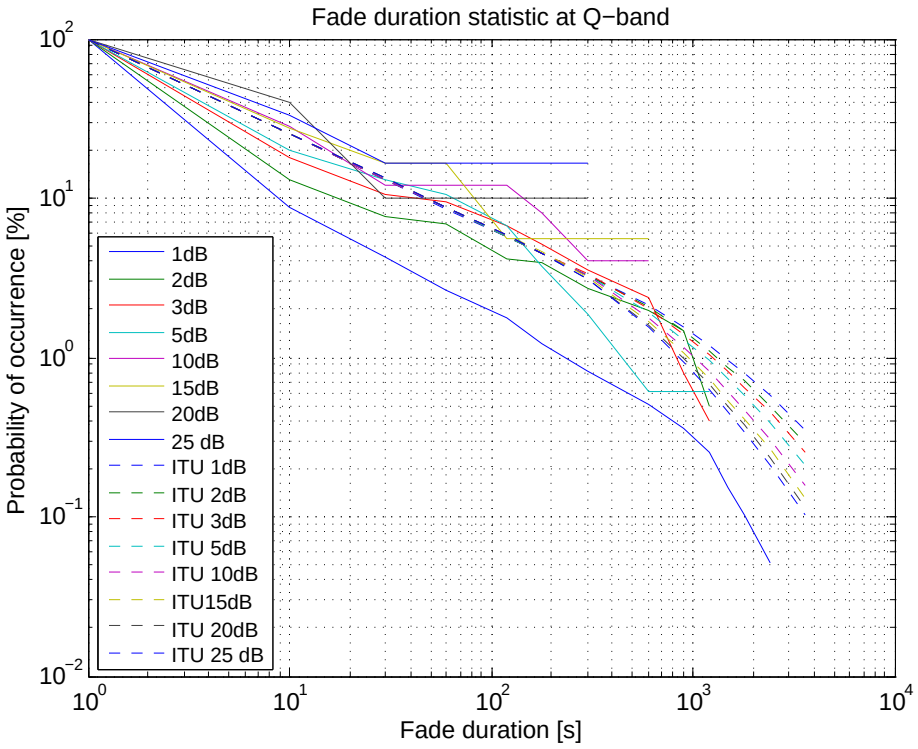

Figure 42: Fade duration probability of occurrence at Alphasat Q-band

The evaluation results of both Q-band statistics based on the testing variable are presented in Table 24 and Table 25.

Attenuation threshold [dB]	**1**	**2**	**3**	**5**	**10**	**15**	**20**	**25**
mean	1.38	0.3	0.15	0.3	-0.33	-0.36	-0.4	-0.74
standard deviation	0.58	0.29	0.38	0.43	0.34	0.42	0.49	0.63

Table 24: Fade duration probability of occurrence ITU model evaluation at Q-band

Attenuation threshold [dB]	**1**	**2**	**3**	**5**	**10**	**15**	**20**	**25**
mean	-0.73	-0.33	-0.34	-0.44	-0.06	-0.05	-0.13	-0.53
standard deviation	0.18	0.27	0.29	0.22	0.53	0.43	0.7	1.09

Table 25: Fade duration probability of exceedance ITU model evaluation at Q-band

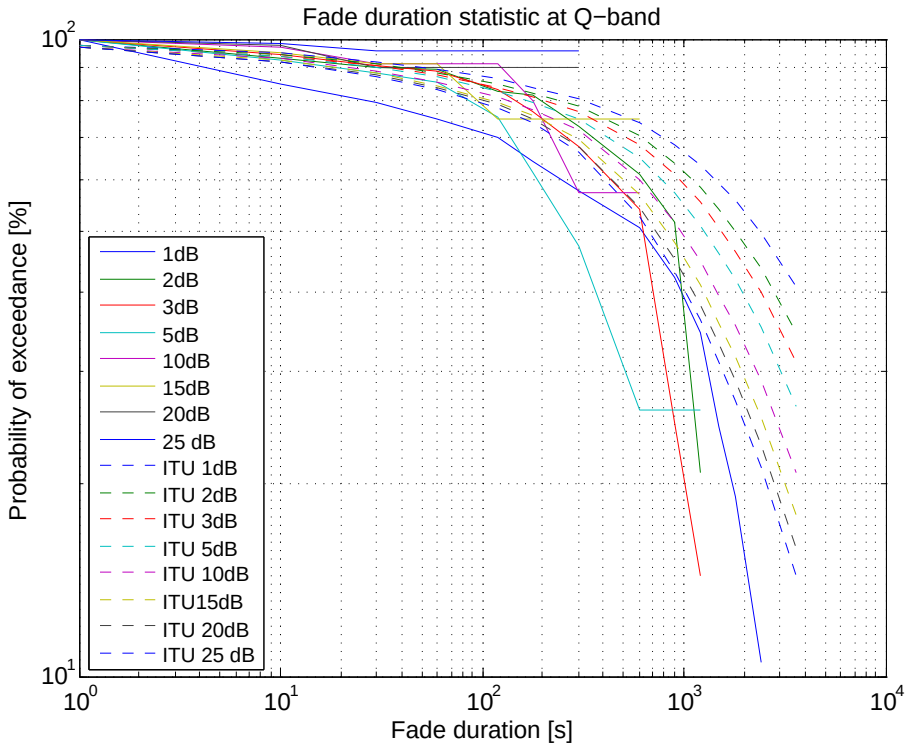

Figure 43: Fade duration probability of exceedance at Alphasat Q-band

The comparison of Olympus evaluation results indicates that the ITU model predicts the probability of occurrence more accurately at higher frequencies. Also for Q-band the evaluation results show a good match. The probability of exceedance at Q-band was evaluated with good results as well. Nevertheless, the testing variables revealed that the most accurate prediction was achieved at attenuation levels between 3 dB to 5 dB.

It is noticeable that the mean values of the testing variables derived at different frequencies show a similar behaviour. The mean values are highest at very low and very high attenuation. This effect is caused by the unusual behaviour of the ITU fade duration model output which was also reported by Garcia del Pino et al. [16] as shown in the chapter 8. Based on this fact, the matching of predicted attenuations in the range of the 5 dB threshold is more accurate.

9.2.9 Task 9 - Interfade duration

The recommendation ITU-R P.1623 [42] does not provide a model to predict interfade duration. Nevertheless, it is assumed that the distribution of the interfade occurrence probability follows the shape of a log-normal distribution. Despite the fact that evaluation is not possible in this task, interfade duration statistics of Olympus measurements at 12 GHz and Alphasat and Q-band measurements have been computed.

Interfade duration statistics for the 12 GHz Olympus beacon signal are presented in the following. Figure 44 presents the probability of occurrence and in Figure 45 the probability of exceedance is shown.

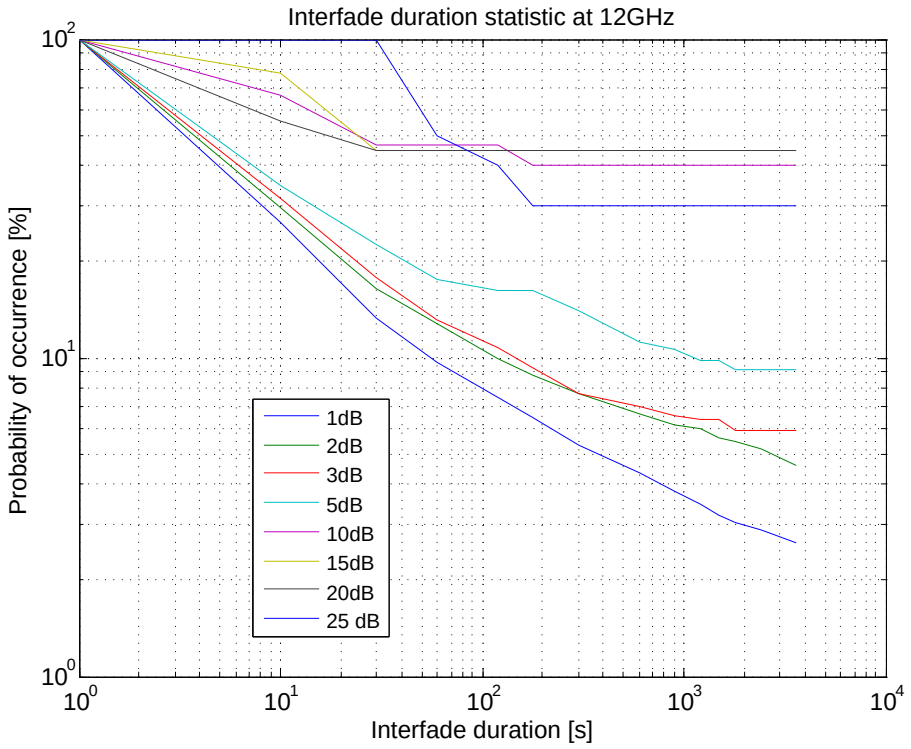

Figure 44: Probability of occurrence interfade duration statistic at 12 GHz

First interfade duration statistics have been derived for Alphasat beacon measurements for less than 30 days of observation. The occurrence probabilities of interfade durations and exceedance probabilities for Q-band are presented in Figure 46 and Figure 47.

It is noticeable that statistics of interfade duration are not very common in open literature. Therefore, not much results for comparison are available.
The log-normal shape of the distribution as assumed by the ITU recommendation P.1623 [42] could be confirmed by the probability of occurrence results derived from measurement data. In this section interfade duration statistics derived at 12 GHz and 40 GHz are compared. The comparison shows that interfade durations at 12 GHz are longer than 40 GHz because at 40 GHz the influence of atmospheric events on the signal is much stronger. Thus, in general, a larger number of occurring fades causes more interfade interruptions and therefore leads to shorter individual interfade times.

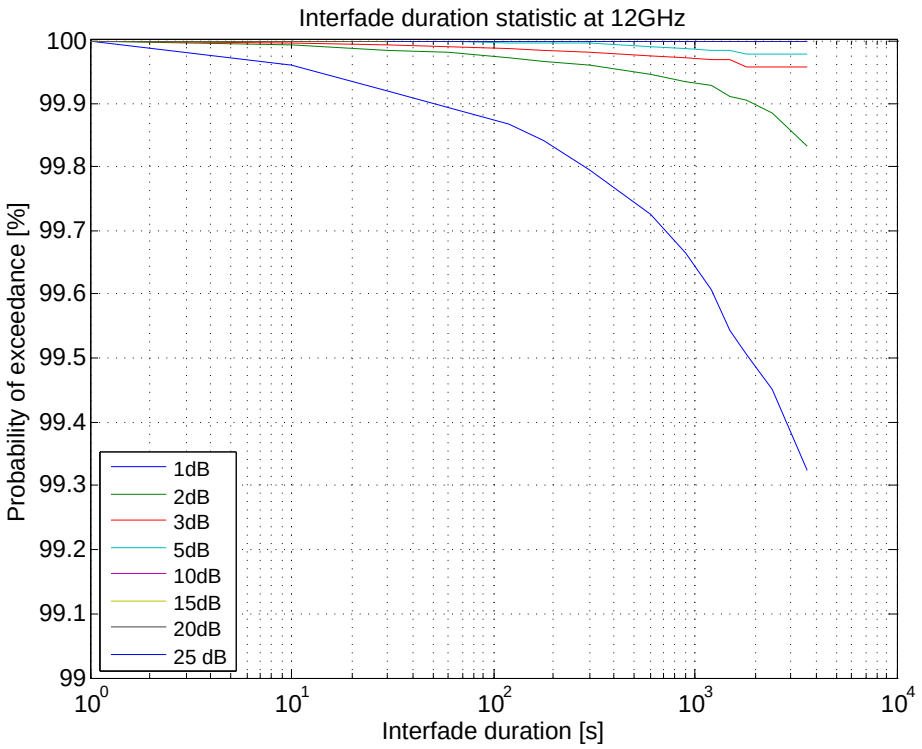

Figure 45: Probability of exceedance interfade duration statistic at 12 GHz

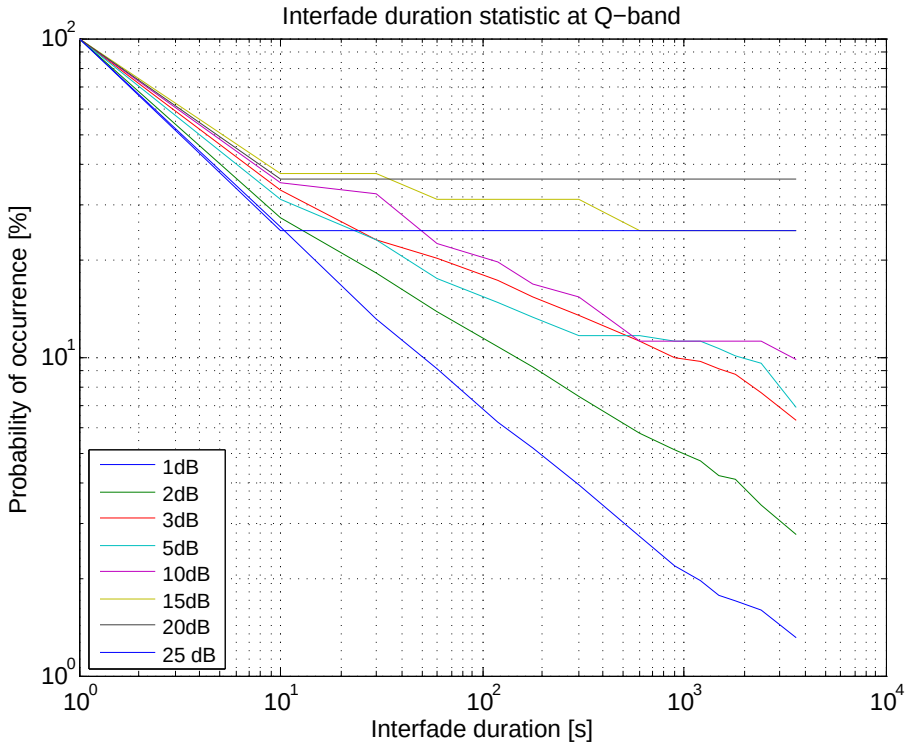

Figure 46: Probability of occurrence interfade duration statistic of Alphasat Q-band

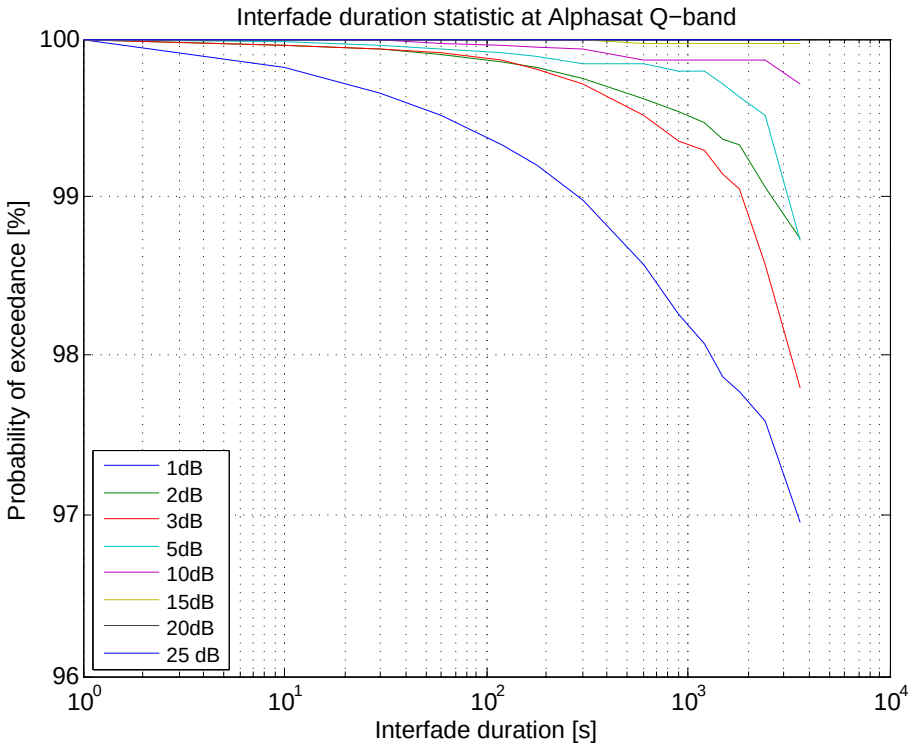

Figure 47: Probability of exceedance interfade duration statistic of Alphasat Q-band

9.2.10 Task 10 - Fade slope

The modelled fade slope statistics at 12 GHz, 20 GHz and 30 GHz obtained by the ITU model provided in ITU-R P.1623 [42] were evaluated by fade slope statistics computed from Olympus beacon data. The fade slope statistics were determined for 7 different attenuation thresholds in the range between 1 dB and 25 dB. Additionally, the absolute fade slope statistics at 12 GHz, 20 GHz and 30 GHz are presented as well. In the following figures, results obtained from ITU models are indicated as dashed line and fade slope statistics derived from Olympus beacon measurements are presented as solid line.

The fade slope derived from beacon measurements at 12 GHz is presented in Figure 48. The absolute fade slope statistic at 12 GHz is shown in Figure 49.

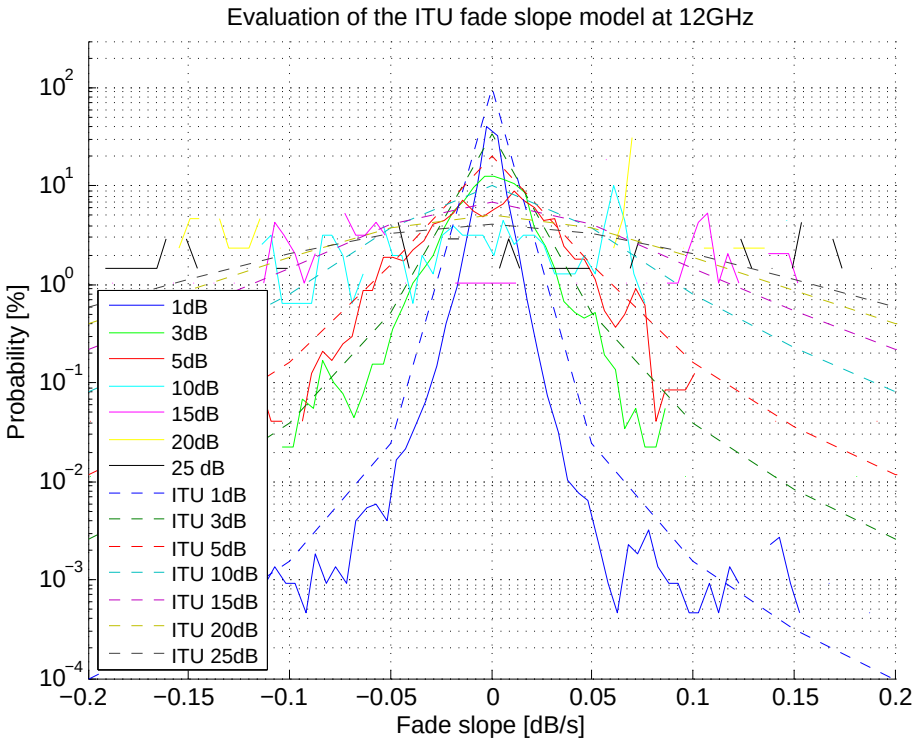

Figure 48: Evaluation of the ITU fade slope model at 12 GHz

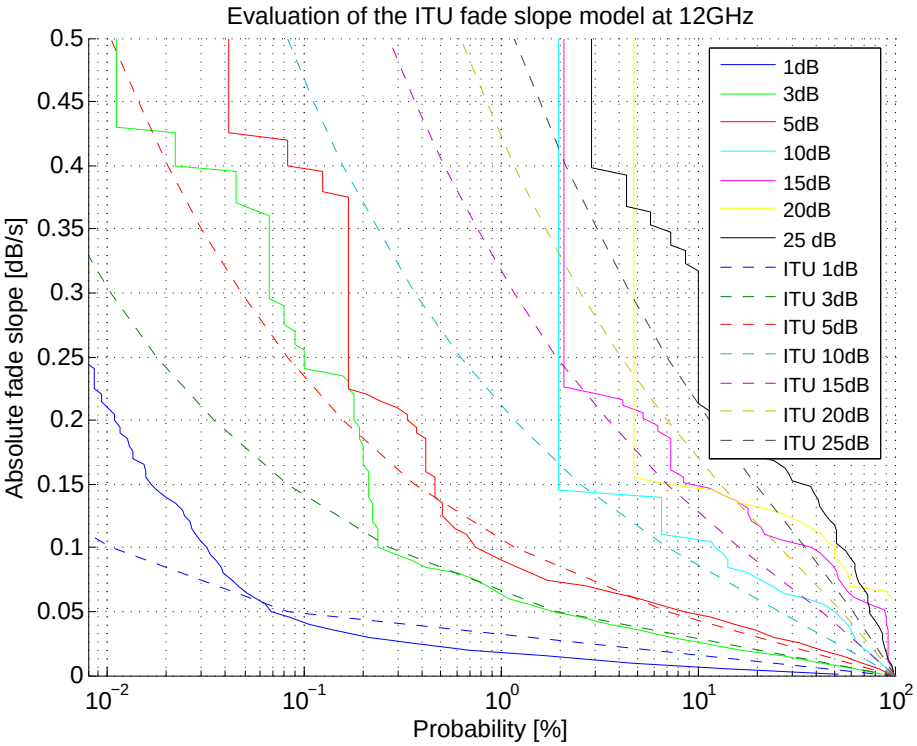

Figure 49: Evaluation of the ITU fade slope for absolute fade slope at 12 GHz

The fade slope statistic at 20 GHz is presented in Figure 50 and Figure 51 illustrates the results of the absolute fade slope statistic.

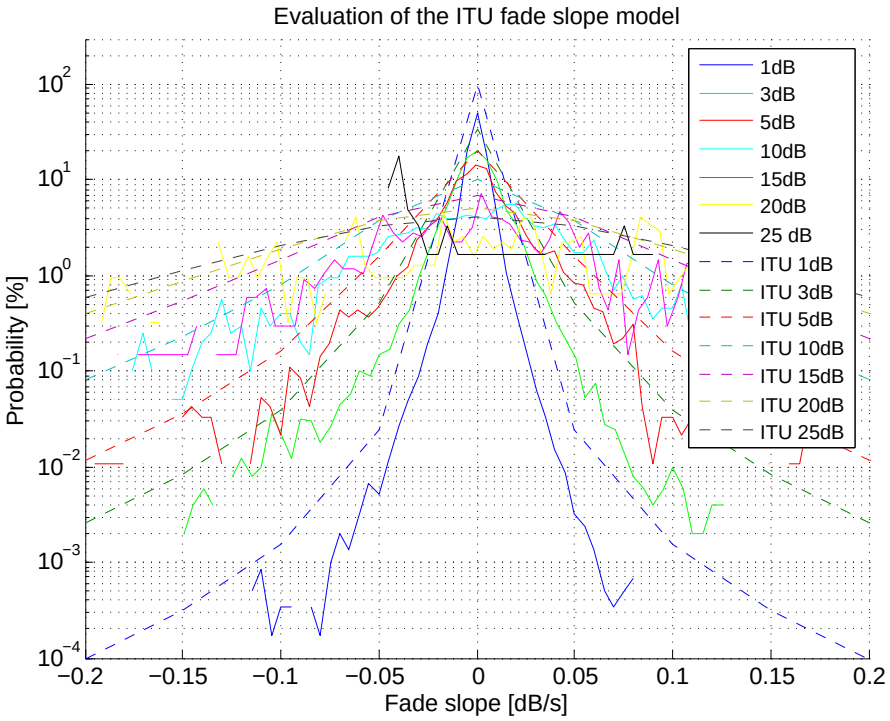

Figure 50: Evaluation of the ITU fade slope model at 20 GHz

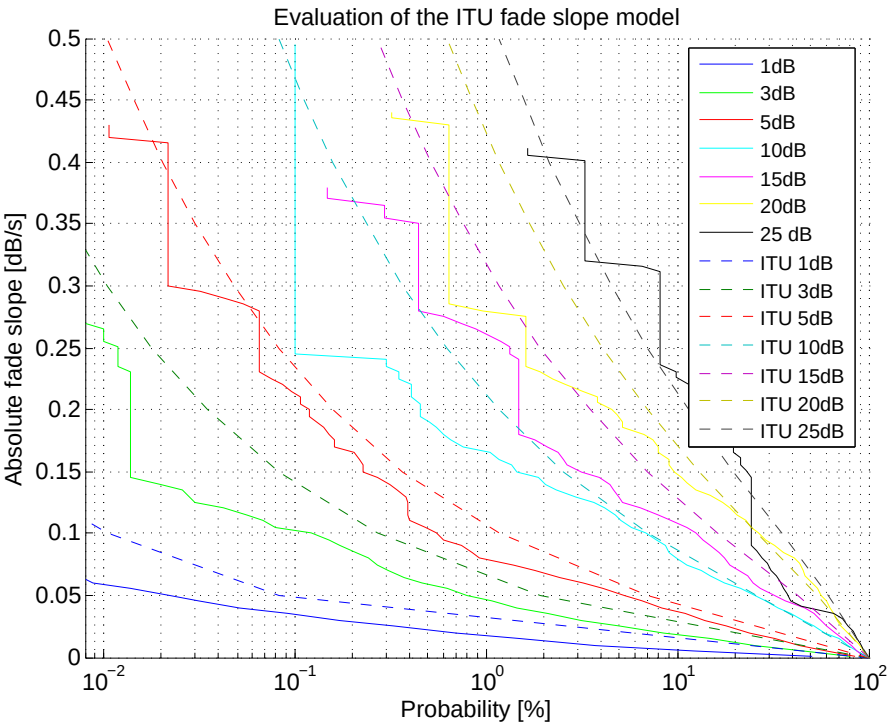

Figure 51: Evaluation of the ITU fade slope for absolute fade slope at 20 GHz

The results for 30 GHz are presented in Figure 52. The absolute fade slope statistic at 30 GHz is shown in Figure 52.

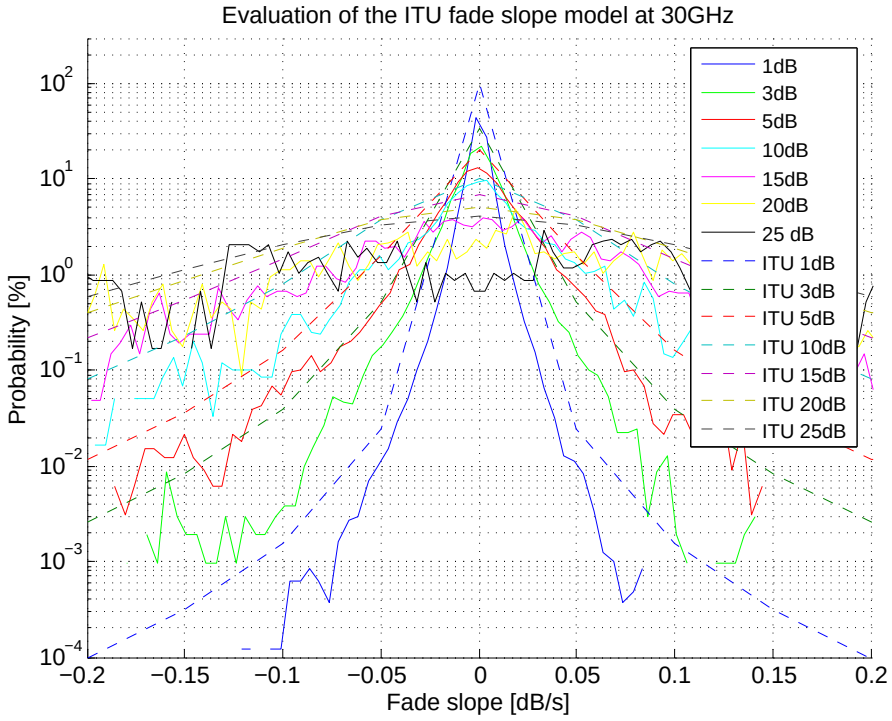

Figure 52: Evaluation of the ITU fade slope model at 30 GHz

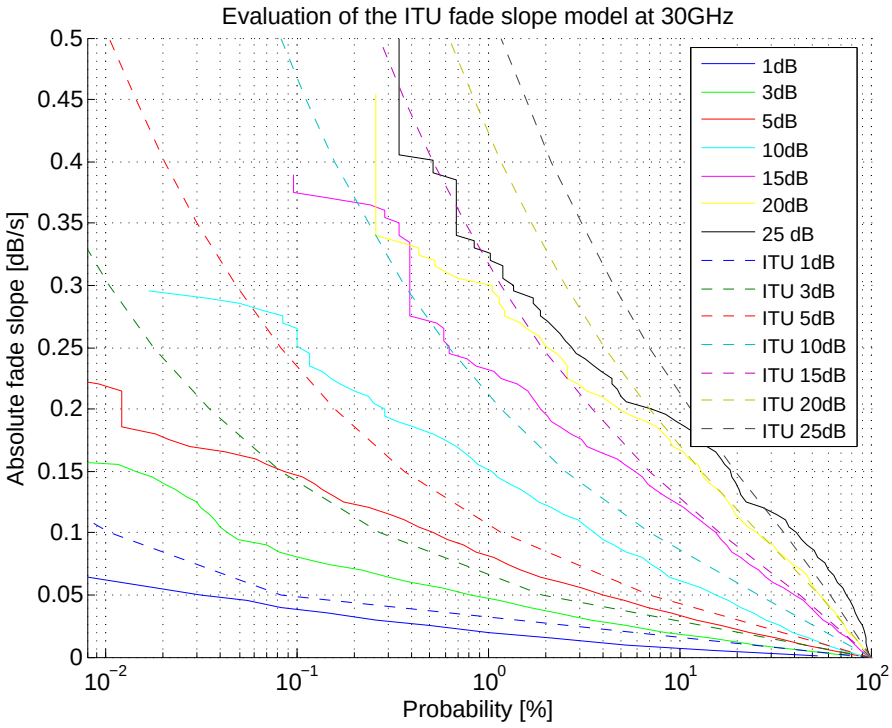

Figure 53: Evaluation of the ITU fade slope for absolute fade slope at 30 GHz

Attenuation threshold [dB]	**1**	**3**	**5**	**10**	**15**	**20**	**25**
mean	1.26	1.56	1.55	1.73	1.59	1.74	1.5
standard deviation	1.31	0.97	0.86	0.67	0.93	0.79	1.0

Table 26: Evaluation of the fade slope statistic model at 12 GHz

Attenuation threshold [dB]	**1**	**3**	**5**	**10**	**15**	**20**	**25**
mean	1.7	1.56	1.4	1.2	1.03	1.14	1.38
standard deviation	0.89	0.73	0.84	0.83	0.86	0.94	1.06

Table 27: Evaluation of the fade slope statistic model at 20 GHz

Attenuation threshold [dB]	**1**	**3**	**5**	**10**	**15**	**20**	**25**
mean	1.69	1.51	1.21	1.07	0.89	0.95	1.04
standard deviation	0.34	0.41	0.42	0.55	0.72	0.78	0.88

Table 28: Evaluation of the fade slope statistic model at 30 GHz

The Tables 26, 27 and 28 show the evaluation results derived by the testing variable of the fade slope statistics at different attenuation thresholds. The ITU model for the prediction of fade slope statistics however is not dependent on frequency. Based on the results derived by the testing variables, the ITU fade slope model prediction matches best the fade slope statistic derived at 30 GHz. However the model tends to overrate the fade slope statistics computed from measurement results. By visual inspection of the absolute statistics though, the ITU prediction of the absolute fade slope statistic achieves best accuracy for the statistic computed from 20 GHz data. The evaluation reveals that also absolute fade slope statistics results derived from the measurements are constantly overrated by the ITU model.

10 Modified models under investigation

ITU members states have the possibility to submit proposals for new or modified ITU models to the ITU. In this chapter potential modifications are reviewed. At the last ITU meeting, many recommendations that are considered in this thesis already have been modified. Therefore, at the moment no new contributions for potential improvements are found at the ITU website.
Evaluation results presented in chapter 9 do not show significant systematic deviations compared to the results predicted by the ITU model. Therefore a specific research for modified models regarding a such model deviation is hardly possible. Nevertheless, in the following, by means of recently proposed models in open literature, approaches for possible modifications of ITU models developed for individual regions are shown.
Many published papers regarding ITU models aim to improve the ITU model for the prediction in tropic regions. A sample for this fact presents the study on cloud attenuation in the tropics carried out by T. V. Omotosho et al. in [34]. The paper concluded that the cloud attenuation in Ka-band predicted by the ITU model underestimates radiosonde observation by approximately 2 dB. Obviously, the models provided by the ITU achieve different accuracies depending on climate zones.

10.1 Frequency scaling model

In [22] a method is proposed to improve the accuracy of the frequency scaling factor compared to the long-term frequency scaling model provided by the ITU. The study was executed with Ka-band data measured at 58 earth stations in China. In this new method, the predicted rain attenuations derived from the ITU-R recommendation P.618 [49] version 8 are used to determine frequency attenuations for different frequencies and rain rate. Based on this knowledge the following frequency scaling formula was derived. As it is stated, this formula is assumed to be valid in the frequency range between 20 and 39 GHz.

$$A_2 = \frac{-0.081 f_2^2 + 50.188 f_2 - 585.04}{-0.081 f_1^2 + 50.188 f_1 - 585.04} \cdot A_1 \quad f \in \{20, .., 39\}\, GHz \tag{62}$$

The evaluation was performed with a downlink frequency f_1 of 20 GHz and an uplink frequency f_2 of 30 GHz.
Figure 54 illustrates the evaluation results as presented by [22]. The green curve represents the measured relations of rain attenuation, the red curve represents the result derived by the new model and the prediction by the ITU long-term frequency scaling model is presented by the blue curve.

As the evaluation in Figure 54 shows, this new method predicts the locally measured rain attenuation quotient of both frequencies with significant higher accuracy. While the predictions of the ITU frequency scaling model for low attenuation levels up to 5 dB

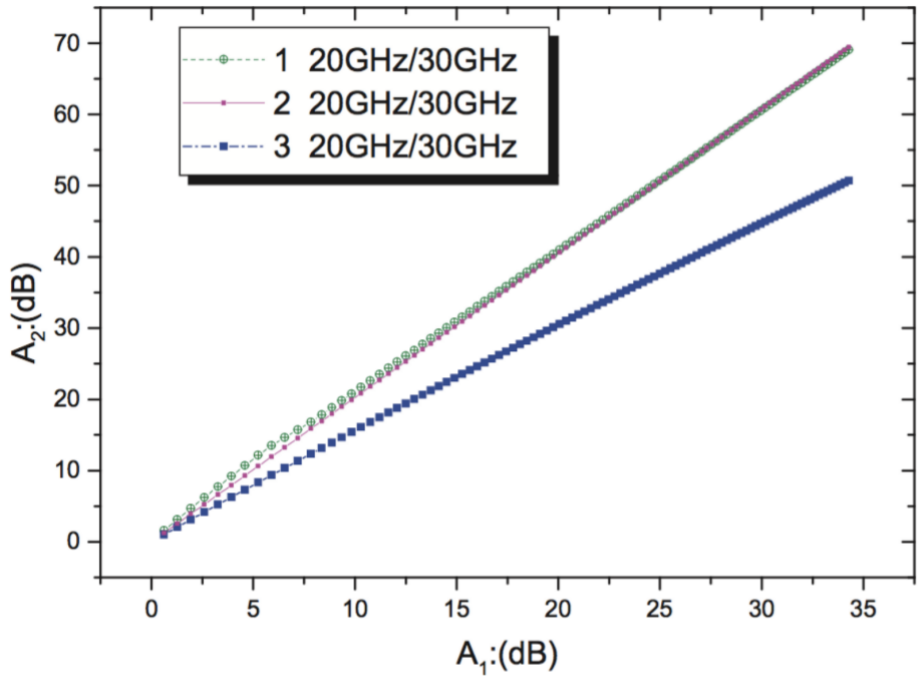

Figure 54: Evaluation of the proposed frequency scaling model at Ka-band [22]

were acceptable, especially at higher frequencies the error increased significantly. The authors conclude that better accuracy is reached by the new formula due to the fact that the formula is better adapted to the local climatic conditions in China than the ITU recommendation.

10.2 Fade slope model

A model to improve the fade slope prediction model recommended by the ITU-R P.1623 [42] is introduced by Xin at al. in [53]. The idea of this new method is to get better accuracy by computing the standard deviation of the conditional fade slope σ_ζ as function of the attenuation and time interval instead of the formula recommended in [42]. With this measure, the predicted slopes should be better adapted to local measurement results.

$$\sigma_\zeta = S(A) \cdot \sigma(\Delta t) \tag{63}$$

$$S(A) = -0.0170A^2 + 0.3538A - 0.4992 \tag{64}$$

$$\sigma(\Delta t) = -7.3162 \cdot 10^{-9} \cdot \Delta t^3 + 2.8292 \cdot 10^{-6} \cdot \Delta t^2 - 3.8974 \cdot 10^{-4} \Delta t + 0.0382 \tag{65}$$

A comparison of the results derived by this new method and the ITU model reveals improved performance because of the modification in computation. The paper finally recommends the improved model for the design of satellite communication links.

10.3 Rain attenuation model

Changsheng et al. introduce in [8] a method to predict rain attenuation based on the so-called EXCELL rain cell model. In this new prediction model a path adjustment factor needed as model input is derived from statistics.
The difficulty in this model is to describe the spatial distribution of the rain rate. The used EXCELL model is based on radar measurements. It describes the rain rate profile inside a rain cell as exponential function. This means there is an exponential decay of the rain rate from a single maximum. For the model it is assumed that the slant path crosses the center of only one rain cell. The step-by-step model as proposed in this paper [8], is explained in the following.
In step 1 the local rain rate R_p that is exceeded for a certain probability $p[\%]$ has to be determined. If no measurement data is available, the model provided by ITU-R P.837 [45] can be used instead.
In step 2 the isotherm height h_0 has to be obtained based on the numerical map provided by ITU-R P.839. Then, the rain height can be computed with the following equation:

$$h_R = h_0 + 0.36 \quad [km] \tag{66}$$

Step 3 computes the length of the slant path. The following equation is valid for elevation angles that are greater than or equal to 5°.

$$L_s = \frac{h_R - h_s}{sin\Theta} \tag{67}$$

where h_s denotes the height above the sea level [km] of the site and Θ is the elevation angle indicated in [degree].
For elevation angles Θ smaller than 5° the following equation has to be applied, where R_e indicates the effective radius of the Earth that is assumed with $R_e = 8500km$.

$$L_s = \frac{2(h_R - h_s)}{((sin^2\Theta + \frac{2(h_R - h_s)}{R_e})^{1/2} + sin\Theta)} \tag{68}$$

Afterwards in step 4 the path adjustment factor is calculated by:

$$r = 1.47 R_{OS}^{-0.55 + \frac{1.59}{L_s}} L^{1.43 f^{-0.76}} \tag{69}$$

here, R_{OS} denotes the point rain fall rate and the parameter f is the frequency indicated in [GHz].
In the final step 5 for an average year the exceeded probability $p[\%]$ of the attenuation is computed.

$$A(p) = k(r(p)R_0(p))^{\alpha} L_S \tag{70}$$

This new method was compared with results derived by the ITU recommendation. As the paper [8] reports, the comparison revealed an improvement of accuracy due to the new proposed method.

11 Potential improvements

In this chapter potential improvements of ITU recommendations are discussed. The proposed potential improvements have been identified in the course of the evaluation process.

11.1 Specific rain attenuation

Bringi et al. analyzed in [7] the drop size distribution of rain events in different climatic areas by disdrometer and radar measurements. There it is shown that for steady rain events the average mass weighted drop diameter D_m vs. the $logN_w$ shows an inverse relationship. Where the parameter N_w $[mm^{-1}m^{-3}]$ is the same as N_0 for an equivalent exponential drop size distribution. More detailed information on these parameters is provided in [7].

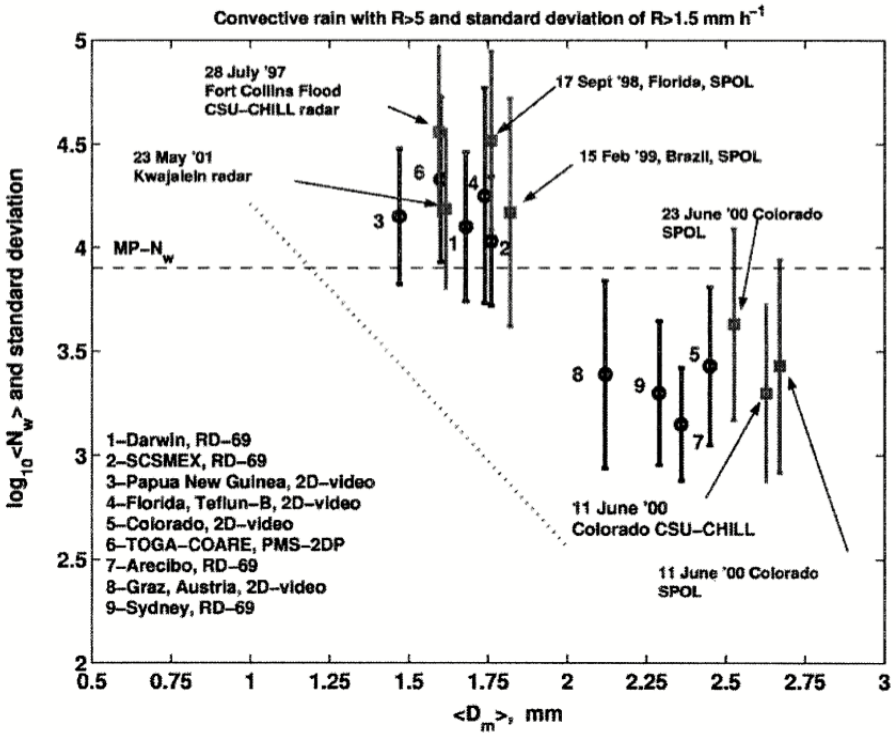

Figure 55: The average of $log_{10}N_w$ vs. D_m derived from disdrometer and radar measurements as indicated for convective rain [7]

Figure 55 presents the measurement results for convective rain as reported by [7]. The parameter $Log_{10}N_w$ is indicated with $\pm 1\sigma$ standard deviation bars. The dotted diagonal line indicates the least squares fit for steady rain events. As this figure shows, the results of the measurement sites can be classified in two groups. The paper calls these two groups "maritime-like" and "continental-like". The sites that are part of the maritime-like group

report drop size distributions that are characterized by a significantly high concentration of small rain drops. In contrast to that the maritime-like cluster, the continental-like cluster recorded a smaller number density but larger sized rain drops.
The rain drop size distribution shows for convective rain variations dependent on the climate. Based on this fact, a prediction method of rain attenuation that relies on local rain rate data is due to the lack of rain specific information not able to accurately predict the actual rain attenuation of a specific rain event. This phenomenon was also observed at the evaluation in task 6. By comparison with disdrometer measurements, the rain attenuation predicted by the ITU underestimates the results.
For improvement of the current ITU rain attenuation model [49], a modified prediction method could be proposed that takes local drop size distribution measurements takes into account.

11.2 Interfade duration

Investigation on interfade duration is a rather rare topic in open literature in the field of propagation. Hence, also the recommendation ITU-R P.1623 [42] does not provide a model to predict interfade duration statistics for different attenuation levels and interfade durations at a frequency and elevation angle of interest. From a satellite service provider's viewpoint though, this statistic provides crucial information about the expected uptime of a system. Eventually, the service provider needs to satisfy the guaranteed system uptime that is usually set at a very high percentage of time.
H. Fenech et al. [20] particularized the importance of exact models for atmospheric effects especially, regarding the quality of service, from the view point of the satellite operator Eutelsat by the following statement:

> "Space-time channel characterization and modeling of the propagation channel will certainly help in the prediction and optimization of quality."

Based on this statement it could be concluded that further investigation in more precise prediction models and therefore also an appropriate interfade duration model is of interest not only for scientific reasons but would be also of great value for commercial use.

11.3 Frequency scope of ITU models

The discussed ITU propagation models show strong variations in their applicable frequency range. In Table 29 the models and their constraints in frequency are listed to provide an overview. As the overview in this table reveals especially for the prediction of scintillation and fade slope there is backlog demand to adapt frequency range of the model.

According to the frequency scope limits of the ITU models, they are not fully applicable to intended future Q/V-band satellite system channels. It can be assumed that satellite missions in Q/V-band result in essential findings that enable modification of ITU models regarding this aspect. However, a quick adaption of the models would for sure benefit to evolve satellite services at Q/V-band as standard mode.

Model	Recommendation	Frequency range
Fade duration	ITU-R P.1623 [42]	10 GHz - 50 GHz
Fade slope	ITU-R P.1623 [42]	10 GHz - 30 GHz
Cloud attenuation	ITU-R P.840 [51]	up to 1000 GHz
Rain attenuation from rain rate	ITU-R P.618 [49]	up to 55 GHz
Conditional frequency scaling	ITU-R P.618 [49]	19 GHz - 55 GHz
Long-term frequency scaling	ITU-R P.618 [49]	7 GHz - 55 GHz
Scintillation	ITU-R P.618 [49]	up to at least 20 GHz (tested between 7 GHz and 14 GHz)
Total attenuation	ITU-R P.618 [49]	above 18 GHz

Table 29: Frequency scope of selected ITU-R propagation models

11.4 Climate change

Another phenomenon that potentially influences the accuracy of ITU models is climate change. It needs to be considered that some ITU atmospheric models are based on long-term weather measurements world wide. For example ERA 40 datasets provided by European Centre for Medium-Range Weather Forecasts (ECMWF), that represent re-analyzed data over a period of four decades, are used to generate numerical world maps for atmospheric parameters. Thus, for some recommendations the climate is considered to be constant. However, due to the ongoing climate change, during the last years also in Austria some meteorological records have been established. Climate change could potentially cause periods of drought to become longer, temperature maxima higher and extreme rain events more often. Then, even if the annual average of precipitation and temperature might possibly not show large variations, especially the monthly and short-term meteorological statistics could be more affected. Therefore, it might potentially happen that current prediction models will become more inaccurate in future since they are based on historical climate observations. This aspect definitely requires more research to identify the potential impact of climate change. In papers like [25] by Kantor and Bito but also in [35] by Paulson the impact of climate change also has been thematized and up to a certain extend analyzed. Based on their measurements, both came to the conclusion that the climate cannot be considered constant and the models recommended by the ITU potentially need to be updated regarding this aspect.
A clear increasing trend in the exceeded rain rate for all observed percentages is illustrated by the fitted lines in Figure 56. Rain statistics of nearly two decades as displayed in Figure 57 reveal the effect of non-constant climate. To emphasis the problem, Paulson [35] explains that for terrestrial links designed for an unavailability rate of 0.01% 20 years ago, nowadays the number of outages on the link would be twice as high. Links designed for 0.001% availability, would experience an outage rate that is even three times higher. Even though this sample is given for terrestrial satellite links, certainly earth-space links are

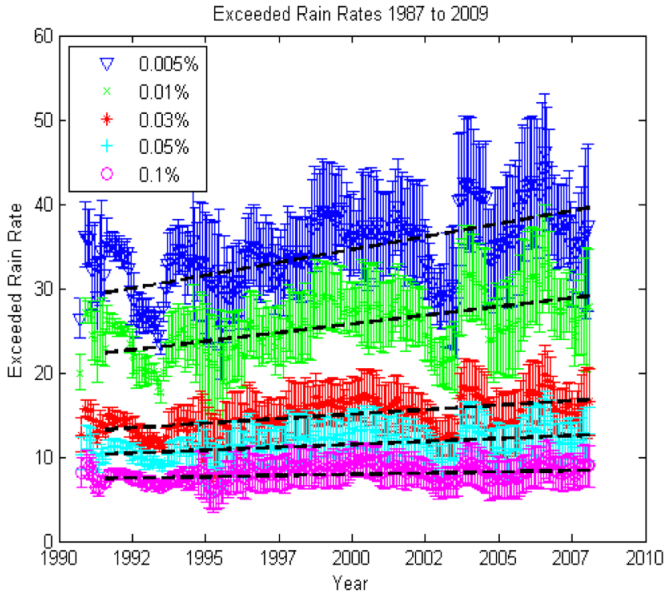

Figure 56: Exceeded rain rate for defined probabilities measured at 150 rain gauge sites in the UK [35]

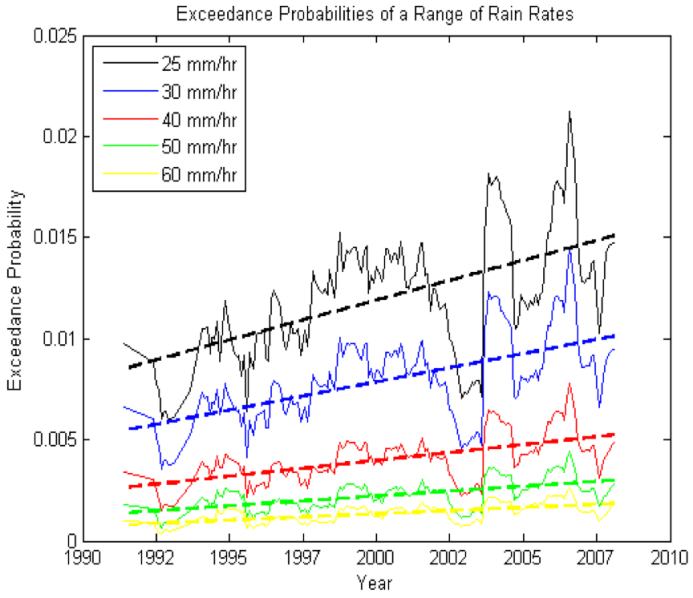

Figure 57: Measured time series of the average annual exceedance probability shown at five different rain rates [35]

affected in a similar way. In the conclusion of this paper [35], Paulson highly recommends to consider the effect of climate change in the ITU prediction models. Only by consideration of latest climate change predictions in ITU models, currently designed satellite links are able to accomplish the specified uptime also during the next decades of operation.

11.5 Alphasat Ka- and Q-band results

The first results of Alphasat Ka- and Q-band statistics measured at the ground station in Graz present a rather short period of observation that encompasses 30 days at maximum. Additional artefacts due to wind events and antenna pattern of preliminary fixed satellite pointing hamper the data processing. Despite these conditions, conservative comparison of derived ITU model and Alphasat statistics was performed.
In consequence of these circumstances serious proposals for modifications of ITU models based on Alphasat measurements unfortunately cannot be made at this stage. As long-term Alphasat Ka- and Q-band beacon measurements are available, it might be very well possible to examine the indicated frequency range of ITU models and perform investigations on a potential interfade duration model. In addition also a long-term study on instantaneous frequency scaling would be of great interest.

12 Conclusion and outlook

This thesis evaluated the accuracy of selected ITU models by comparison with measurement data from beacon receivers, radiometers, a disdrometer and meteorological data. The results of the evaluation with measurement data have been presented and analyzed. The ITU models and measurement data processing routines have been described. Furthermore, a review of modified prediction models available in open literature has been provided as well. In Addition, based on findings during the evaluation process, potential improvements for current ITU models have been discussed.

Generally speaking, the comparison with ITU predictions achieved quite reasonable agreement. However there is still room for improvement of ITU models since frequency dependent variations in prediction accuracy have been observed. Preliminary results of Alphasat beacon statistics have been shown as well. However, these results are statistics over a very short time of observation. Therefore, a serious evaluation with ITU models is not possible at the moment. The number of recently published papers that propose improvements of the current ITU models for tropospheric effects in the tropic zone implies that there is still a need for improvement to reach a constant level of accuracy world wide. Moreover, research to provide general validity of ITU models for high frequencies such as Q-band an above is required.

In the course of this thesis MATLAB was used in order to process measurement data and compute statistics. Especially at high sampling rates such as 10 Hz for example, Matlab reaches its limits in capacity. A possible solution would be down sampling to a sampling rate of 1 Hz to compute first and second order statistics for one year of measurement data. A problem however arose when it comes to scintillation. To measure scintillation, high sampling rates are needed, thus downsampling does not represent an applicable solution. A possible solution would be to realize the computation on another software platform or a cluster.

Unfortunately, only a very limited amount of Alphasat measurement data was available for this thesis. Nevertheless, it is for sure that findings derived by the propagation experiments during the remaining years of the nominal lifetime of the satellite payload will provide vital information for the extension of satellite communication to the Q/V-band.

Significant knowledge of the impairment due to atmospheric effects up to Ka-band was gained during the historic Olympus campaign and ever since still newer methods to understand these monitored effects are being developed. However some of these models have to be changed or reworked because at Q-band and higher frequencies already considered phenomena present an unexpected new appearance. Therefore, the upscaling of ITU model parameters to reach good accuracy at higher frequencies potentially needs to be adapted.

In the course of this thesis test input and output parameters provided by the ITU for the

verification of the implemented models were used, if available. Unfortunately, these sets of test parameters are not available for all prediction models provided by the ITU at the moment. By providing verification data in form of input and expected output values, not only sporadically, but rather for all proposed models, consistency in the model implementation could be ensured and verification facilitated. Certainly, this process would take a lot of effort and time.

Another important point to mention is the non-standardized way to derive propagation parameters from measurement values, respectively statistics from propagation parameters. At the moment there is no standard available that represents algorithms to derive these parameters from the instruments which are part of the basic equipment of a ground receiver terminal. This leads to the fact that experimenters apply their individual algorithms and consecutively difficulties arise when results are compared. Unfortunately, such recommendations as available for the modelling of the atmospheric effects developed by the ITU are not available yet. However, there are already some actions started by experimenters in Europe with the aim of building a standard software library to derive propagation parameters and statistics in a consistent way. Nevertheless, it needs to be stated that even if the processing is consistent, a manual pre-processing and data classification regarding validity still represents the most reliable way of processing. The development of a standard algorithm software library would provide a new basis for discussion and at the same time a common starting point for new modifications. To keep track of these modification a consortium such as the ITU would be necessary to investigate and review the proposed modifications as well as update the standard software library respectively the processing algorithms.

Subsequent to this thesis the evaluation of improved models that derive specific coefficients based on local measurement data as introduced in chapter 10 with measurements derived in Graz is proposed. These models have been developed to aim for better accuracy of the prediction of an atmospheric effect in a tropic region. Though, since they are adopted to local measurements, also an evaluation of these proposed models for the region of Austria, where the ITU models already achieve quite good accuracy, would be of interest. The specific model parameters of course need to be adopted according to the local climate conditions and beacon receiver settings. However, a model that is based on local measurements could potentially be able to reach better accuracy.

Bibliography

[1] ESA/ESTEC A. Martellucci et. al. *Cost Action IC0802. Handbook of Microwave Propagation Measurements for Satellite and Terrestrial Links.* Noordwijk, The Netherlands, 2012. v. 2.0.

[2] M. Adnan, R. Razali, and Md. Azalin Md. Said. A Study of Perturbation Effect on Satellite Orbit Using Cowell's Method, 2003. 4th IAA Symposium.

[3] J. E. Allnutt. *Satellite-to-ground Radio Wave Propagation.* Peter Peregrinus Ltd., London, United Kingdom, 1989.

[4] C. Amaya, T. Nguyen, A. Rocha, J. M. Riera, A. Benarroch, P. Garcia del Pino, J. M. Garcia-Rubia, G. Carrie, and L. Castanet. Comparison of Multi-year Ka-Band Propagation Characteristics at Four Sites in North America and Europe, 2012. Conference Proceeding: 18th Ka and Broadband Communications, Navigation and Earth observation Conference. Ottawa, Canada.

[5] J.P.V. Poiares Baptista and P.G. Davies, editors. *OPEX Reference book on Attenuation Measurement and Prediction*, volume 1, Noordwijk, The Netherlands, 1994. ESA ESTEC.

[6] Les Barclay. *Propagation of Radiowaves.* IET electromagnetic wave series 502. The Institution of Engineering and Technology, London, United Kingdom, 2nd edition edition, 2003.

[7] V. N. Bringi, V. Chandrasekar, J. Hubbert, W. L. Randeu, and M. Schoenhuber. Raindrop Size Distribution in Different Climatic Regimes from Disdrometer and Dual-Polarized Radar Analysis. *Journal of the atmospheric sciences*, 60:354–365, 2003.

[8] L. Changsheng, Z. Zhenwei, L. Leke, and Z. Xin. A Novel Prediction Model of Rain Attenuation along Earth-space Path. *International Conference on Microwave and Millimeter Wave Technology (ICMMT)*, 4:1–4, 2012.

[9] M. Cheffena and L. E. Braten. Low-Cost Digital Beacon Receiver Based on Software-Defined Radio. *IEEE Antennas and Propagation Magazine*, pages 50–55, 2011.

[10] K.-S. Chen, C.-Y. Chu, and Y.-C. Tzeng. A semi-empirical model of rain attenuation at Ka-band in northern Taiwan. *Progress In Electromagnetics Research M*, 16:213–223, 2011.

[11] Robert E. Collin. *Antennas and Radiowave Propagation.* McGraw-Hill Book Company, 1985.

[12] C. Cornacchini, A. Vernucci, G. Codispoti, and E. Russo. The Alphasat TDP#5 mission segment, 2012. Satellite Telecommunications (ESTEL), 2012 IEEE First AESS European Conference.

[13] Microsoft Corporation. Bing maps. Website: http://www.bing.com/maps/. last checked: 1/05/2014.

[14] M. E. da Costa Rodrigues. *Synthesis of rain attenuation time series for earth-space paths in tropical and equatorial areas.* PhD thesis, Pontificia Universidade Catolica do Rio de Janeiro, Departamento de Engenharia Eletrica, PUC-Rio, 2010. http://www.dbd.puc-rio.br/pergamum/tesesabertas/0610795_10_cap_02.pdf. Last checked: 01/05/2014).

[15] P. Garcia del Pino and A. Benarroch J. M. Garcia, J. M. Riera. Tropospheric scintillation measurement on a Ka-band satellite link in Madrid. Website: http://www.ursi.org/proceedings/procGA08/papers/F04p3.pdf. last checked: 01/05/2014.

[16] P. Garcia del Pino, J. M. Riera, and A. Benarroch. Dynamic characteristics of fading on a 50 GHz slant path. *Conference on Antennas and Propagation, EuCAP 2006*, pages 1–6, 2006.

[17] P. Garcia del Pino, J. M. riera, and A. Benarroch. Fade and interface duration statistics on an earth-space link at 50 GHz. *IET Microwaves, Antennas and Propagation*, 5:790–794, 2011.

[18] ESA Media Relations Office European Space Agency. Alphasat: a double-decker in space. Website: http://esamultimedia.esa.int/docs/technology/Alphasat_factsheet.pdf, 2013. last checked: 01/05/2014. fact sheet.

[19] European Space Agency ESA plain text press releases. No 40-1993: OLYMPUS: END OF MISSION. Website: http://www.esa.int/For_Media/Press_Releases/OLYMPUS_End_of_mission, 1993. last checked: 01/05/2014.

[20] H. Fenech, A. Tomatis, S. Amos, J. Serrano Merino, and V. Soumpholphakdy. An Operator's Perspective on Propagation. *Conference on Antennas and Propagation, EuCAP 2014*, pages 4162–4165, 2014.

[21] Zentralanstalt für Meteorologie und Geodynamik (ZAMG). Website: http://www.zamg.ac.at. last checked: 01/05/2014.

[22] Jiying Huang, Shuhong Gong, and Benxiao Cai. The frequency scaling ratio factor of rain attenuation in Ka waveband along earth-space path in China. *Second International Conference on Mechanic Autimation and Control Engineering (MACE), 2011*, pages 7831–7833, 2011.

[23] Radiocommunication Study Groups International Telecommunication Union. Validation examples for study group 3 earth-space propagation. Excelsheet: http://www.itu.int/oth/R0A04000002/en, 2011. last checked: 1/05/2014.

[24] L. J. Ippolito. *Propagation Effects Handbook for Satellite Systems Design.* Stanford Telecom, USA, 1999. Fifth edition, Section 2 - Prediction.

[25] P. Kantor and J. Bito. Influence of Climate Variability on Performance of Wireless Microwave Links. *IEEE 24th International Symposium on Personal, Indoor and Mobile Radio Communications: Fundamentals and PHY Track*, pages 891–895, 2013.

[26] E. Kubista, W.L. Randeu, W. Riedler, and N. Witternigg. Analysis report on 1985 activities. Technical Report 2, ESTEC/Contract No 5357/83/NL/GM, 1987.

[27] Jr. Louis J. Ippolito. *Satellite Communications Systems Engineering Atmospheric Effects, Satellite Link Design and System Performance*. John Wiley and Sons Ltd, 2008.

[28] DP Technologies Ltf. Dishpointer. Website: http://www.dishpointer.com. last checked: 1/05/2014.

[29] L. Luini, C. Riva, and C. Capsoni. Reduced liquid water content for cloud attenuation prediction: the impact of temperature. *Electronics Letters*, Vol. 49(20):pp. 1259 – 1261, September 2013.

[30] A. Martellucci and SP-1252 European Space Agency R.A. Harris. *Cost Action 255. Radiowave Propagation Modelling for SatCom Services at Ku-Band and Above*. Noordwijk, The Netherlands, 2002.

[31] V. Mattioli. Alphasat TFP5 GS G/T measurement campaign and IOT GS4-MWR, Graz Austria. definition of radiometric coefficients, 2013. version 02.

[32] N.Witternigg, W.L. Randeu, W. Riedler, and E. Kubista. Analysis report on 1980/81 activities, 12GHz quadruple-site radiometer, diversity experiment report. Technical Report 1, Intelsat Contract IS-900, 1986.

[33] Radiocommunication Bureau of the International Telecommunication Union (ITU). ITU-R Study Groups. Geneva, Switzerland, May 2013.

[34] T. V. Omotosho, J. S. Mandeep, and M. Abdullah. Cloud-Cover Statistics and Cloud Attenuation at Ka- and V-Bands for Satellite Systems Design in Tropical Wet Climate. *IEEE Antennas and Wireless Propagation Letters*, 10:1194–1196, 2011.

[35] K. S. Paulson. The Effects of Climate Change on Microwave Telecommunications. *11th International Conference on Telecommunications - ConTEL 2011*, pages 157–160, 2011.

[36] W. L. Randeu. Über die Entwicklung und den Bau eines mehrparametrigen frequenzagilen Wetterradars im Rahmen der Erforschung von Ausbreitungsstörungen auf Satellitenfunkstrecken, 1986. Habilitation dissertation, Technical University Graz/Austria.

[37] W. L. Randeu, E. Kubista, M. Schönhuber, N. Witternigg, F. Stampfl, and W. Riedler. Propagation Modelling Using Dual-Polarisation Radar, final report. Technical report, ESTEC/Contract No. 7417/87/NL/PB (SC), 1992.

[38] W. L. Randeu and W. Riedler. Radar-Supported Microwave Propagation Research in Graz - An Overview, 1991. Proceedings of the International Workshop on Multi-Parameter Radar Applied to Microwave Propagation, Graz (Austria), Sept. 03-06, 1991, pp. 45-58.

[39] A. C. Rocha and J. C. Neves. Cloud and gases attenuation by radiometer measurements., 2001. 11th International Conference on Antennas and Propagation, 17-20 April, Conference Publication No. 480, IEE.

[40] M. Ruggieri, C. Riva, M. De Sanctis, and T. Rossi. Alphasat TDP#5 mission: Towards future EHF satellite communications, 2012. Satellite Telecommunications (ESTEL), 2012 IEEE First AESS European Conference.

[41] Michael Schönhuber. *About interaction of precipitation and electromagnetic waves.* PhD thesis, Graz Technical University, 1998.

[42] International Telecommunication Union. *ITU-R P.1623-1 Prediction method of fade dynamics on Earth-space paths*, 2005.

[43] International Telecommunication Union. *ITU-R P.838-3 Specific attenuation model for rain for use in prediction methods*, 2005.

[44] International Telecommunication Union. *ITU-R P.453-10 The radio refractive index: its formula and refractivity data*, 2012.

[45] International Telecommunication Union. *ITU-R P.837-6 Characteristics of precipitation for propagation modeling*, 2012.

[46] International Telecommunication Union. *ITU-R P.1057-3 Probability distributions relevant to radiowave propagation modelling*, 2013.

[47] International Telecommunication Union. *ITU-R P.311-14 Acquisition, presentation and analysis of data in studies of radio wave propagation*, 2013.

[48] International Telecommunication Union. *ITU-R P.372-11 Radio Noise.* Geneva, Switzerland, 2013.

[49] International Telecommunication Union. *ITU-R P.618-11 Propagation data and prediction methods required for the design of Earth-space telecommunication systems*, 2013.

[50] International Telecommunication Union. *ITU-R P.676-10 Attenuation by atmospheric gases*, 2013.

[51] International Telecommunication Union. *ITU-R P.840-6 Attenuation due to clouds and fog*, 2013.

[52] Maximilianus M. J. L. van de Kamp. *Climatic Radiowave Propagation Models for design of Satellite Communication Systems.* PhD thesis, Technical University Eindhoven, 1999.

[53] Z. Xin, Z. Zhenwei, L. Leeke, and L. Changsheng. Rain Fade Slope on 12.5 GHz Earth-space Link at Qingdao. *International Conference on Microwave and Millimeter Wave Technology (ICMMT)*, 4:1–4, 2012.

Appendix

The appendix provides figures of measured brightness temperatures and atmospheric attenuation statistics that were used for the ITU model evaluation in chapter 9.

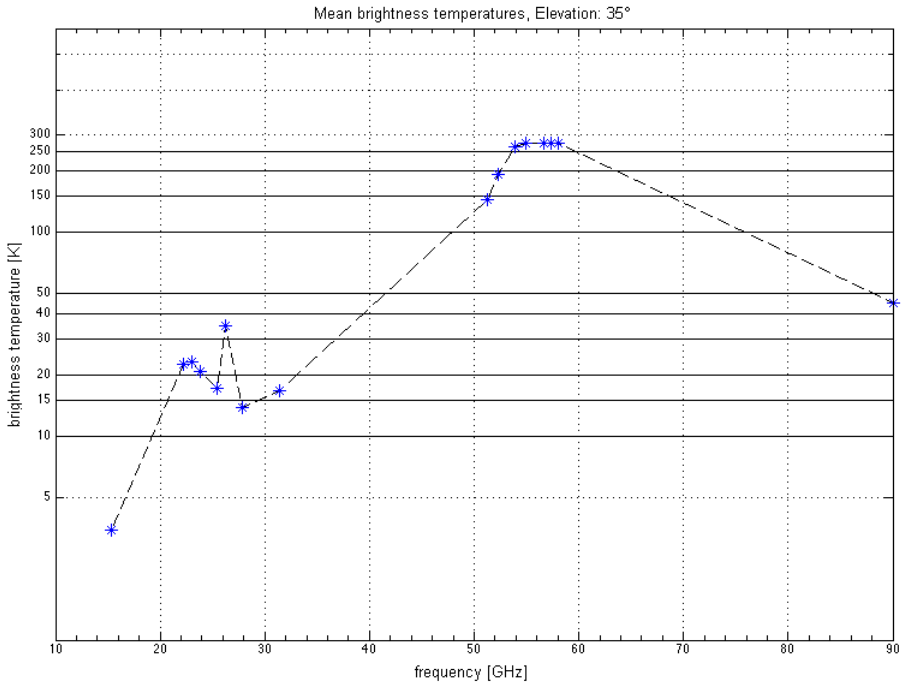

Figure 58: Clear sky brightness temperatures at 35° elevation measured on Hilmwarte

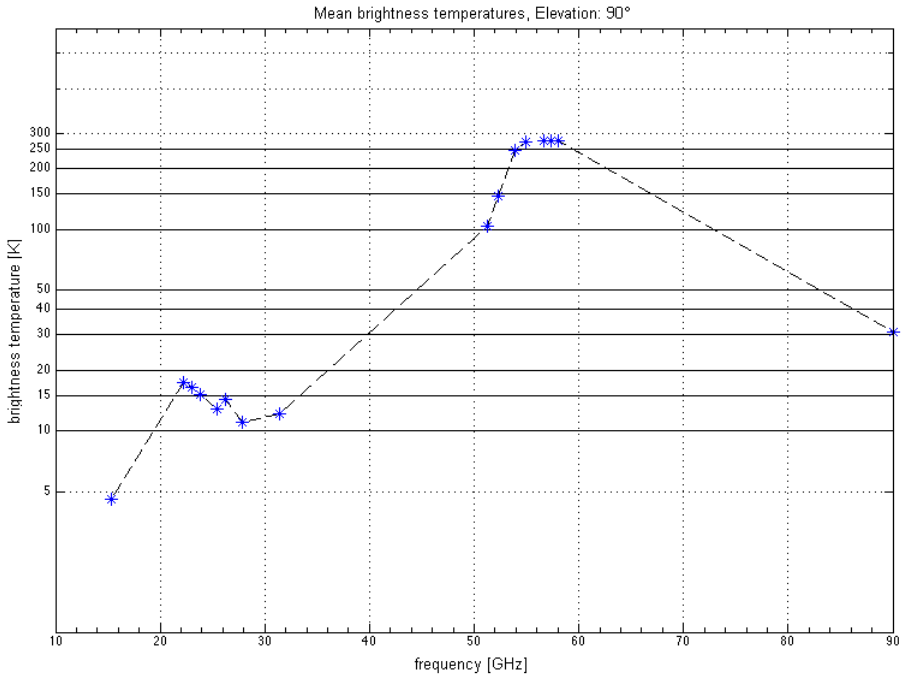

Figure 59: Clear sky brightness temperatures at 90° elevation measured on Hilmwarte

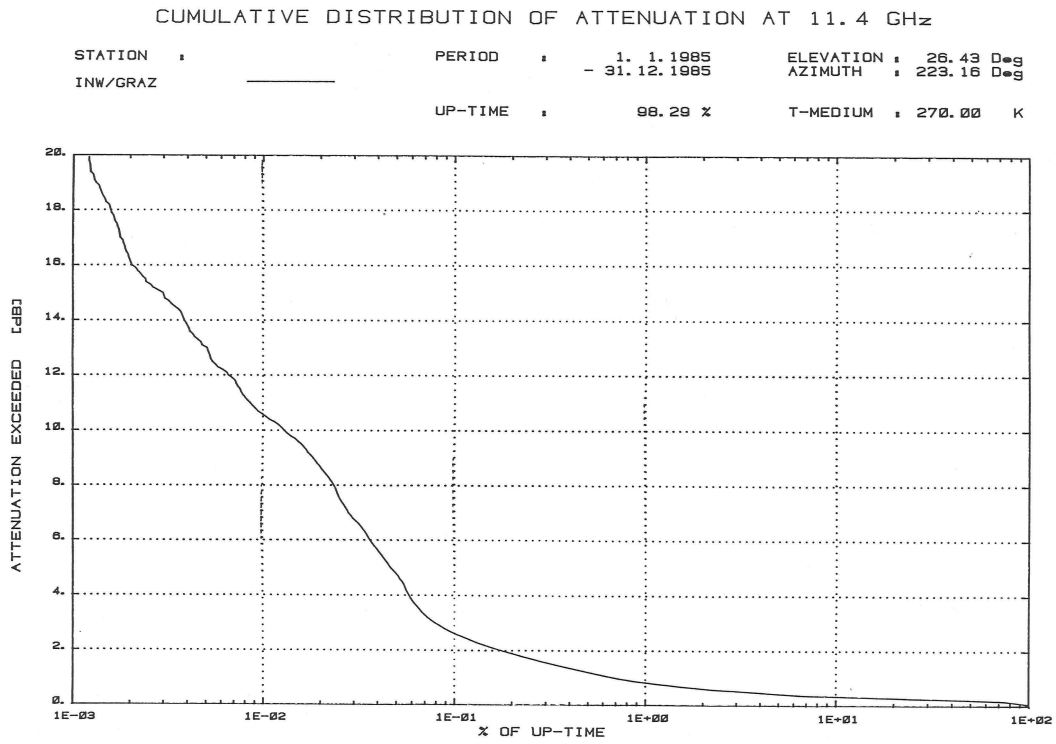

Figure 60: Atmospheric attenuation derived from radiometer measurements at 11.4 GHz provided by [26]

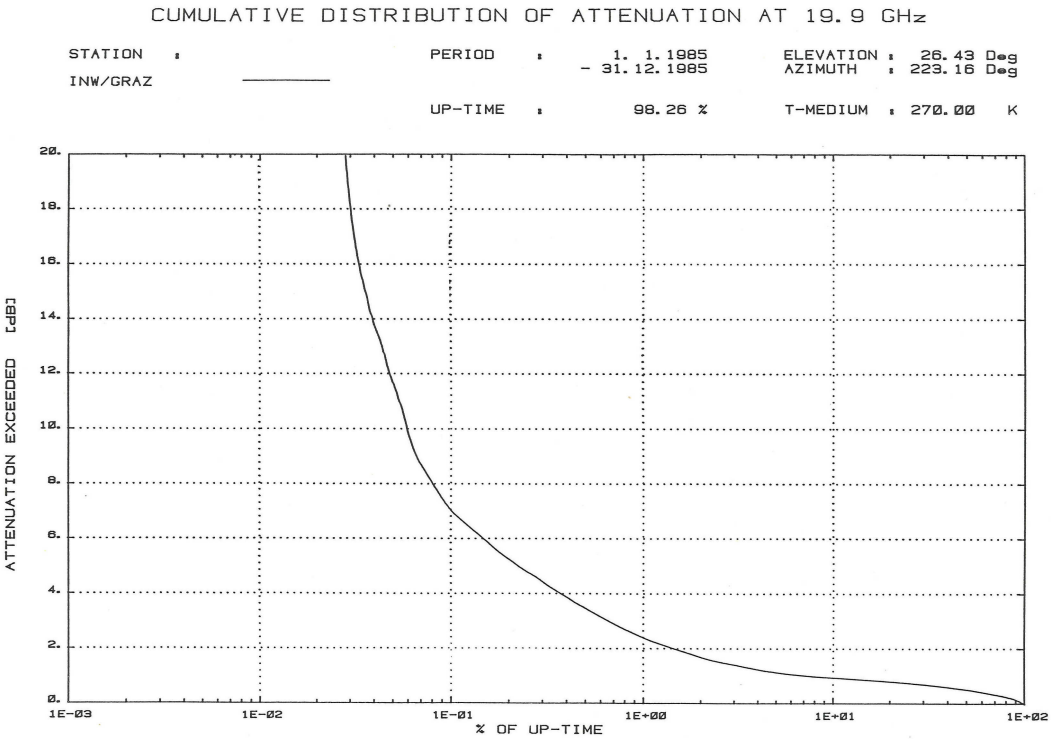

Figure 61: Atmospheric attenuation derived from radiometer measurements at 19.9 GHz provided by [26]

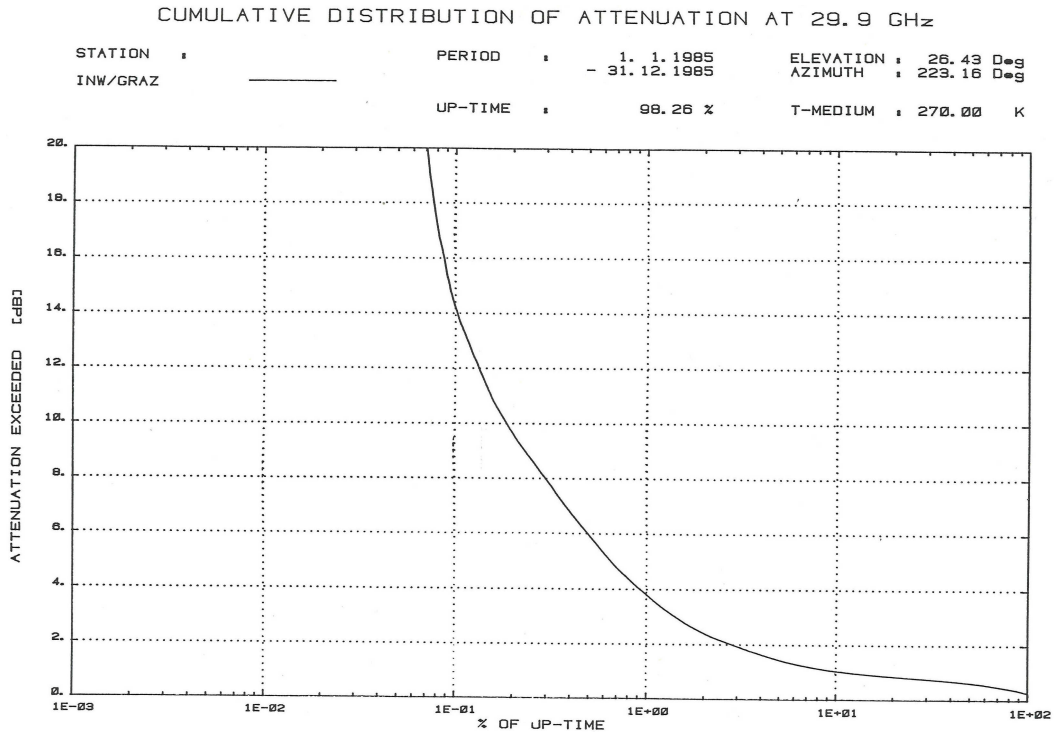

Figure 62: Atmospheric attenuation derived from radiometer measurements at 29.9 GHz provided by [26]